

University of Thessaly

Polytechnic School

Department of Mechanical Engineering

Laboratory of Thermodynamics and Thermal Engines

**Computational Fluid Dynamic Analysis of an Automotive
Centrifugal Compressor**

By

Papagiannis Dimitrios

Giakouvis Ioannis

Submitted in partial fulfillment of the requirements for the degree of Diploma
in Mechanical Engineering at the University of Thessaly

Supervisor: A.M. Stamatellos

Volos, October 2022

© 2022 PAPAGIANNIS DIMITRIOS & GIAKOUVIS IOANNIS

All rights reserved. The approval of the present Diploma Thesis by the Department of Mechanical Engineering, School of Engineering, University of Thessaly, does not imply acceptance of the views of the author (Law 5343/32 art. 202).

Approved by the Members of the Three-member Examining Committee:

First Examiner: Dr. Anastasios Stamatelos
(Supervisor) Professor, Mechanical Engineering Department
University of Thessaly

Second Examiner: Dr. Georgios Charalampous
Asst. Professor, Mechanical Engineering Department
University of Thessaly

Third Examiner: Dr. Konstantinos Ritos
Asst. Professor, Mechanical Engineering Department
University of Thessaly

Acknowledgements

Firstly, we would like to thank our supervisor, Dr. Stamatelos Anastasios, for allowing us to work on such an interesting subject in the Laboratory of Thermodynamics and Thermal Engines, and also for his guidance throughout our thesis. We are really glad to have attended all his lectures in the academic courses Internal Combustion Engines and Turbomachinery and gained all the necessary knowledge to address the subject of this thesis. Furthermore, we would like to thank Dr. Konstantinos Ritos and Dr. Georgios Charalampous for their valuable advice concerning our study.

We'd also like to thank our friends for being there for us over the last five years, in both good and bad times, and for their help with our studies and this dissertation.

Lastly, we would like to thank our parents and brothers for their continuous support and love throughout our lives. Without their selfless help, it would be really difficult for us to follow our dream and study Mechanical Engineering. Our effort in this dissertation is dedicated to them.

Yours sincerely,
Dimitris Papagiannis
Ioannis Giakouvis

Volos, October 2022

Computational Fluid Dynamics Analysis of an Automotive Centrifugal Compressor

Papagiannis Dimitrios & Giakouvis Ioannis

Department of Mechanical Engineering, University of Thessaly, 2022.

Supervisor: Dr. Stamatelos Anastasios

Professor of Internal Combustion Engines

Abstract

In this thesis, we present the preliminary design and computational fluid dynamic analysis of a centrifugal compressor with application to an internal combustion engine. Based on a previous study for the compressors' impeller, this thesis extends to an analysis of the full turbomachine, including the diffuser and the volute. Moreover, an analysis of a version of the compressor with a vaned diffuser is included. The results are compared, and several improvements are proposed. The design of such machines requires special attention as their performance depends on several parameters and must work at a large speed range. The high speed of the flow inside the compressor makes the study of the flow absolutely necessary in order to limit compressibility effects and minimize losses.

The compressor we study belongs to the Laboratory of Thermodynamics & Thermal Engines of the University of Thessaly and was part of the two-stroke Detroit Diesel 12V-71TA engine. The first task of our thesis was to develop a detailed preliminary design of all the parts of the compressor and perform thermodynamic calculations at every stage. Using an Excel spreadsheet, the geometric characteristics are inserted and the appropriate equations and estimated critical parameters of the performance of the compressor.

Throughout the Computational Fluid Dynamic analysis, the results of the simulations are evaluated and compared to those from Excel. Also, several improvements are made where necessary in order to reduce the deviation to acceptable levels. The results extracted were the basic thermodynamic quantities evaluated by means of balances and averaging at inlet and outlet of each part, velocity triangles, and Mach numbers at various points within the compressor for the engine's nominal operating point, which was determined from existing test data.

Υπολογιστική Ρευστοδυναμική Ανάλυση Φυγοκεντρικού Συμπιεστή Αυτοκινήτου

Παπαγιάννης Δημήτριος & Γιακουβής Ιωάννης

Τμήμα Μηχανολόγων Μηχανικών του Πανεπιστημίου Θεσσαλίας, 2022.

Επιβλέπων Καθηγητής: Δρ. Σταματέλλος Αναστάσιος

Καθηγητής των Μηχανών Εσωτερικής Καύσης

Περίληψη

Σε αυτή την πτυχιακή εργασία παρουσιάζουμε το σχεδιασμό και την υπολογιστική ρευστοδυναμική ανάλυση ενός φυγοκεντρικού συμπιεστή που εφαρμόζει σε έναν κινητήρα εσωτερικής καύσης. Βασισμένη σε προηγούμενη μελέτη για τη φτερωτή του συμπιεστή, η πτυχιακή εργασία παρουσιάζει όχι μόνο μια ολοκληρωτική μελέτη για τον φυγοκεντρικό συμπιεστή, αλλά και την ανάλυση μιας εκδοχής του συμπιεστή με πτερυγοφόρο διαχύτη. Τα αποτελέσματα συγκρίνονται και προτείνονται διάφορες βελτιώσεις. Ο σχεδιασμός τέτοιων μηχανών απαιτεί ιδιαίτερη προσοχή καθώς η απόδοση εξαρτάται από πολλές παραμέτρους. Η υψηλή ταχύτητα της ροής εντός του συμπιεστή καθιστά τη μελέτη της ροής απολύτως αναγκαία ώστε να περιοριστεί η συμπίεστικότητα και να ελαχιστοποιηθούν οι απώλειες.

Ο υπό μελέτη συμπιεστής ανήκει στο Εργαστήριο Θερμοδυναμικής και Θερμικών Μηχανών του Πανεπιστημίου Θεσσαλίας και ήταν μέρος του δίχρονου κινητήρα Detroit Diesel 12V-71TA. Το πρώτο καθήκον της διπλωματικής εργασίας μας ήταν να αναπτύξουμε μια λεπτομερή προκαταρκτική μελέτη για όλα τα μέρη του συμπιεστή και να εκτελέσουμε θερμοδυναμικούς υπολογισμούς για κάθε στάδιο. Χρησιμοποιώντας ένα υπολογιστικό φύλλο στο Excel, εισήγαμε τα γεωμετρικά χαρακτηριστικά και εκτιμήσαμε καθοριστικές παραμέτρους της απόδοσης του συμπιεστή.

Κατά της διάρκεια της Υπολογιστικής Ρευστοδυναμικής Ανάλυσης, τα αποτελέσματα των προσομοιώσεων αξιολογούνται και συγκρίνονται με αυτά στο Excel. Επίσης, γίνονται αρκετές αλλαγές όπου είναι αναγκαίο ώστε να μειώσουμε την απόκλιση στα αποδεκτά επίπεδα. Τα αποτελέσματα που εξήγαμε ήταν τα βασικές θερμοδυναμικά μεγέθη, τα τρίγωνα ταχυτήτων, οι αριθμοί Mach σε διάφορα σημεία του συμπιεστή για το ονομαστικό σημείο λειτουργίας του κινητήρα, το οποίο καθορίστηκε από δεδομένα.

Contents

Acknowledgements	vi
Abstract	vii
Περίληψη	viii
Contents	ix
Figure Index	xii
Table Index	xv
Symbol List	xvi
Indicators	xvii
1. Turbocharging and Centrifugal Compressors	1
1.1 Introduction.....	1
1.2 Forced Induction Systems and ICE.....	2
1.3 Supercharging	2
1.4 Centrifugal Compressor Parts.....	4
1.4.1 Impeller	5
1.4.2 Diffuser	5
1.4.3 Volute.....	6
1.5 Mollier Diagram.....	7
1.6 Compressor Map.....	8
2. Preliminary Design	10
2.1 Detroit-Diesel 2-stroke 12V-71TA	10
2.2 Preliminary Analysis.....	11
2.2.1 Calculations at Impeller Inlet.....	13
2.2.2 Calculations at Impeller Outlet	14
2.2.3 Thermodynamic Properties Calculation	15
2.2.4 Calculations of the Vaneless Diffuser.....	16
2.2.5 Calculations of the Vaned Diffuser.....	18
2.2.6 Calculations at the Volute.....	19
2.3 Final Calculations	19
2.4 Results of the Preliminary Design	20

2.5 Velocity Triangle	23
3. Geometry and Mesh Generation	25
3.1 Geometries Creation	25
3.1.1 Geometry of the Impeller.....	25
3.1.2 Geometry of the Vaneless Diffuser.....	26
3.1.3 Geometry of the Vaned Diffuser.....	27
3.1.4 Geometry of the Volute	28
3.2 Mesh in Turbogrid	31
3.2.1. Impeller Mesh	32
3.2.2. Diffuser Mesh	37
3.2.3 Mesh in Ansa	39
3.3 Mesh Independency Study	41
3.3.1 Calculation of Mesh Size of the Vaneless Diffuser	41
3.4 Mesh Generation Criteria.....	43
3.4.1 Final Mesh Generation.....	43
4. Computational Fluid Dynamics Analysis	44
4.1 Modeling.....	44
4.2 Boundary Conditions	48
4.3 Solver Setup	50
4.4 Solver Functions	51
4.4.1 Transfer equations.....	52
4.5 Averaging the Navier-Stokes.....	53
4.5.1 Constitutive Equation.....	53
4.6 Turbulence Models	54
4.6.1 k-epsilon model.....	55
4.6.2 k-omega model.....	55
4.6.3 SST model.....	55
4.6.4 Modeling of y^+	55
4.7 Finite Volumes.....	56
5. Computational Fluid Dynamics Analysis Results.....	58
5.1 Impeller-Vaneless Diffuser.....	58
5.2 Impeller-Vaneless Diffuser-Volute.....	66

5.3 Impeller- Vaned Diffuser	73
5.4 Impeller-Vaned Diffuser-Volute.....	84
5.5 Comparison of CFD Results with the two types of diffusers	89
6. Concluding remarks	92
6.1 Software	92
6.2 Time Management	92
6.3 Conclusions.....	93
6.4 Recommendations.....	94
6.5 Time plan	94
Bibliography	96

Figure Index

Figure 1 : Types of Compressors.....	1
Figure 2 : Turbocharger and Supercharge System [3].....	2
Figure 3 : Roots Blower Design [5].....	2
Figure 4 : Power Indicator Diagram [6].....	3
Figure 5 : Power Indicator Comparison [6].....	4
Figure 6 : Pure Radial Impeller [9].....	5
Figure 7 : Impeller with splitters [9].....	5
Figure 8 : Impeller with Backward Leaned Blades [9].....	5
Figure 9 : Vaned Diffuser Design [9].....	6
Figure 10 : Large Transitory Stall [11].....	6
Figure 11 : Volute Design [12].....	7
Figure 12 : Cross-Section of Overhang Volute [6].....	7
Figure 13 : H-S Mollier Diagram [6].....	8
Figure 14 : Compressor Map [6].....	9
Figure 15 : Upper side of the compressor.....	11
Figure 16 : Upper side of compressor.....	11
Figure 17 : Slides 1 and 2 of the App.....	23
Figure 18 : Velocity Triangle at Tip Inlet.....	24
Figure 19 : Velocity Triangle at Hub Inlet.....	24
Figure 20 : Velocity Triangle at Outlet.....	24
Figure 21 : Velocity Triangle at Outlet.....	24
Figure 22 : Blade Dimensions.....	26
Figure 23 : Wrap angle and thickness.....	26
Figure 24 : Final Impeller Geometry.....	26
Figure 25 : Cross Section of the Impeller.....	26
Figure 26 : Cross Section of the Impeller and Vaneless Diffuser.....	27
Figure 27 : Final Impeller and Vanless Diffuser Geometry.....	27
Figure 28 : Radial Diffuser Dimensions.....	28
Figure 29 : Final Vaned Diffuser Geometry.....	28
Figure 30 : Cross Section of the Final Diffuser.....	28
Figure 31 : Volute in Solidworks.....	29
Figure 32 : Geometrical Characteristics of Volutes' exit Diffuser from Vaneless Centrifugal Compressor in Solidworks.....	29
Figure 33 : Geometrical Characteristics of the Volute Casing from Vaneless Centrifugal Compressor in Solidworks.....	30
Figure 34 : Geometrical Characteristics of the Volutes' exit Diffuser from Vaned Centrifugal Compressor in Solidworks.....	31
Figure 35 : Graphic Interface of Turbogrid.....	31
Figure 36 : Geometry input in Turbogrid.....	31
Figure 37 : Machine Data definition.....	32

Figure 38 : Gap between the blade and the shroud.....	32
Figure 39 : Inlet and Outlet Definition.....	33
Figure 40 : Topology Definition.....	33
Figure 41 : Mesh parameters	34
Figure 42 : Near wall method specification	34
Figure 43 : Blade Mesh Parameters.....	35
Figure 44 : Layers in the corresponding ranges at the Impeller	35
Figure 45 : Tetrahedron and Hexahedron cells [18].....	36
Figure 46 : Structured and Unstructured Grid [19] [20].....	37
Figure 47 : Mesh generation of the impeller.....	37
Figure 48 : Mesh of inlet, hub, and vanes of the Diffuser	38
Figure 49 : Layers in the corresponding ranges at the Diffuser.....	38
Figure 50 : Mesh at the Diffuser.....	39
Figure 51 : Volute Mesh Generation	39
Figure 52 : $y +$ Calculator.....	40
Figure 53 : Volute Volume mesh.....	40
Figure 54 : CFX quality criteria Standard	41
Figure 55 : Total Pressure variation according to Mesh size.....	41
Figure 56 : Total Temperature variation according to Mesh size.....	42
Figure 57 : Efficiency factor variation according to Mesh size.....	42
Figure 58 : Interface of CFX.....	44
Figure 59 : First slide of Turbo Mode.....	45
Figure 60 : Component Definition.....	45
Figure 61 : Physics Definition	46
Figure 62 : Frozen Rotor Interface Definition	47
Figure 63 : Mixing Plane Interface Definition.....	48
Figure 64 : Boundary Conditions Definition	48
Figure 65 : Blades are set as 'Wall'	49
Figure 66 : Solver Setup Interface	50
Figure 67 : Solver Control Definition.....	50
Figure 68 : Time-averaged Vs Instantaneous velocity [25].....	52
Figure 69 : $k-\epsilon$ and $k-\omega$ [26]	55
Figure 70 : y^+ [27]	56
Figure 71 : 2-D Finite element volume [29]	57
Figure 72 : Contour of Total Pressure at Vaneless Diffuser.....	58
Figure 73 : Contour of Pressure at Vaneless Diffuser	59
Figure 74 : Velocity Streamlines at Vaneless Diffuser.....	60
Figure 75 : Contour of Total Temperature at Vaneless Diffuser.....	60
Figure 76 : Contour of Static Temperature at Vaneless Diffuser	61
Figure 77 : Contour of Density in Vaneless Diffuser	62
Figure 78 : Mach number at the Impeller	62
Figure 79 : Mach Number at the Vaneless Diffuser	63
Figure 80 : Flow Field of Vaneless Diffuser	64

Figure 81 : Static Entropy at the Vaneless Diffuser	64
Figure 82 : Contour of Static Pressure.....	66
Figure 83 : Contour of Static Pressure at XY plane	67
Figure 84 : Contour of Total Pressure	68
Figure 85 : Total Pressure distribution at XZ plane.....	68
Figure 86 : Velocity Streamlines	69
Figure 87 : Contour of Total Temperature.....	70
Figure 88 : Contour of Total Temperature at XY plane	70
Figure 89 : Contour of Static Temperature.....	71
Figure 90 : Contour of Static Temperature at XY plane.....	71
Figure 91 : Contour of Density at XY plane.....	72
Figure 92 : Density Distribution at ZY plane	72
Figure 93 : Static Pressure Variation	73
Figure 94 : Total Pressure Variation.....	74
Figure 95 : Pressure Loss Coefficient Variation.....	75
Figure 96 : Pressure Recovery Coefficient.....	75
Figure 97 : Diffuser Effectiveness Variation.....	76
Figure 98 : Isentropic Efficiency factor.....	76
Figure 99 : Contour of Static Pressure at Vaned Diffuser	78
Figure 100 : Contour of Total Pressure at Vaned Diffuser.....	78
Figure 101 : Streamlines in Vaned Diffuser	79
Figure 102 : Streamlines over and under the vanes.....	80
Figure 103 : Contour of Total Temperature at the Vaned Diffuser	80
Figure 104 : Contour of Static Temperature in Vaned Diffuser	81
Figure 105 : Contour of Density of Vaned Diffuser.....	82
Figure 106 : Flow Field at Vaned Diffuser.....	82
Figure 107 : Static Entropy at Vaned Diffuser	83
Figure 108 : Contour of Static Pressure at XY plane	85
Figure 109 : Contour of Total Pressure at XY plane	86
Figure 110 : Velocity Streamlines	87
Figure 111 : Contour of Static Temperature.....	87
Figure 112 : Contour of Density	88
Figure 113 : Contour of Turbulence Kinetic Energy.....	89

Table Index

Table 1: Specifications of Detroit Diesel 2-stroke 12V-71TA	10
Table 2 : Compressor Geometrical Specifications.....	12
Table 3 : Operating Point of the Research	13
Table 4 : Assumptions for inlet conditions	15
Table 5 : Characteristics of the Vaned Diffuser.....	18
Table 6 : Calculated Velocities at the Inlet.....	20
Table 7 : Calculated Velocities at the Impeller Outlet.....	20
Table 8 : Calculated Velocities at the Vaneless Diffuser Outlet.....	21
Table 9 : Calculated Velocities at the Vaned Diffuser Outlet.....	21
Table 10 : Comparison between the Vaneless and the Vaned Diffuser.....	21
Table 11 : Thermodynamic Calculations in the compressor.....	22
Table 12 : Results in the Volute.....	22
Table 13 : Presentation of Results.....	22
Table 14 : Final Mesh Size	43
Table 15 : Detailed Definition for every Boundary Condition	49
Table 16 : Results of CFD vs pre-design for the Vaneless Diffuser.....	65
Table 17 : Results CFD vs Pre-design for the Vaned Diffuser.....	84
Table 18 : Comparison between the CFD results	90
Table 19 : Final Calculations	91
Table 20 : Review of the tasks of the thesis.....	93
Table 21 : Time plan for the thesis	95

Symbol List

A	Cross Section Area
b_{mep}	Brake Mean Effective Pressure
V_d	Engine Cylinder Volume
P_e	Engine Power Output
N_e	Number of RPM
LHV	Lower Heating Value
η_{th}	Thermal efficiency
η_v	Volumetric efficiency
n_r	Number of crankshaft revolutions in one Stroke
ρ	Density
$(\frac{A}{F})_{st}$	Stoichiometric Air Fuel ratio
λ	Air to Fuel ratio related to stoichiometry
ϕ	Inverse of λ
AF	Air to Fuel ratio
m	Mass Flow rate
cp	Heat capacity
R_{air}	Ideal gas constants for air
γ	Isentropic exponent
Z	Number of Main blades
Z_s	Number of Splitter blades
t_b	Thickness of blades
L	Length of impeller
D	Diameter
R	Radius
H	Height
P_{rt}	Total Pressure ratio
P_c	Compressor Power Output
η_s	Compressor efficiency
α	Flow angle
β	Blade angle
N	Number of RPM of compressor
ω	Angular velocity
M_{rel}	Relative Mach number
M_{bl}	Blade Mach number
M	Absolute Mach number
a	Speed of sound
c	Absolute Velocity
c_x	Meridional component of absolute velocity
c_u	Tangential component of absolute velocity
c_r	Velocity perpendicular to the exit cross-section
U	Blade speed
w	Relative speed
σ	Slip factor

ΔW	Compressor specific work
ϕ	Flow coefficient
ψ	Load factor
P	Static pressure
T	Static temperature
h	Static enthalpy
ρ	Static density
P0	Total pressure
T0	Total temperature
h0	Total enthalpy
ρ_0	Total density

Indicators

1	Impeller Inlet
2	Impeller Outlet
2_a	Diffuser Outlet
3	Volute Outlet
h	Blade hub
m	Blade mean
t	Blade tip

1. Turbocharging and Centrifugal Compressors

1.1 Introduction

Gas compressors have many applications in today's industry, from pipeline transport and petroleum refineries to road vehicles and jet engines. That is why scientists need to study compressors thoroughly and find ways to optimize their function. There are many types of compressors, and they are divided into 2 major categories: Positive Displacement Compressors and Dynamic Compressors. Unlike a positive displacement compressor, which works with a constant flow, a dynamic compressor works at a constant pressure. Also, another main difference is related to the number of revolutions that each one performs. The 2 major categories consist of different types of compressors as it can be seen in Figure 1 [1].

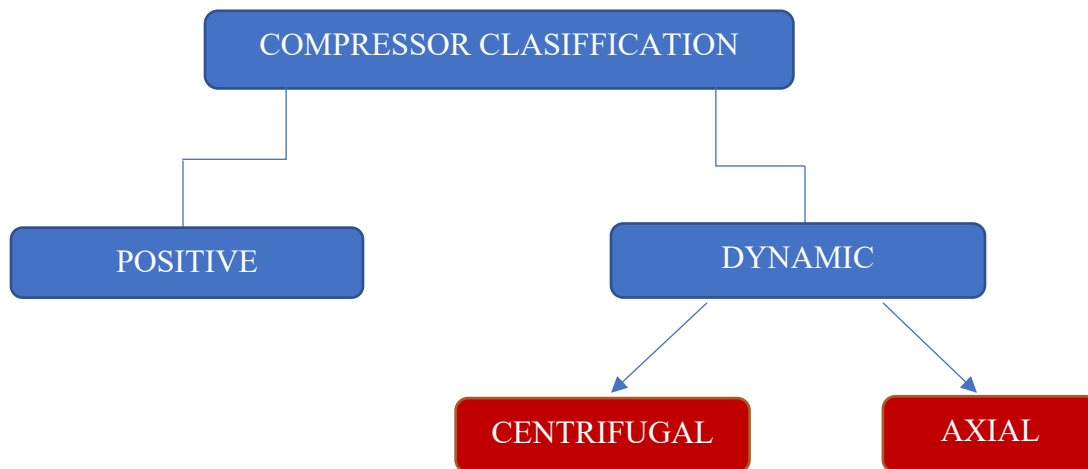


Figure 1 : Types of Compressors

As stated, this thesis investigates how a centrifugal compressor operates and analyzes the different phenomena that alter the state of the gas from the inlet to the outlet. The basic function of a compressor is to achieve pressure increase of a fluid by reducing its volume. This phenomenon is described by the laws of thermodynamics, and in simple terms by the equation of state:

$$P \cdot V = n \cdot R \cdot T \quad (1)$$

The basic principles of operation of the compressor are similar to those of a pump, but with a different compressible fluid (air). When air goes through such a device, it is compressed, usually many times and through different stages, in order to reach the desired pressure values. Each stage takes up a part of the overall pressure rise.

In contrast to the naturally aspirated engines, which suck air in atmospheric conditions (1 atm), the turbocharged engines take air that has a pressure value of over 1.5 atm. This increases the air density and thus the air mass in the cylinder, assuming same intake temperatures. Increased mass leads to more power generation, and one can achieve good results with more compact engines, saving space but also money, due to reduced weight.

1.2 Forced Induction Systems and ICE

In Internal Combustion Engines (ICE), forced induction systems are very common. These systems use centrifugal compressors to push compressed air into the engine. The compressed air gives space for extra air (oxygen) to reach the engine, providing an extra boost of power. This can be achieved either by a turbocharger or a supercharge [2]. The main difference between each system is the energy source. Superchargers are powered directly by the engine, commonly through a belt, while turbochargers use the engine's exhaust gas to be rotated, as described in Figure 2.

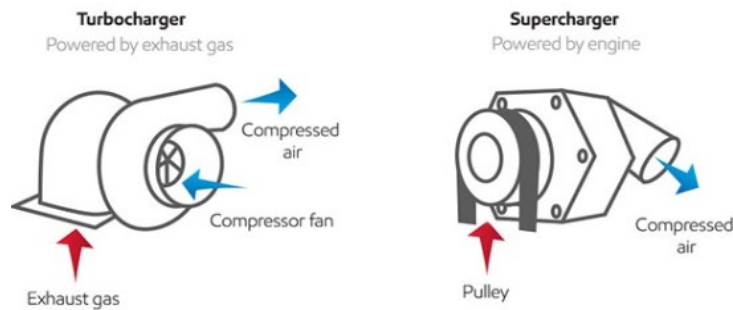


Figure 2 : Turbocharger and Supercharge System [3]

This fact allows superchargers to provide the optimum boost throughout the rev band without any lag. This direct connection to the engine makes superchargers more powerful than turbochargers, but this also makes superchargers considerably less efficient, as they consume engine power in order to run. On the other hand, turbochargers are preferred for their fuel economy benefits, despite the turbo lag that may exist. The turbo lag is actually the slower throttle response, and it depends on the time it takes the engine to create enough exhaust pressure to spin the turbo and pump compressed intake air into the engine. It is clear enough that the longest turbo lag appears in a low-rpm range of an engine. However, in high-performance cars and racing applications, there are applied set-ups like sequential turbocharging, which uses one turbocharger for lower engine speeds and a second or both turbochargers at higher engine speeds to eliminate turbo lag.

The centrifugal compressor used in both systems also has a small size and high efficiency, achieving good results with smaller engines, which is very important for many aspects of the industry. With the application of a centrifugal compressor, pressure ratios higher than 2.5 can be achieved.

The most well-known positive displacement compressor is the Roots Blower, and its design is shown in Figure 3. This type of compressor pumps air with two meshing lobes. The fluid is essentially trapped in pockets around those lobes and transferred from the inlet side to the exhaust [4]. The most common application of this type is found in two-stroke Diesel engines. As referred to, this type of compressor rotates at a much lower RPM than a dynamic one, and pressure ratios up to 1.6 can be achieved.

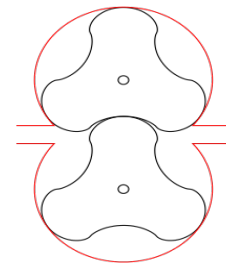


Figure 3 : Roots Blower Design [5]

The entrance of air into a cylinder with a higher density than that of the environment is called "supercharging". The goal is to improve power output. Figure 4 below, displays the Power Indicator diagram of an ideal cycle of a Diesel engine.

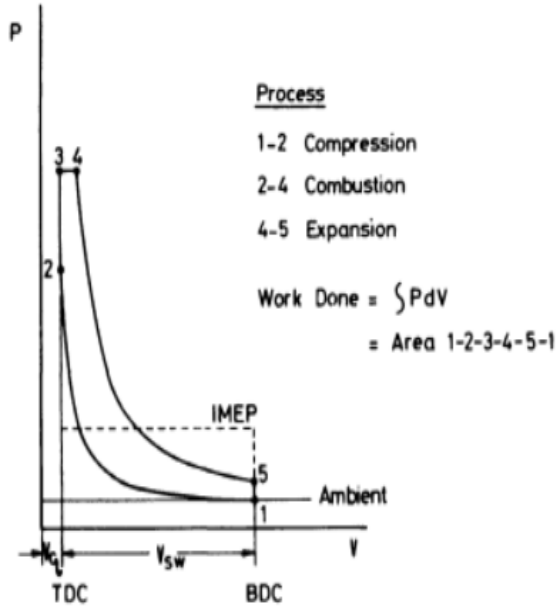


Figure 4 : Power Indicator Diagram [6]

As described from N. Watson and M. S. Janota (1982) [6], the useful work of the entire process is acquired through stages 3-4-5. However, this works against the required work in process 1-2, in order to compress the gas. The work can be calculated from:

$$W = P \cdot dV \quad (2)$$

From J.B. Heywood [7], the power in an ICE is proportional to the Mean Effective Pressure (*bmep*), the rotational speed (*N*) and displacement of the cylinder (*S* or Stroke):

$$P = \frac{bmep \cdot N \cdot S}{n_r} \quad (3)$$

, where *bmep* is the break mean effective pressure, *N* is the number of revolutions, *S* the Stroke and *n_r* is the number of crankshaft revolutions in one stroke. While the *bmep* term is described as:

$$bmep = \frac{\rho \cdot n_v \cdot n_{th} \cdot LHV}{\lambda} \quad (4)$$

, where ρ is the density of the fluid, n_v is the charging efficiency, n_{th} is the thermal efficiency, *LHV* is the Lower Heating Value of fuel and λ is the Air to Fuel ratio related to stoichiometry.

An observation from the diagram is that at stations 3 and 4, the pressure remains constant. Rudolf Diesel tried to inject the fuel in small quantities in order to achieve heat addition from

burning the fuel at constant pressure inside the cylinder chamber. This is considered a way to achieve high efficiency.

Intercooling may occasionally be employed to increase the density of the gas before it reaches the combustion chamber. Compression also results in higher temperatures that are most often unwanted and, in some cases, dangerous. Intercoolers help achieve lower temperatures.

Figure 5 compares the naturally aspirated cycle with the supercharged one and shows that the power produced, as well as the mean effective pressure, reaches higher values. Using the mean effective pressure, also called dimensionless torque, one can compare engines with different volumes and conclude that supercharged engines excel the rest in terms of performance. This higher power output requires a higher fuel demand.

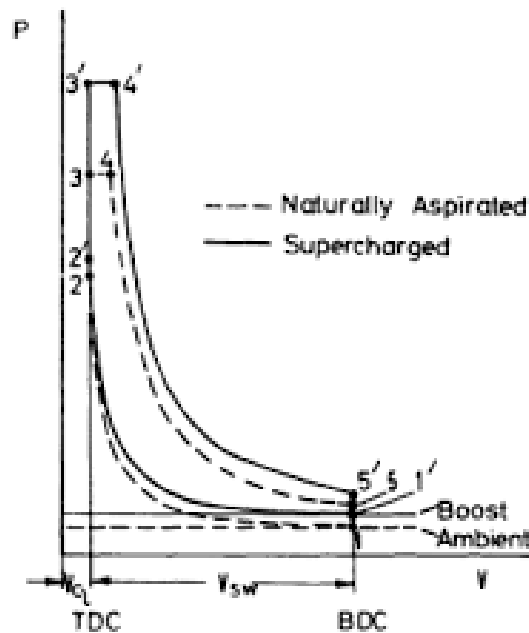


Figure 5 : Power Indicator Comparison [6]

Supercharging has also contributed to the downsizing of the engine because a supercharged low displacement engine can produce the same power and torque as a larger naturally aspirated one. This fact has led not only to cheaper manufacturing costs but also to a general improvement in vehicle performance. The lower weight, combined with the lower center of gravity of the engine, improves the drivability of not only racing but also conventional vehicles. All these also lead to a lower ratio of power (kW) to weight (kg) of each engine, a value that can be used to estimate the overall efficiency of the system.

1.4 Centrifugal Compressor Parts

Centrifugal compressors are compressors that provide radial airflow. The main components of the centrifugal compressor consist of the Impeller, Diffuser, and Volute. The air goes through the inlet of the device, reaching the rotating impeller. The air is often twisted before entering the compressor through blades to obtain the most suitable angle of attack for the impeller blades.

Through rotation, the fluid gains velocity and pressure, and after exiting the impeller, it reaches the diffuser. At the diffuser, the fluid loses some of its kinetic energy and converts it into a static pressure rise. Finally, the fluid is collected and transferred at the outlet via the volute casing, which is shaped like a spiral duct. The role of the volute is not only to guide the flow but also to convert the kinetic energy into static pressure through the gradual increase of its cross-section.

1.4.1 Impeller

The impeller, whose design is depicted in Figure 6, is the part of the compressor that transfers all the work needed to the fluid, resulting in increasing both its velocity and static pressure. It is made up of a number of main blades, the number of which depends on the size of the impeller [8]. The relative Mach number is a critical point when designing an impeller because if the flow becomes sonic either in the inlet or the outlet, there will be choking and probably shock waves will appear, which cause not only a huge decrease in the efficiency but also structural failures. The solution to this problem is to use backward-leaning vanes to slow down the flow in the inlet, as shown in Figure 8. Moreover, blades with angles different from zero can also reduce the Mach number at the outlet, causing bigger bending stresses in the blades. Blades with an angle equal to zero are used mainly in diesel engines because they lack air mass flow rate and they operate at a limited number of revolutions.

Apart from the main blades, many devices consist of splitters, as the one in Figure 7. These splitters are placed between two main blades and extend from part way through the inlet up to the impeller tip to aid flow control while minimizing the blockage in the eye. At high speeds, the vacuum created helps increase the air mass flow rate even more. However, their main role is to help guide the flow and compress air as it is accelerated according to the impeller rotation. Detailed analysis is performed on the shape and the material used for the impeller in every application in order to reduce the weight and, consequently, its moment of inertia so as to achieve faster acceleration.



Figure 6 : Pure Radial Impeller [9]



Figure 7 : Impeller with splitters [9]



Figure 8 : Impeller with Backward Leaned Blades [9]

1.4.2 Diffuser

After exiting the impeller, the fluid reaches the diffuser part. The shape of the diffuser helps to convert the air velocity into a pressure rise, as reported by Dixon S.L. and Hall C.A. (2013) [10]. The diffusers consist of two categories: the vaneless diffusers and the vaned ones. On the one hand, the vaneless diffusers demand a bigger radial area in order to diffuse the fluid, resulting in bigger flow losses. On the other hand, the vaned diffusers, which is in Figure 9, can achieve the same

pressure rise in the fluid with fewer losses because there is better guidance of the flow. Generally, this helps to increase the efficiency but also greatly reduces the air mass flow rate operating range. So, the vaned diffusers will only be used in low-speed engines. In most cases, the number of diffuser vanes is less than the number of impeller vanes, so that the flow will be distributed more evenly from one diffuser channel to another. Also, it is critical to determine the exact dimension of the vaneless space before and after the vanes, which results in normalizing and stabilizing the flow.



Figure 9 : Vaned Diffuser Design [9]

The design of a diffuser is a demanding task. The reason is that the greater part of the losses caused by the diffuser (up to 70%) are due to the detachment of the boundary layers at the wall. More generally, there is an upper limit to how much the flow area can be increased and how much the stall pressure can be reduced in a diffuser. The maximum increase in static pressure will be reached just before the point where boundary layer separation will occur. Figure 10 below depicts the transitory stall.

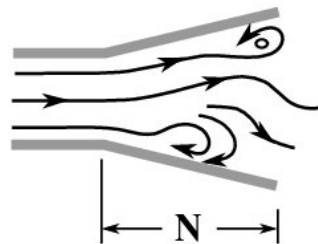


Figure 10 : Large Transitory Stall [11]

1.4.3 Volute

The Volute represents the connecting element between the last stage of the compressor and the external environment. For every application, the casing has many differences in shape. However, in every case, its casing has a cross-sectional area that continually increases. This results in the diffusion of the flow as well as maintaining its velocity through it. The function of the volute is simply to collect the diffuser exit flow and guide it as efficiently as possible to the exit without compromising the effectiveness of the diffuser. That's why the volute can also play a significant

and sometimes dominant role in stage performance. According to Watson, the total losses in the volute are considered about half of the dynamic pressure of the diffuser [6].

The design of a volute does not begin with the volute but rather with the upstream elements. Therefore, emphasis must also be placed on how the flow comes. The flow must be prepared for the type of volute being used. Apart from the inlet flow conditions, the design of the volute involves several factors, such as proper volute sizing, throat placement, tongue configuration, and exit conical diffuser. On the intake side, there is an opening perimetrically to the shell which allows the entrance of the fluid. In most cases, this design, which is called the overhang design, shown below, is preferred, as it reduces the overall diameter of the compressor. Moreover, it is claimed that mixing losses at the entry are decreased. The cross sections of the volute are sized to achieve constant angular momentum of the flow but can also be slightly increased in size to account for boundary layer growth. Furthermore, the larger the radius tongue is, the wider the operating range will be achieved. However, higher losses will be caused. Also critical, like the tongue design, is the final part of the volute, the diffuser exit. For this section, there can be a sizable area ratio and a suitable length in order to aim for good diffusion of the flow [12]. The shape of the volute is illustrated through Figure 11 and 12.

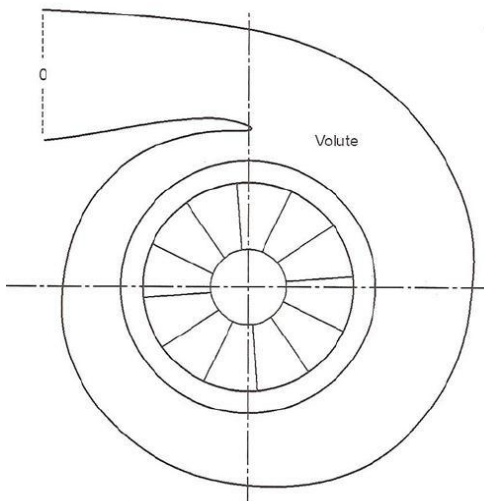


Figure 11 : Volute Design [12]

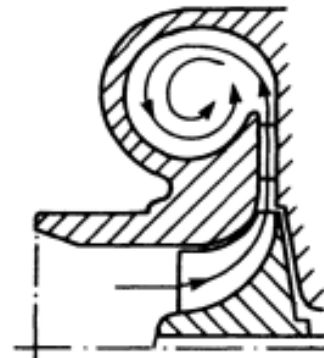


Figure 12 : Cross-Section of Overhang Volute [6]

1.5 Mollier Diagram

Compressor performance cannot be accurately predicted without detailed knowledge of the behavior of the fluid. The Mollier Diagram in Figure 13 helps to deeply understand the function of the compressor. All the plots in this enthalpy-entropy (h-s) diagram can describe the changes in the fluid at every stage of the compressor. For a better understanding of the diagram, some important thermodynamic formulas are mentioned:

$$P_{01} = P_i + \frac{1}{2} \cdot \rho \cdot c_i^2 \quad (5)$$

$$h_{01} = h_i + \frac{1}{2} \cdot c_i^2 \quad (6)$$

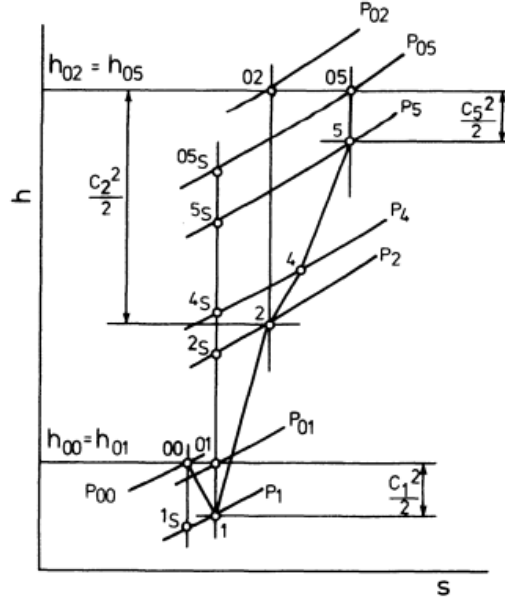


Figure 13 : H-S Mollier Diagram [6]

Station 01 represents the ambient conditions of the air. When the air enters the eye of the impeller, it accelerates, causing a pressure drop from P₀₁ to P₁. The energy transfer to the air takes place through the rotating impeller, and the process is indicated by line 1-2. This results in not only a huge increase in pressure but also an enthalpy rise. If the total kinetic energy of the air leaving the impeller is converted isentropically to pressure, the final pressure would be P₀₂. Since the diffusion process is not accomplished isentropically and some kinetic energy remains at the diffuser exit, the static pressure at point 5 is P₅. Here, the total enthalpy between station 02 and station 05 remains the same, as no work is produced through the diffuser. However, the total pressure decreases due to losses in the diffuser [6]. As mentioned, the diffuser losses are significantly calculable, so the design is required to be detailed.

1.6 Compressor Map

The compressor map is a chart that engineers use to examine if a compressor is suitable for an ICE, as it contains information concerning the behavior of the compressor throughout its operating range. This chart illustrates the mass flow of air in relation to the revolutions (rpm) of the engine in relation to the operation map. Figure 14 shows a map that only serves as an example; it does not describe the compressor that is the subject of the inquiry. In this map, the x axis corresponds to dimensionless mass flow ($m \sqrt{T_{01}} / P_{01}$) and y to Pressure ratio (P_{02} / P_{01}). Furthermore, there are curves of constant dimensionless speed ($N / \sqrt{T_{01}}$) and areas corresponding to the compressor efficiency.

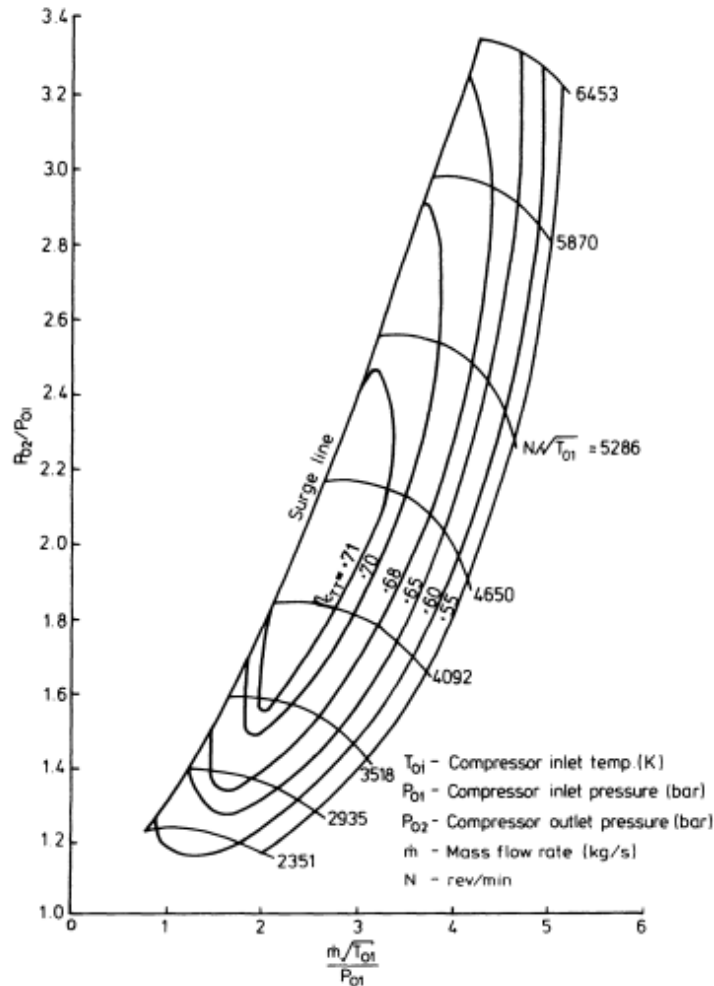


Figure 14 : Compressor Map [6]

There are three essential areas on a compressor map. The central area is the stable operating zone. This area is separated from the unstable one on its left by the surge line and on its right by the choke line. When operating over the surge line, the mass flow rate is low enough and flow reversal in boundary layers is observed. This results in many flow oscillations, which will lead to compressor failure. On the other hand, the flow is characterized by high speeds, which increases the Mach number. When the Mach number overcomes the value of 1, the flow becomes supersonic. In these cases, just when Mach equals the unit, the flow choking takes place. When choking occurs, compressor speed may rise substantially with no increase in mass flow rate. From Figure 14, one can see that the curves of constant speed tend to become vertical when choking exists. For these reasons, a compressor must remain within its stable range, especially inside the areas where it has maximum efficiency. This means that for any application, the operating range should be known to select the suitable compressor.

There are many cases where the compressor is unsuitable for the specific engine and performs outside its stable range. When a compressor runs on the left side of the surge line, it means that it is bigger than needed for the specific engine, while when it runs on the opposite side, it means that the compressor is smaller than the optimum one and cannot sustain the high mass flow rate.

2. Preliminary Design

This chapter presents the analysis of the preliminary design. Preliminary design has always been the most powerful and important tool for every engineer. Through this process, the engineer can estimate the effect of every geometrical change on performance and thermodynamic properties. Consequently, using this process, any industry can not only save a lot of time but also money.

The preliminary design of the Centrifugal compressor of Detroit-Diesel 2-Stroke 12V-71TA is presented in a Microsoft Excel spreadsheet and it is based on the calculations and assumptions of Dixon and Hall [10]. The calculations start with the impeller, continue with the diffuser, and conclude with the volute. This study contains both the aspects of a vaneless and a vaned diffuser. The preliminary design refers to a single operating point, which is in the middle of the operation range of the compressor.

2.1 Detroit-Diesel 2-stroke 12V-71TA

This engine was produced in the decade of 1950 by General Motors, and the analysis of its parts remains remarkable. The fact that this engine is part of the laboratory of Thermodynamics and Thermal Science gave us the opportunity to take a closer and more detailed look at its parts. It is a 12V cylinder engine, and each side has a centrifugal compressor and a roots blower, which are connected in series.

Before the preliminary design, there are some important calculations concerning the engine that need to take place. These calculations refer to the mass air flow of the engine, which is the most critical parameter of its performance. The mass flow of the engine will be used further for the calculations of the centrifugal compressor. The data of the engine are presented in Table 1 below:

Table 1: Specifications of Detroit Diesel 2-stroke 12V-71TA

Specifications Detroit Diesel 2-stroke 12V-71TA			
Engine Displacement	V_d	0.0140	m ³
Bore	B	0.108	m
Stroke	S	0.127	m
Max Power	Pe	336	kW
RPM of Max Power	Ne	2300	rpm
Thermal Efficiency	n_{th}	0.37	
Volumetric Efficiency	n_v	0.65	
Stoichiometric Air Fuel Ratio	$\left(\frac{A}{F}\right)_{st}$	14.5	
Air Fuel Ratio	λ	1.4	
Lower Heating Value	QLHV	44	MJ/kg

$$m_f = \frac{P_e}{n_f * Q_{LHV}} \quad (7)$$

$$\lambda = \frac{\left(\frac{A}{F}\right)}{\left(\frac{A}{F}\right)_{st}} \quad (8)$$

$$m_{air} = \frac{\lambda * \left(\frac{A}{F}\right)_{st} * m_f}{2} \quad (9)$$

, where P_e is the Power of compressor and n_{th} is the thermal efficiency.

The calculation of mass air flow for the centrifugal compressor studied is based on the formulas above and found to be 0.2 kg/sec.

The compressor is made up of eight main and eight splitter blades as portrayed in Figure 15 and Figure 16. The splitter blades and the backswept blades are used to decrease the velocity of the air coming into the impeller in order to eliminate any chance of a sonic phenomenon in the inlet. Also, the blades become radial at the outlet, resulting in lower stress on them.

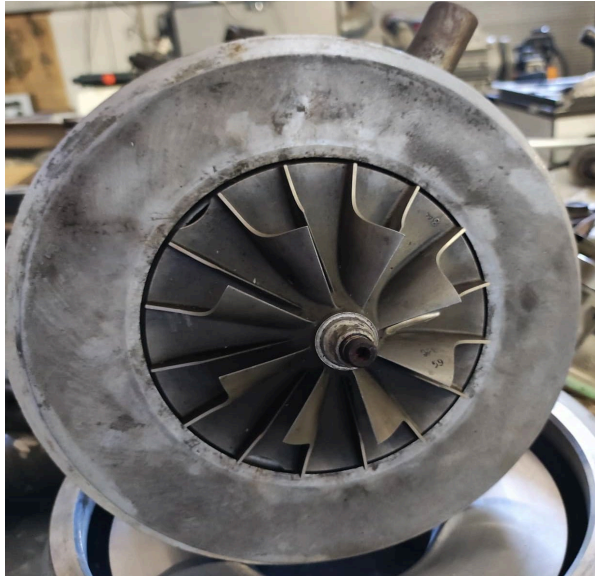


Figure 15 : Upper side of the compressor



Figure 16 : Upper side of compressor

2.2 Preliminary Analysis

All measurements on critical parts of the compressor have been conducted with the help of the appropriate equipment in the laboratory. Some measurements are used as input in the preliminary design, while others constitute a value of comparison between them and the output results from the preliminary design. All geometrical characteristics are summarized and represented in Table 2.

Table 2 : Compressor Geometrical Specifications

Geometrical Specifications			
Number of main blades	Z	8	
Number of splitter blades	Z_s	8	
Thickness of blades	t_b	0.001	m
Length of impeller	L	0.032	m
Inlet of Impeller			
Hub radius	R_{hub}	0.01	m
Tip radius	R_{tip}	0.04	m
Hub blade angle	$\beta_{1,h}$	43	deg
Mean blade angle	$\beta_{1,m}$	60.15	deg
Tip blade angle	$\beta_{1,t}$	68.75	deg
Area of Inlet	A_i	0.0051	m ²
Impeller Outlet			
Outside Diameter	D_o	0.125	m
Height of Blades	H_{tip}	0.009	m
Area of Exit	A_o	0.003	m ²
Blade angle	β_2	0	deg
Diffuser Diameter	D_d	0.2	m

Where A_i is the inlet area of the air that comes in the impeller and A_o is the outlet area of the air that comes out:

$$A_i = \pi \cdot (R_{tip}^2 - R_{hub}^2) \quad (10)$$

$$A_o = D_o - Z + Zstb \cdot (H_{tip} - H_{hub}) \quad (11)$$

Table 3 represents the operating point of the research.

Table 3 : Operating Point of the Research

Operating Point			
Power Output	P_c	13000	W
Number of Revolutions	N	40000	rpm
Mass flow rate	m	0.2	kg/s
Angular velocity	ω	4189	rad/s

The angular velocity is determined from:

$$\omega = \frac{2 \cdot \pi \cdot N}{60} \quad (12)$$

The preliminary design is performed for both the compressor with the vaneless diffuser and the one with the vaned diffuser. Consequently, there are differences in the calculations concerning the diffuser and the volute in each device.

2.2.1 Calculations at Impeller Inlet

As mentioned previously, the preliminary design is important for the calculation of the thermodynamic properties and the velocity of the air. Since the inlet conditions are constantly changing, the velocity triangle must be designed in at least 3 positions (hub, mean, and tip). As far as the inlet, the calculations are performed at these three positions since the conditions at the leading edge of the blade are changing across it [13].

The process starts with the calculations at the tip. The tip and hub diameters are measured (R_{1tip} , R_{1hub}), and from the following formula, derive the values of $M_{1t,rel}$ and M_{1t} :

$$\frac{R_{1hub}}{R_{1tip}} = \sqrt{1 - \frac{\omega^2 \cdot m \cdot (1 + \frac{1}{5} \cdot M_{1t,rel}^2 \cdot \cos(\beta_{1t}))^4}{\pi \cdot P_{o1} \cdot \gamma \cdot a_{o1} \cdot M_{1t,rel}^3 \cdot \sin^2(\beta_{1t}) \cdot \cos(\beta_{1t})}} \quad (13)$$

$$a_{o1} = \sqrt{\gamma \cdot R \cdot T_{o1}} \quad (14)$$

$$M_{1t} = M_{1t,rel} \cdot \cos(\beta_{1t}) \quad (15)$$

The calculation of the velocity triangle remains an important aspect of the analysis of the compressor. The following formulas are necessary in order to calculate the exact velocity triangle:

$$c_{x1t} = M_{1t} \cdot \alpha_1 \quad (16)$$

$$\alpha_1 = \frac{\alpha_{o1}}{\sqrt{1 + \frac{1}{5} \cdot M_{1\tau}^2}} \quad (17)$$

$$w_{1t} = \frac{c_{x1t}}{\cos(\beta_{1t})} \quad (18)$$

$$u_{1t} = w_{1t} \cdot \sin(\beta_{1t}) \quad (19)$$

The same process is also performed for the mean and hub, and the results are presented further in this chapter.

2.2.2 Calculations at Impeller Outlet

Continuing with the outlet, the slip factor is calculated using the Stanitz method for the radial impeller. This factor indicates that the relative velocity of the flow isn't driven perfectly, even under ideal conditions. So, the deviation of the flow must be predicted and counted in the further design. It is known that this specific compressor produces 13 kW at $N = 40.000$ rpm. So, the energy produced per kilogram of fluid (W) is calculated:

$$\sigma = 1 - \frac{0,63 \cdot \pi}{Z + Z_s} \quad (20)$$

$$\Delta W = \frac{P}{\dot{m}} \quad (21)$$

$$u_2 = \sqrt{\frac{\Delta W}{\sigma}} \quad (22)$$

Moving on with the calculation of the tangential component of the absolute velocity, c_{u2} . Following other designers' strategies [6], it was assumed that the radial component of the velocity c_{r2} is equal to the axial component of the flow at the inlet. Below are the formulas used for the above calculations:

$$c_{r2} = c_{x1t} \quad (23)$$

$$c_{u2} = \sigma \cdot u_2 \quad (24)$$

$$c_2 = \sqrt{c_{u2}^2 + c_{r2}^2} \quad (25)$$

Through this process, the relative velocity w_2 was calculated using the following formulas:

$$w_2 = \sqrt{(u_2 - c_{u2})^2 + c_{r2}^2} \quad (26)$$

$$\alpha_2 = \tan^{-1}\left(\frac{c_{u2}}{c_{r2}}\right) \quad (27)$$

$$\beta_2 = \cos^{-1}\left(\frac{c_{r2}}{w_2}\right) \quad (28)$$

2.2.3 Thermodynamic Properties Calculation

The aim of this process is to calculate the overall efficiency and pressure ratio of the compressor. By making assumptions (Table 4) and performing calculations for each part, we can conclude the desired calculations. The procedure is the same for both the vaneless and vaned compressors.

Table 4 : Assumptions for inlet conditions

Assumptions			
Inlet Total Pressure	P_{01}	105	<i>kPa</i>
Inlet Total Temperature	T_{01}	293	<i>K</i>
Impeller isentropic efficiency	n_{is}	0.9	

Based on the above values, the total density of the air and total enthalpy at the inlet can be calculated:

$$\rho_{01} = \frac{P_{01}}{R_{air} \cdot T_{01}} \quad (29)$$

$$h_{01} = c_p \cdot T_{01} \quad (30)$$

The calculation of the static temperature in the inlet is performed using the formula below and the static pressure using the conservative equation:

$$T_1 = T_{01} - \frac{c_{x1t}^2}{2 \cdot c_p} \quad (31)$$

$$\rho_1 = \frac{\rho_{01}}{\left(1 + \frac{1}{5} \cdot M_{1t}^2\right)^{2,5}} \quad (32)$$

$$P_1 = \rho_1 \cdot R_{air} \cdot T_1 \quad (33)$$

With the use of specific work, the total temperature at the outlet of the impeller was calculated. Further, using the isentropic efficiency of the compressor, the isentropic total temperature at the outlet was calculated and used to evaluate the total pressure.

$$\frac{T_{02}}{T_{01}} = \frac{\Delta W}{c_p \cdot T_{01}} + 1 \quad (34)$$

$$T_{02} = \frac{T_{02}}{T_{01}} \cdot T_{01} \quad (35)$$

$$\frac{T_{02s}}{T_{01}} = n_{is} \cdot \left(\frac{T_{02}}{T_{01}} - 1 \right) + 1 \quad (36)$$

$$\frac{P_{02}}{P_{01}} = \left(\frac{T_{02s}}{T_{01}} \right)^{\left(\frac{\gamma}{\gamma-1} \right)} \quad (37)$$

$$T_2 = T_{02} - \frac{c_2^2}{2 \cdot c_p} \quad (38)$$

$$P_2 = \frac{P_{02}}{\left(\frac{T_{02}}{T_2} \right)^{\gamma \cdot (\gamma-1)}} \quad (39)$$

Using the conservative equation for the outlet:

$$\rho_{02} = \frac{P_{02}}{R_{air} \cdot T_{02}} \quad (40)$$

$$\rho_2 = \frac{P_2}{R \cdot T_2} \quad (41)$$

2.2.4 Calculations of the Vaneless Diffuser

The total speed at the outlet of the diffuser derives from appropriate measurements concerning the radius of the diffuser and the impeller. According to Cumpsty (1989) [14], the minimum value of the ratio r_{2d}/r_2 is 1.1. A great way to decrease the Mach number at the diffuser is to have a higher value for this ratio, increasing the diffusion of the fluid.

$$c_{u2d} = \frac{1}{\frac{r_{2d}}{r_2}} \cdot c_{u2} \quad (42)$$

$$c_{r2d} = \frac{1}{\frac{r_{2d}}{r_2}} \cdot c_{r2} \quad (43)$$

The speed at a radius of r_{2d} is calculated using the incompressible approach of a logarithmic helix.

$$\alpha_{2d} = \cos^{-1} \left(\frac{c_{r2d}}{c_{u2d}} \right) \quad (44)$$

$$c_{2d} = \sqrt{c_{u2d}^2 + c_{r2d}^2} \quad (45)$$

Using the same thermodynamic equations leads to the final values:

$$T_{2d} = T_{02} - \frac{c_{2d}^2}{2 \cdot c_p} \quad (46)$$

$$P_{2d} = \frac{P_{02}}{\left(\frac{T_{02}}{T_{2d}} \right)^{\frac{\gamma-1}{\gamma}}} \quad (47)$$

$$\rho_{2d} = \frac{P_{2d}}{R_{air} \cdot T_{2d}} \quad (48)$$

$$P_{02d} = P_{2d} + \frac{1}{2} \cdot \rho_{2d} \cdot c_{2d}^2 \quad (49)$$

$$q_{2d} = \frac{1}{2} \cdot \rho_{2d} \cdot (c_{2d})^2 \quad (50)$$

Also, the Mach number is crucial to be calculated and make sure that the value is below the critical value of unit.

$$a_{2d} = \sqrt{\gamma \cdot R_{air} \cdot T_{2d}} \quad (51)$$

$$M_{2d} = \frac{c_{2d}}{a_{2d}} \quad (52)$$

The above approach is performed with the assumption of incompressible flow. That's why the results had to be verified also for compressible flow and highlight any differences. This second approach uses the following formula:

$$\frac{r_2 \cdot M_{2r}}{(1 + \frac{1}{5} \cdot M_{2r}^2)^3} = \frac{r_{2d} \cdot M_{2dr}}{(1 + \frac{1}{5} \cdot M_{2dr}^2)^3} \quad (53)$$

This equation was solved by writing a small script in MATLAB. The result found with the second approach differs slightly from the first one (7.8% deviation).

2.2.5 Calculations of the Vaned Diffuser

Firstly, some geometrical characteristics that have a huge effect on the efficiency of the whole compressor should be determined. Choosing the distance between the impeller and the leading edge of the vanes, which, according to Dixon and Hall [10], is about 10 to 20% of the impeller's outer diameter. The number of vanes in the diffuser also constitutes a critical parameter for the efficiency and the surge margin of the compressor. Generally, in vaned diffusers, the stall appears in bigger mass flows in contrast to the vaneless diffusers. So, in order to aim for a large operating range, the diffuser vanes should be up to half the number of the impeller blades. Moreover, the angle of attack of the flow to the diffuser vanes is also concluded. This value is set with respect not only to lower the losses as possible but also to achieve a bigger pressure rise in the flow and also to minimize the detachment of the boundary layers that lead to crucial flow losses. Last but not least, the ratio of L/W is selected, where L corresponds to the length and W to the width of the diffuser. All of these characteristics are summarized in Table 5:

Table 5 : Characteristics of the Vaned Diffuser

Geometrical Characteristics of the Vaned Diffuser			
Impeller and vanes distance	s	0.0126	<i>m</i>
Number of vanes	<i>Vanes</i>	16	
Length to Width ratio	L/W	3	

The space between the outlet of the impeller and the leading edge of the diffuser vanes is studied like a vaneless diffuser. So, it is clear now that the vaned diffuser consists of a vaneless part and a vaned one, and each must be studied separately. The vaneless part was studied based on the previous formulas, and the calculated values are used for the vaned part.

The static pressure and the velocity of the flow at the outlet of the vaned diffuser are found through the equations:

$$P_3 = P_{2d} + c_p \cdot q_{2d} \quad (54)$$

$$q_{2d} = \frac{1}{2} \cdot \rho_{2d} \cdot (c_{2d})^2 \quad (55)$$

$$c_3 = c_{2d} \cdot (1 - c_{p,id})^{0,5} \quad (56)$$

2.2.6 Calculations at the Volute

The volute, as a diffuser, neither produces nor consumes work, so the total temperature must remain constant ($T_{03} = T_{02d}$). The following formula specifies the density of the flow:

$$\rho_3 = \frac{P_3}{R_{air} \cdot T_3} \quad (57)$$

Where:

$$T_3 = T_{03} - \frac{c_{2d}^2}{2 \cdot c_p} \quad (58)$$

According to Watson, the total losses in the volute are considered to be about half of the dynamic pressure of the diffuser.

$$P_{03} = P_3 + \frac{1}{2} \cdot \frac{1}{2} \cdot \rho_3 \cdot c_3^2 \quad (59)$$

2.3 Final Calculations

After the previous computations, it is time to find the efficiency and the pressure ratio for both versions of the compressor.

$$P_r = \frac{P_{03}}{P_{01}} \quad (60)$$

For the efficiency, the total losses should be taken into consideration. These losses take place in the impeller, the diffuser, and the volute. The losses at each stage are:

$$H_{imp} = \frac{0,1 \cdot U_2 \cdot c_{\theta 2}}{g} \quad (61)$$

$$H_{dif} = (1 - n_d) \cdot \frac{(c_2^2 - c_{2d}^2)}{2 \cdot g} \quad (62)$$

$$H_{imp} = \frac{1}{2} \cdot \frac{c_3^2}{2 \cdot g} \quad (63)$$

The total efficiency is:

$$n_c = \frac{\frac{\Delta W}{g} - L1 - L2 - L3}{\frac{\Delta W}{g}} \quad (64)$$

2.4 Results of the Preliminary Design

After the completion of the procedure, the calculated velocities at the impellers' inlet and outlet are represented in Table 6 and Table 7, respectively.

Table 6 : Calculated Velocities at the Inlet

Velocities at the Inlet					
		Tip	Mean	Hub	Units
Blade Velocity	u_1	140.4	95.7	51.4	<i>m/s</i>
Absolute Velocity	c_{x1}	54.6	54.9	55.1	<i>m/s</i>
Relative Velocity	w_1	150.6	110.3	75.3	<i>m/s</i>
Relative Mach Number	$M_{1,rel}$	0.43	0.32	0.22	-

The values of the Mach number are satisfactory, as they ensure that there is no choking phenomenon. Also, the velocities decrease from tip to hub, as the mean radius of the flow decreases.

Table 7 : Calculated Velocities at the Impeller Outlet

Velocities at the Impeller Outlet			
Slip factor	σ	0.88	<i>m/s</i>
Blade velocity	u_2	272.4	<i>m/s</i>
Absolute Velocity	c_2	244.9	<i>m/s</i>
Tangential velocity	$c_{\theta 2}$	238.7	<i>m/s</i>
Radial Velocity	c_{r2}	54.9	<i>m/s</i>
Relative Velocity	w_2	64.4	<i>m/s</i>
Absolute Mach Number	M_2	0.67	-
Relative Mach Number	$M_{2,rel}$	0.56	-

Below are Tables 8 and 9 which contain the results at the outlet of the vaneless and the vaned diffusers respectively. Table 10 compares some of their characteristics and their % difference.

Table 8 : Calculated Velocities at the Vaneless Diffuser Outlet

Results at the Vaneless Diffuser Outlet			
Radius Ratio	$\frac{r_{2d}}{r_2}$	1.64	-
Tangential Velocity	$c_{\theta 2d}$	144.6	<i>m/s</i>
Radial Velocity	$c_{r 2d}$	33.3	<i>m/s</i>
Absolute Velocity	c_{2d}	148.6	<i>m/s</i>
Angle of flow	α_{2d}	77	<i>deg</i>
Mach Number	M_{2d}	0.39	-

Table 9 : Calculated Velocities at the Vaned Diffuser Outlet

Results at the Vaned Diffuser Outlet			
Radius Ratio	$\frac{r_{2d}}{r_2}$	1.20	-
Static Pressure	P_3	226824	<i>Pa</i>
Absolute Velocity	c_3	91.3	<i>m/s</i>
Mach Number	M_{2d}	0.2	-

Table 10 : Comparison between the Vaneless and the Vaned Diffuser

Comparison between the Vaneless and Vaned Diffuser					
		Vaneless	Vaned	Units	Difference %
Diffuser Diameter	D_{2d}	0.2	0.164	<i>m</i>	18
Static Pressure	P_{2d}	1.77	2.26	<i>bar</i>	27.6
Absolute Velocity	c_{2d}	148.6	91.3	<i>m/sec</i>	38.57
Mach Number	M_{2d}	0.4	0.2	-	48.7

The vaned diffuser demands a significantly smaller diameter than the vaneless one. There is an 18 % reduction in diameter, even with greater diffusion of the flow. The vaned diffuser, even though it is shorter in length, causes a higher drop in the speed of the flow. That is why there is a change in the Mach number from the value of 0,39 to the value of 0,2. The aim is to get a smaller Mach number in order to make the flow more controllable.

Table 11 below, provides the calculation of some thermodynamic characteristics in the compressor concerning the impeller and diffuser parts. The results concerning the volute are depicted in Table 12.

Table 11 :Thermodynamic Calculations in the compressor

Results at the Impeller & Diffuser					
	Impeller Inlet	Impeller Outlet	Vaneless Diffuser Outlet	Vaned Diffuser Outlet	Units
Static Pressure	103148	145956	177511	226824	<i>Pa</i>
Static Temperature	291.6	327.8	346.7	353.5	<i>K</i>
Static Density	1.22	1.49	1.72	2.16	<i>kg/m³</i>
Static Enthalpy	293043	329469	338634	355297	<i>j/kg</i>
Total Pressure	105000	197985	196540	182583	<i>Pa</i>
Total Temperature	293	357.7	357.7	357.7	<i>K</i>
Total Density	1.23	1.86	1.86	2.22	<i>kg/m³</i>
Total Enthalpy	294465	359458	359458	359458	<i>j/kg</i>

Table 12 : Results in the Volute

Results at the Volute			
	Vaneless Diffuser	Vaned Diffuser	Units
Total Pressure	187026	231323	<i>Pa</i>

According to tables 11 and 12 above, the volute is a part of the compressor that not only guides the flow but also produces diffusion for it. As a result, it contributes to higher static pressure recovery and pressure ratio. Below, in Table 13, are presented the results of the pressure ratio and total efficiency concerning the volute of the compressor of the vaneless and the vaned diffuser.

Table 13 : Presentation of Results

Results			
	Volute with the Vaneless Diffuser	Volute with the Vaned Diffuser	Units
Pressure Ratio	1.78	2.2	<i>kg/m³</i>
Total Efficiency	0.82	0.8	<i>kg/m³</i>

From Tables 12 and 13, one can conclude that the compressor with the vaned diffuser contributes to a higher pressure ratio. It is expected to be so due to the greater diffusion of the flow through the vanes. The difference between these two ratios is significant, and so gives us good reason to go on with the research. As far as the efficiency is concerned, it is directly connected with the flow losses, which depend on the geometrical characteristics of all parts of the compressor. Therefore, detailed research must be performed using Computational Fluid Dynamics Simulation in order to optimize the characteristics and validate those found in the preliminary design.

2.5 Velocity Triangle

As it is mentioned, due to the backward leaned blades of the impeller, the flow angle and the flow conditions are constantly changing across the blade. For this reason, the velocity triangle is designed in 3 different positions (tip, mean, and hub) at the inlet and outlet.

The velocity triangle is automatically calculated and plotted using an app in MATLAB's App Designer. The user only has to insert all the necessary inputs shown in the slides below. In this way, the user can make any geometrical change in the impeller and see the results. The app is presented in Figure 17 below.

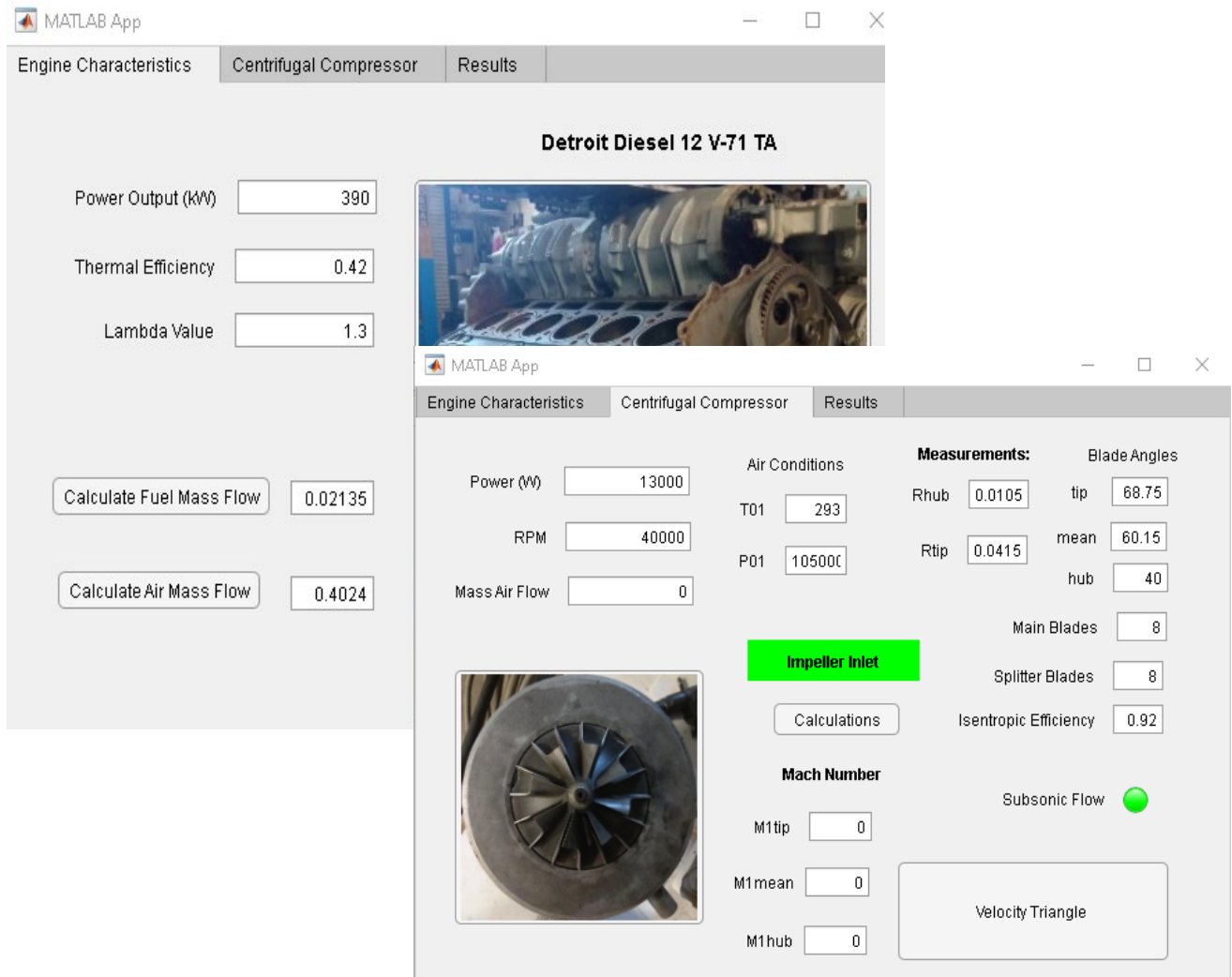


Figure 17 : Slides 1 and 2 of the App

The velocity triangles at every position are displayed below in Figures 18, 19, 20 and 21.

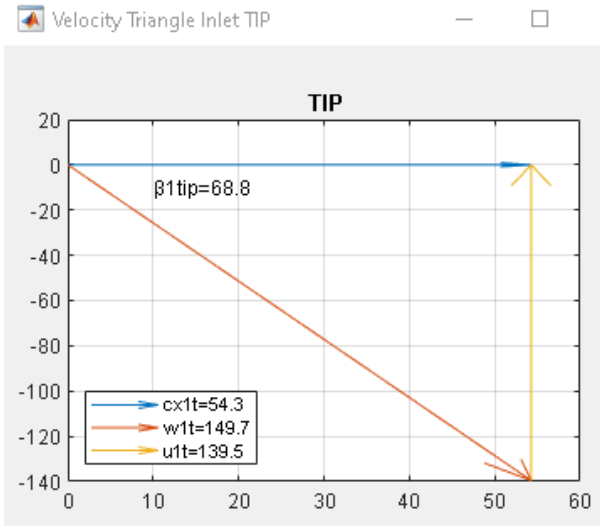


Figure 18 : Velocity Triangle at Tip Inlet

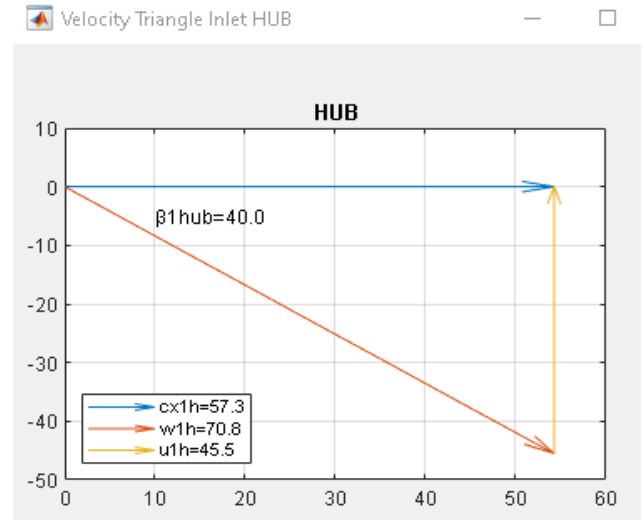


Figure 19 : Velocity Triangle at Hub Inlet

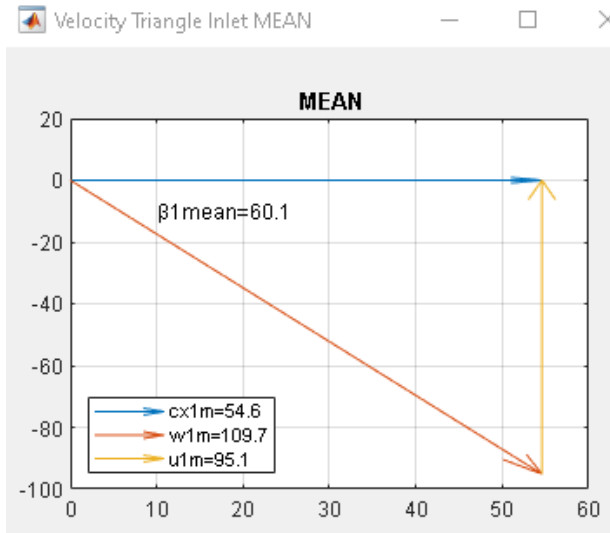


Figure 20 : Velocity Triangle at Outlet

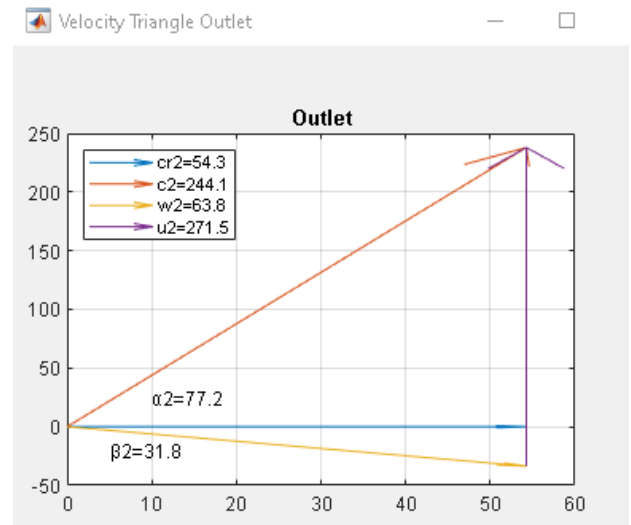


Figure 21 : Velocity Triangle at Outlet

3. Geometry and Mesh Generation

Following completion of the preliminary design, the study will address three-dimensional fluid-dynamics phenomena inside the compressor. The first step in the analysis and set up of the model is mesh generation. The mesh is a representation of a larger geometric domain made up of smaller discrete cells. It is used to compute solutions of partial differential equations, render computer graphics, and analyze geographical and cartographic data. A mesh partitions space into elements over which the equations can be solved, which then approximates the solution over a greater domain.

For internal flows, as in this case, it is necessary to create a volume mesh and the elements that completely fill the volume of the compressor. The size and quality of the mesh have a huge impact on the accuracy of the results and the convergence time of the simulation. That's why they must be deeply studied and carefully applied.

This chapter presents the creation of the geometries and the mesh for every part of the compressor. Using the program "Bladegen", the design of the geometries of the impeller and the radial vaned diffuser is achieved [15]. Additionally, "Turbogrid" defines the mesh size and quality for the diffusers and impellers (the vaneless and the vaned). The size of the mesh was decided after mesh dependency research. For the volute, the geometry was created in "Solidworks" and the generation of its mesh was done in "Ansa". All of the above will be presented further in this chapter.

3.1 Geometries Creation

As already mentioned, the reconstruction of the impeller and the radial diffuser geometry is made through Bladegen. The geometries are easy enough to create. The user has only to set the appropriate parameters in order to declare the geometries.

3.1.1 Geometry of the Impeller

On the first slide, the type of turbomachinery and the basic geometrical characteristics must be declared. Figures 22 and 23 show the setting of the number of the main blades of the impeller, the thickness of the blades, and the wrap angle between the leading and trailing edge of the blade.

The angle θ was set equal to zero and then the angles at the leading edge of the blade in each one of the three tree sections (hub, mean, and hub) were determined. All these values, as mentioned in Chapter 2, were measured in the Laboratory of Thermodynamics and Thermal Engines, with the available equipment. Figure 24 and Figure 25 display the final geometry of the impeller.

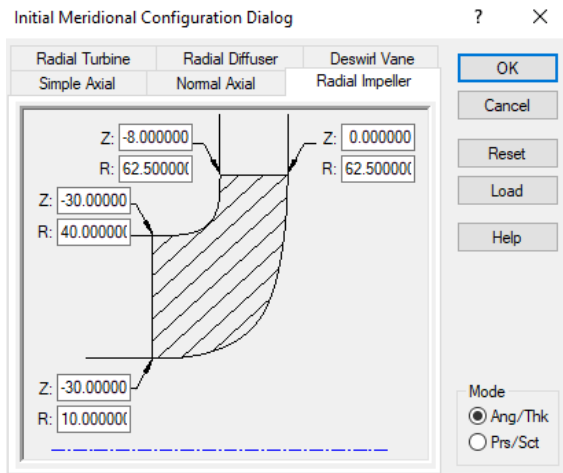


Figure 22 : Blade Dimensions

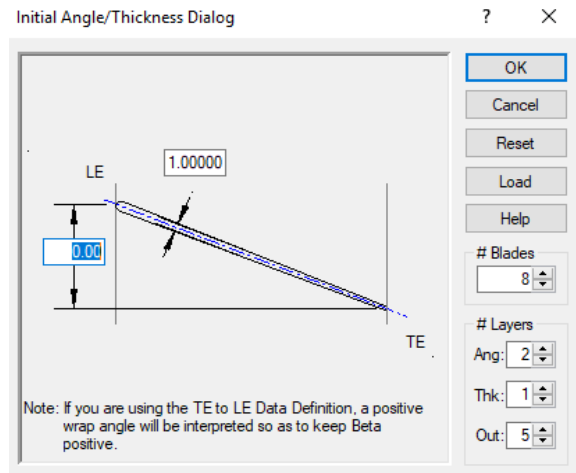


Figure 23 : Wrap angle and thickness

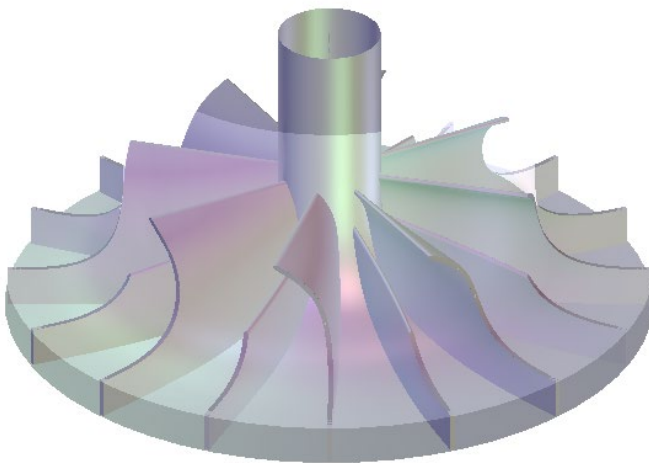


Figure 24 : Final Impeller Geometry

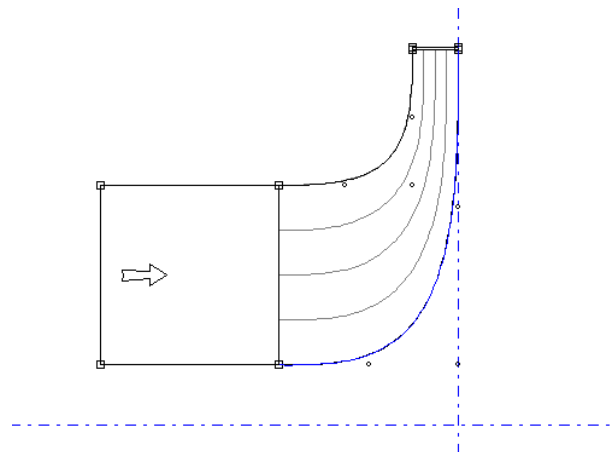


Figure 25 : Cross Section of the Impeller

3.1.2 Geometry of the Vaneless Diffuser

The Bladegen file containing the impeller for the Vaneless Diffuser is used. The impeller is the same in both compressors. The next step is the expansion of the diffuser part, reaching the measured value of 100 mm, which is the radius of the diffuser (Vert). The height of the diffuser is 7.7 mm based on the dimensions of the machine. There must be a separation of the rotating part of the impeller from that of the stationary diffuser using suitable boundary conditions, which will be explained in the next chapter. The vaneless diffuser cross section and the system of the impeller and the vaneless diffuser can be seen in Figure 26 and Figure 27 respectively.

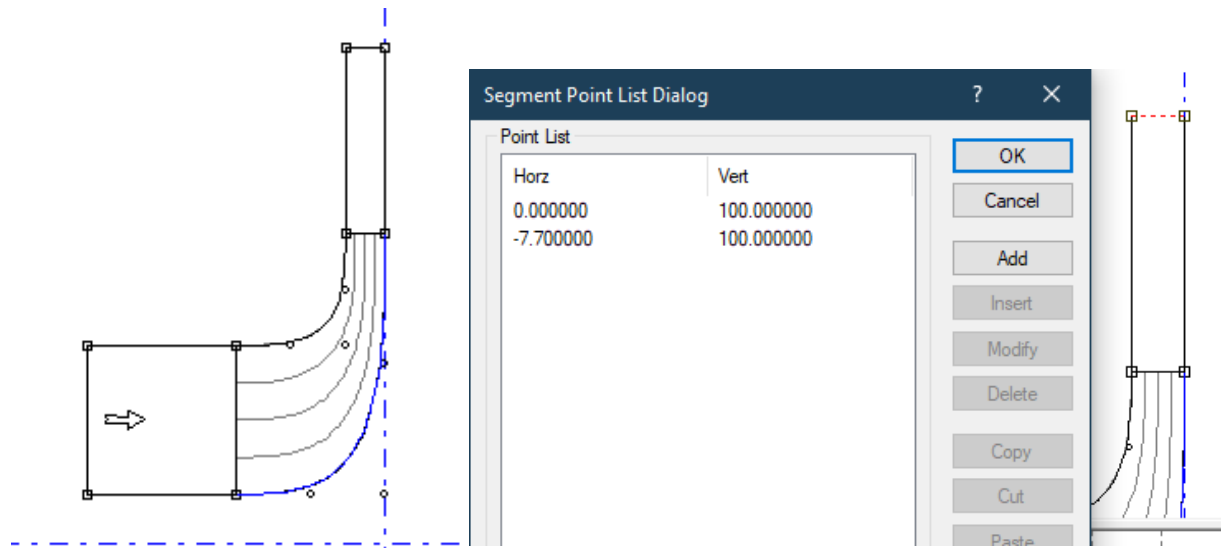


Figure 26 : Cross Section of the Impeller and Vaneless Diffuser

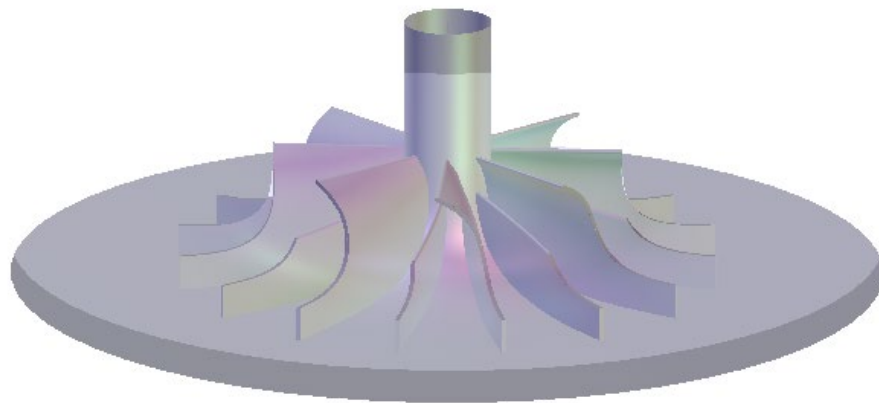


Figure 27 : Final Impeller and Vanless Diffuser Geometry

3.1.3 Geometry of the Vaned Diffuser

As far as the vaned diffuser goes, a new part is created, and the corresponding values and options are also set. The values displayed are calculated properly in order to achieve the optimum performance of the compressor.

The general geometrical characteristics, like the diffusers inner and outer diameter are inserted in Bladegen as shown in Figure 28.

The number of the diffuser vanes and their length were optimized through the simulation by analyzing their effect on thermodynamic properties. The changes made and their results will be detailed and presented in Chapter 5. The number of the diffuser vanes displayed in Figure 29 is 24. Figure 30 shows the cross section of the vaned diffuser.

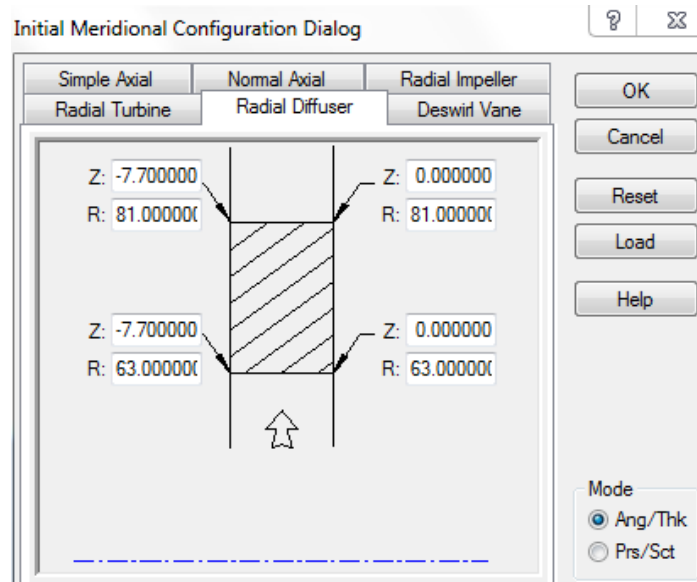


Figure 28 : Radial Diffuser Dimensions

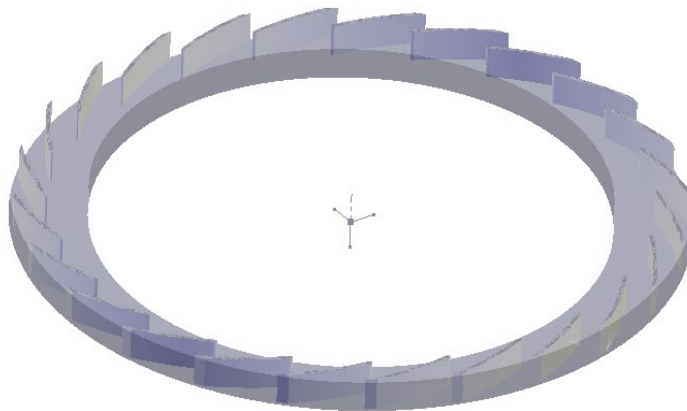


Figure 29 : Final Vaned Diffuser Geometry

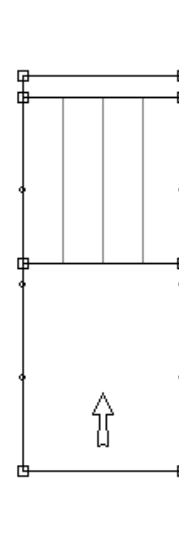


Figure 30 : Cross Section of the Final Diffuser

3.1.4 Geometry of the Volute

As mentioned, the volute was designed using Solidworks. It was necessary to create two different geometries, one for the vaneless diffuser and another for the vaned one, as they have different outer diameters.

The process began by measuring some geometrical characteristics of the volute in the Laboratory of Thermodynamics and Heat Engines (the volute of the vaneless centrifugal compressor). However, it was not easy to extract much information, except the diameter of the

outlet, the diameter of the inlet of the diffuser, the length of the diffuser, and the inlet of the volute. The final design is represented in Figure 31.

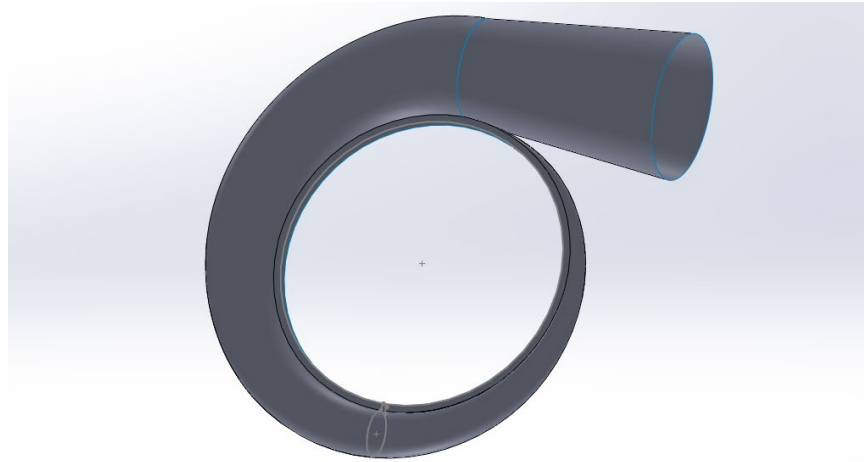


Figure 31 : Volute in Solidworks

With these measurements, the geometry is created using Solidworks, and since it is not enough to go on, some assumptions were made concerning the diameter of the curved funnel at certain points. The casing was created via the command "Surface Loft". To use it, you have to define the diameter of this casing at some points and use this command to create a volume based on the given geometry. Eight points were chosen, and eight different shapes were created, with increasing diameters, as shown in Figure 33.

Figure 32 shows the geometry of the volutes' exit diffuser for the compressor with the vaneless diffuser. Although changes were made to this portion of the volute, no detailed parametrical analysis was done, and this is a topic that requires additional research.

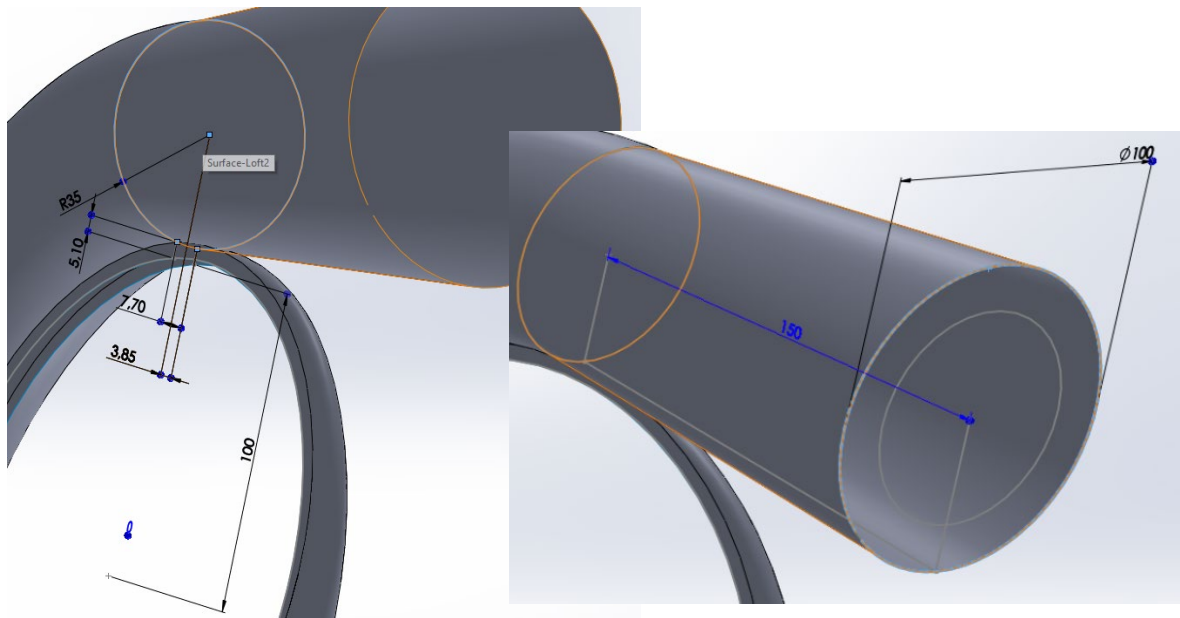


Figure 32 : Geometrical Characteristics of Volutes' exit Diffuser from Vaneless Centrifugal Compressor in Solidworks

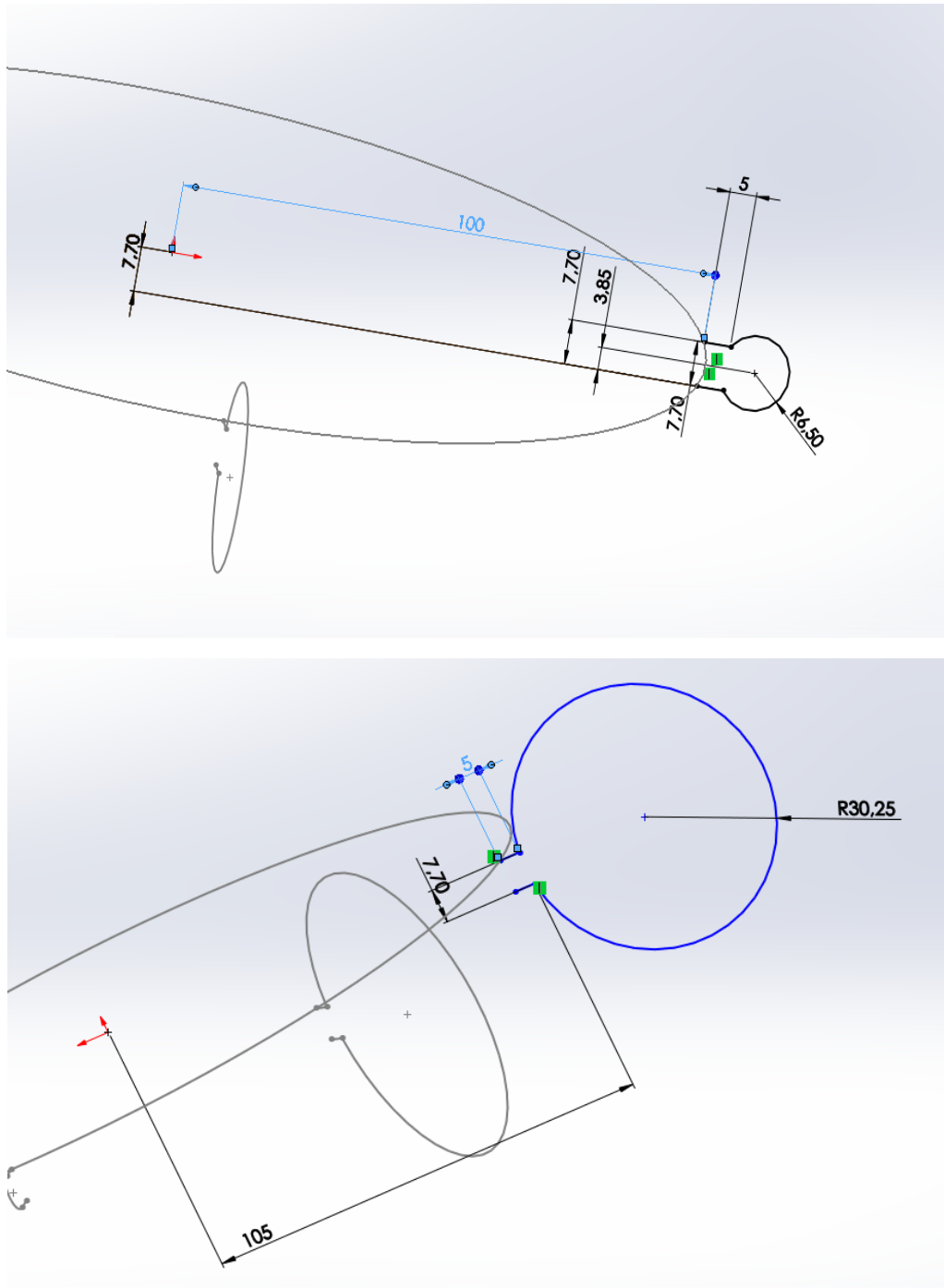


Figure 33 : Geometrical Characteristics of the Volute Casing from Vaneless Centrifugal Compressor in Solidworks

Regarding the Vaned Diffuser Compressor, which is studied in this thesis, some assumptions about its geometry took place, altering some geometry values from the previous volute in order to adjust the shape to the smaller diffuser. In Figure 34 one can see the volutes' exit diffuser geometry.

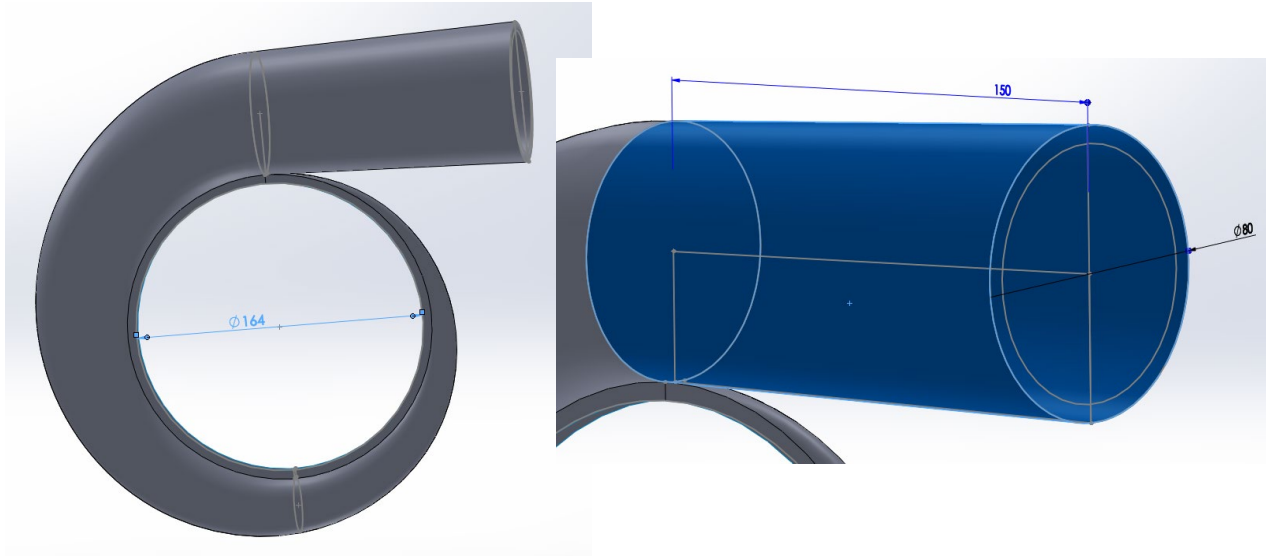


Figure 34 : Geometrical Characteristics of the Volute's exit Diffuser from Vaned Centrifugal Compressor in Solidworks

3.2 Mesh in Turbogrid

The interface of Turbogrid is represented in Figure 35 and it consists of some topics, all of which must be carefully given certain parameters and settings.



Figure 35 : Graphic Interface of Turbogrid

The transfer of the geometry of the impeller and the diffusers to Turbogrid is very easy to do. All the data is automatically transferred and refreshed with just the connection as shown in Figure 36.

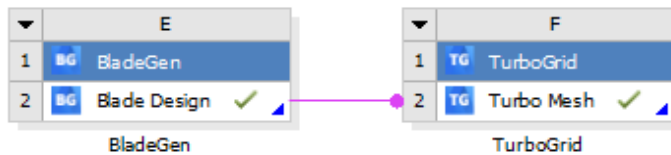


Figure 36 : Geometry input in Turbogrid

In the following photo, Figure 37, the machine type is defined, as well as the units of length.

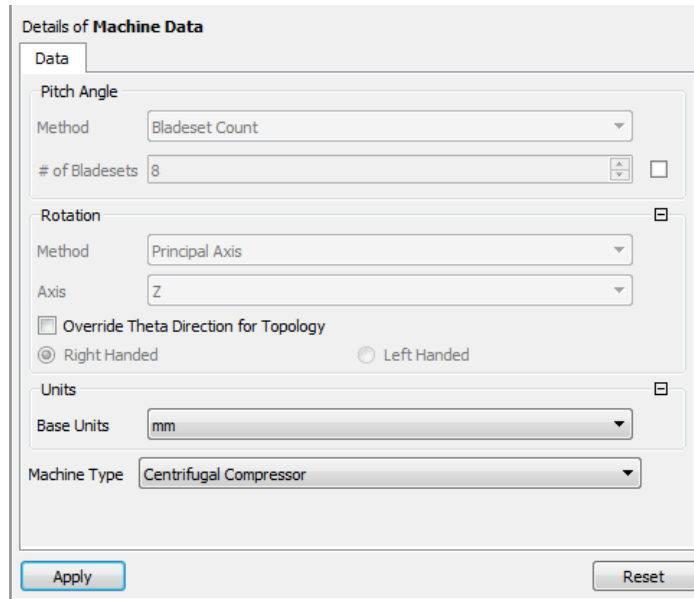


Figure 37 : Machine Data definition

3.2.1. Impeller Mesh

The way that it depicts all the surfaces of the blades is simple. The process is achieved by using the curves of the blades produced by Bladegen and scanning all the curves at the same time. It should be noted that the approach only concentrates on a pair of blades (one main and one splitter blade) and the matching portion of the diffuser before beginning to study the process. Due to the periodicity in these parts of the compressor, computer needs are much lower, and computational time is also lower.

Figure 38 below shows the clearance between the shroud and the tip blade, which is set to 0.2 mm. As Zahed and Bayomi [16] mention, this value needs to be as low as possible in order to avoid flow detachment, ensuring that these faces will never come into contact.

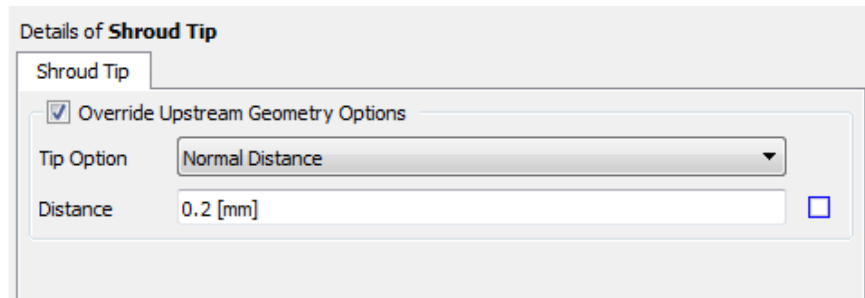


Figure 38 : Gap between the blade and the shroud

The creation of the mesh continues with the “Topology Set” and the definition of the inlet and outlet for every part as shown in Figure 39. In this case, the outlet of the impeller is used as the

inlet for the diffuser. For this reason, the definition must be done carefully. The best way to define these areas is to use the option “parametric”, which declares the distance from the inlet and outlet areas parametrically, according to the leading and trailing edge of the blades, respectively. The zero value is unacceptable, as an interaction between the inlet or outlet areas and the blade is possible.

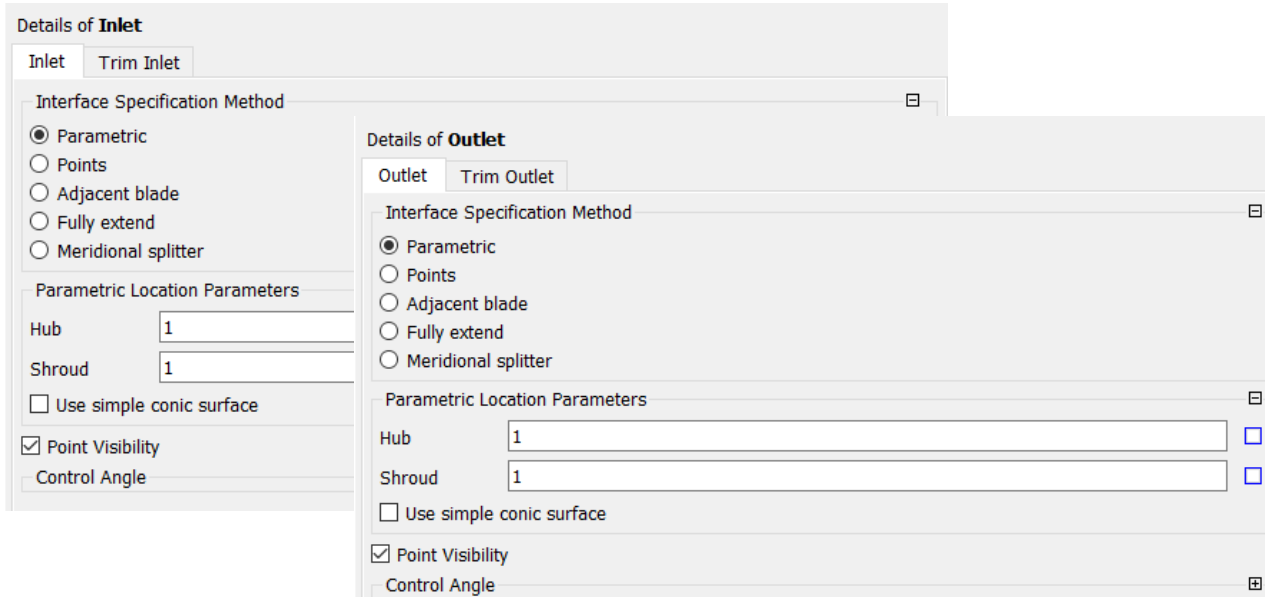


Figure 39 : Inlet and Outlet Definition

The most vital part is the topology of the mesh, where the method of Automatic Topology and Meshing is used. The topology set environment is portrayed in Figure 40.

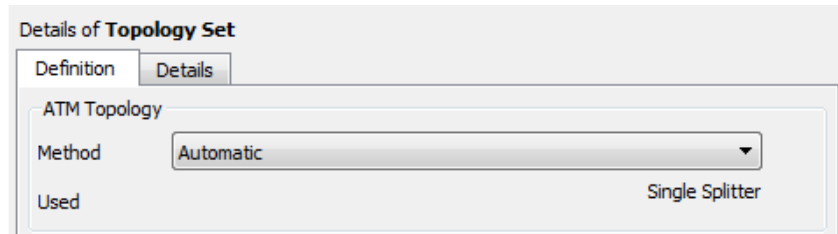


Figure 40 : Topology Definition

This method enables you to control the global mesh size as well as the mesh size at the boundary layer. The Mesh Data inputs are shown in Figure 41. The "Global Size" factor technique, which defines the mesh's overall density as one, is utilized, as shown in the first slide of the Details of Mesh Data. As the value increases, the mesh takes a more desirable shape. The overall mesh size is non-linearly proportional to this factor.

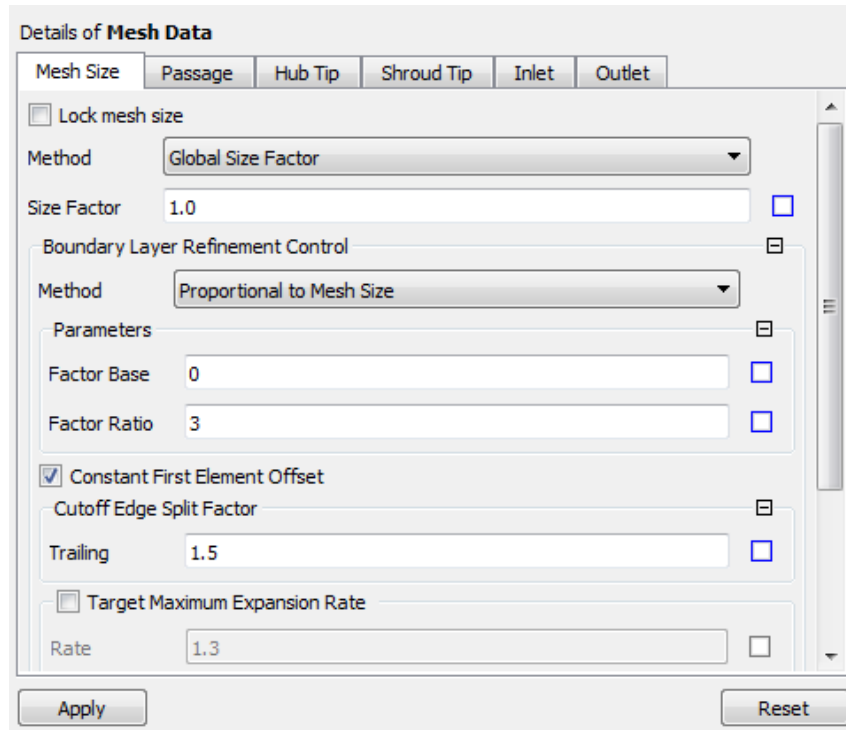


Figure 41 : Mesh parameters

For the mesh at the boundary layer, the proportional to mesh size method is considered. This checks the number of points along with the area of the boundary layer according to “Factor Base” and “Factor Ratio” values, which affect the number of elements [17].

At the trailing edge of the blades, the flow is very complicated. Therefore, using the Cutoff Edge Split Factor, the mesh in both areas changes. A possible boundary layer detachment demands more special control, and it is accomplished by a finer mesh. The “Target Maximum Expansion Rate” should maintain values close to 1.1 in order to have a good quality.

Next comes the setting of the near-wall element specification, as pictured in Figure 42. This term describes the distance between a surface and the first layer of the mesh. The two available methods are the following:

- Absolute: The Absolute method enables you to set the near wall spacing directly on the Passage Hub tip and Shroud tip tabs.
- y^+ : The y^+ method sets a target value for the near wall spacing.

The “Absolute” option is the default in the program.

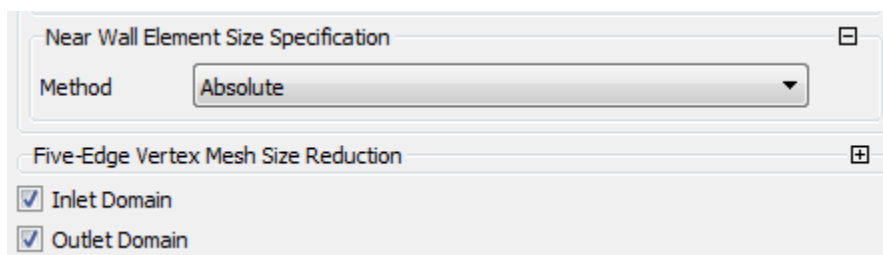


Figure 42 : Near wall method specification

The next slide setting is the method of “Element Count and Size” in the Passage setting in Mesh Data, which checks the number of cells on the blades (Figure 43). Making changes in these values while also observing the quality of the mesh, gives the final ones.

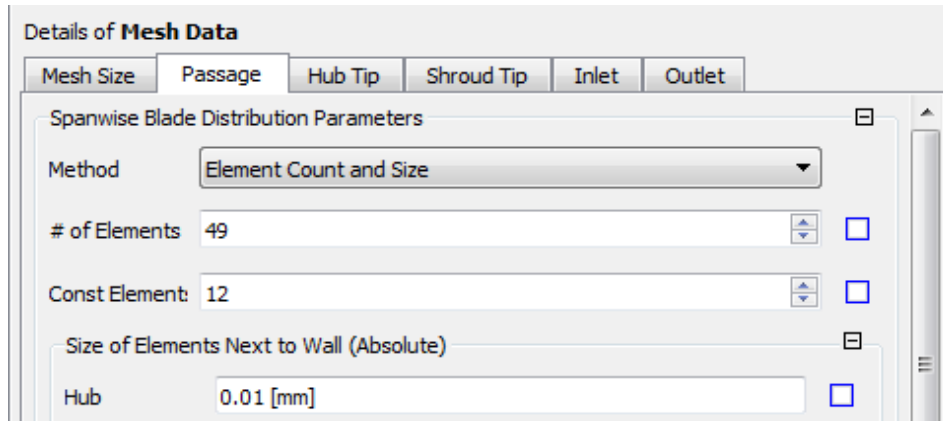


Figure 43 : Blade Mesh Parameters

The mesh created consists of hexahedral elements, which connect with the nearby ones, and they have the same edges and nodes. In this way, the mesh is integrated into all volume mesh. However, it may be difficult to process the mesh. However, by using layers, the user can improve the topology of the mesh across the whole range of the component. The layers are represented in Figure 44.

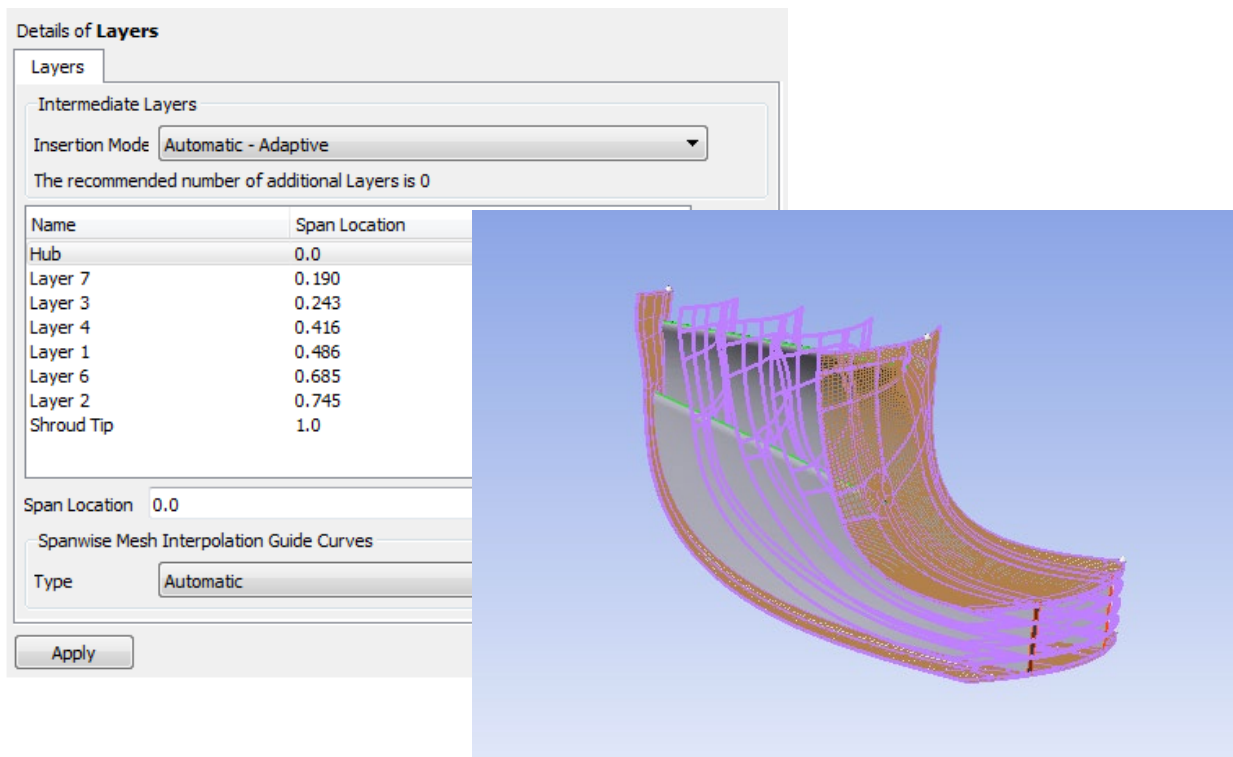


Figure 44 : Layers in the corresponding ranges at the Impeller

Generally, the fluid flow in turbomachinery demands a high-quality hexahedral mesh to simulate the flow path. For the following reasons, the hexahedral mesh is preferred over the tetrahedral one:

- Less cell amount needed to resolve the geometry
- Ensures more accuracy to the solution
- Easier boundary layer resolution

However, the cell quality suffers with increased geometric complexity. In these cases, the hexahedral mesh becomes thin, and a tetrahedral mesh is preferred for some components. In this research, a hybrid mesh is generated, using a hexahedral mesh for the impeller and the diffuser and a tetrahedral mesh for the volute, since it is a more complicated surface. The interface at that point may present non-conformal mesh connectivity and must be checked it out. Figure 45 below illustrates the geometry of the cells.



Figure 45 : Tetrahedron and Hexahedron cells [18]

Of the 3D elements mentioned, that the tetrahedron consists of 4 vertices and 6 edges, while the hexahedron consists of 8 vertices and 12 edges.

Last but not least, there were topical changes in the mesh by hand, especially in critical areas. The solution of the simulation is even more precise since these areas are not only the inlet and outlet of every part but also the areas before and after the vanes of the diffusers since there are expected transitions in the flow.

The mesh produced around the blade of the impeller and the vanes of the diffuser is important to have good quality. The aim is to have a denser mesh on the under-pressure area compared with the overpressure in order to solve with accuracy the boundary layer and capture the possible separation of the flow. The phenomenon of structured grids is also observed in these areas. Here, the volume elements are well ordered, and the grid is identified by regular connectivity.

In figure 46, a structured grid is displayed in contrast to an unstructured one. The advantages of a structured grid over an unstructured one are better convergence and higher resolution. On the

other hand, the unstructured grid is easier to produce and is more commonly used for more complex geometries.

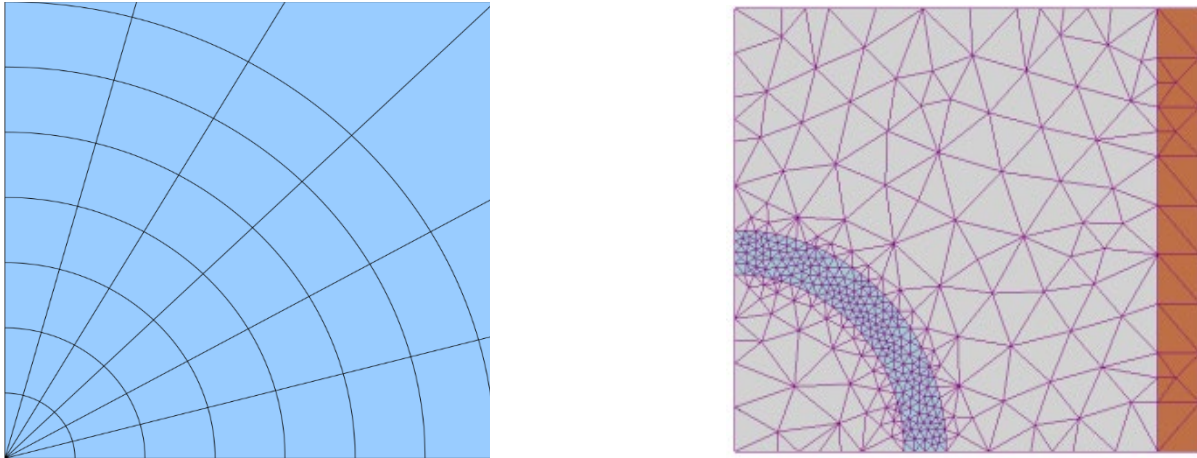


Figure 46 : Structured and Unstructured Grid [19] [20]

The mesh created for the impeller is presented in Figure 47.

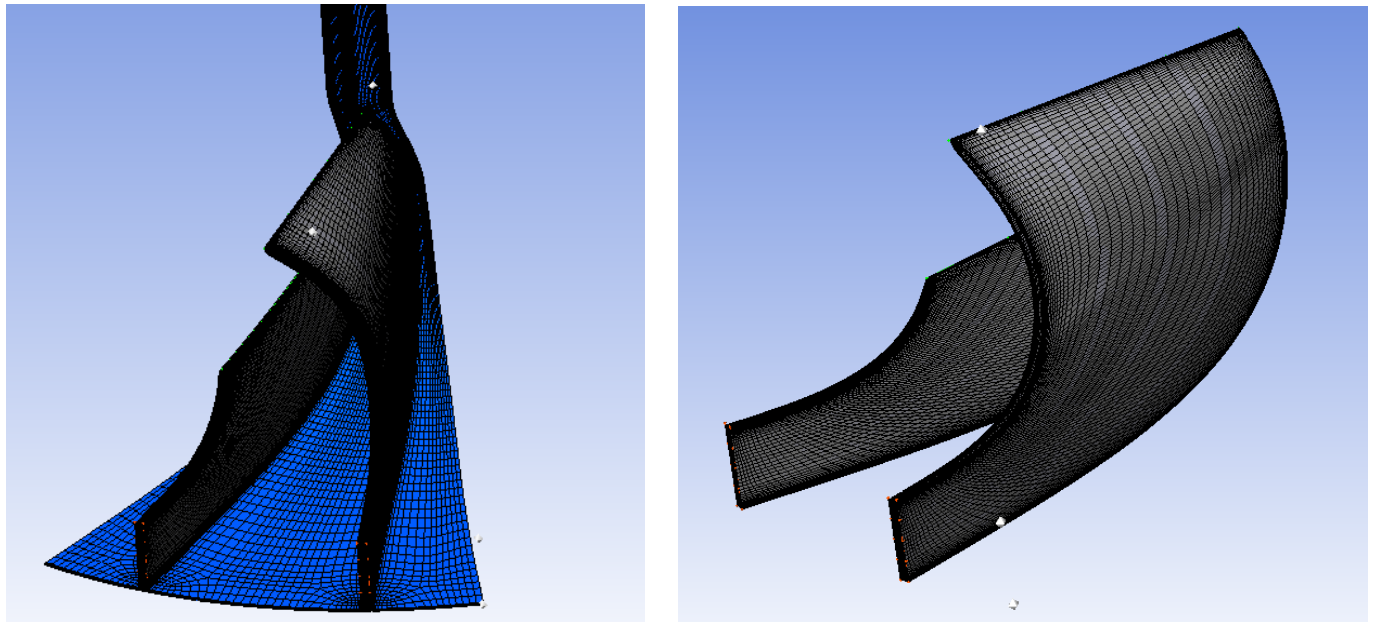


Figure 47 : Mesh generation of the impeller

3.2.2. Diffuser Mesh

The mesh in the diffuser was done in the same way as the impeller, following the same logic. The mesh takes the following shape, as shown in figures 48, 49, and 50.

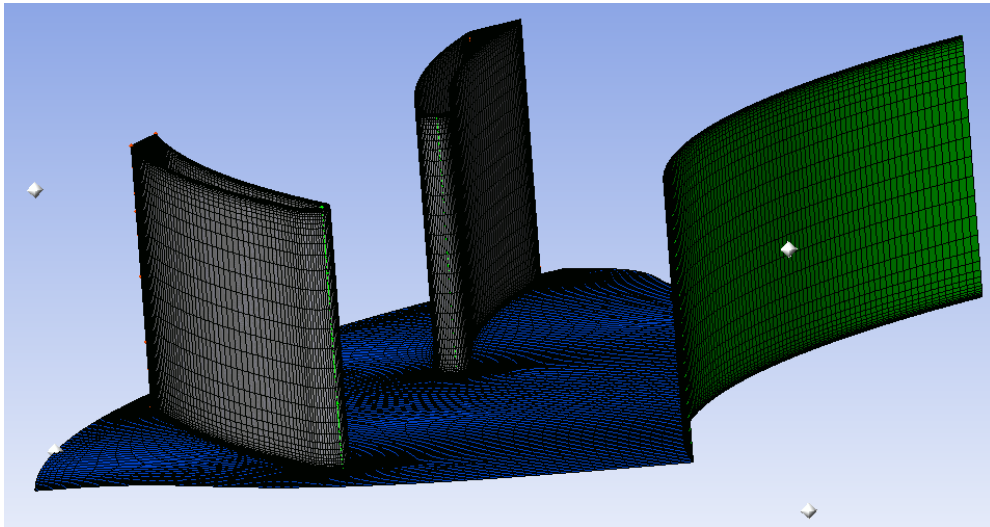


Figure 48 : Mesh of inlet, hub, and vanes of the Diffuser

Details of Layers

Layers

Intermediate Layers

Insertion Mode Automatic - Adaptive

The recommended number of additional Layers is 0

Name	Span Location
Hub	0.0
Layer 3	0.507
Layer 1	0.752
Layer 2	0.917
Layer 4	0.918
Shroud	1.0

Span Location

Spanwise Mesh Interpolation Guide Curves

Type Automatic

Apply

Figure 49 : Layers in the corresponding ranges at the Diffuser

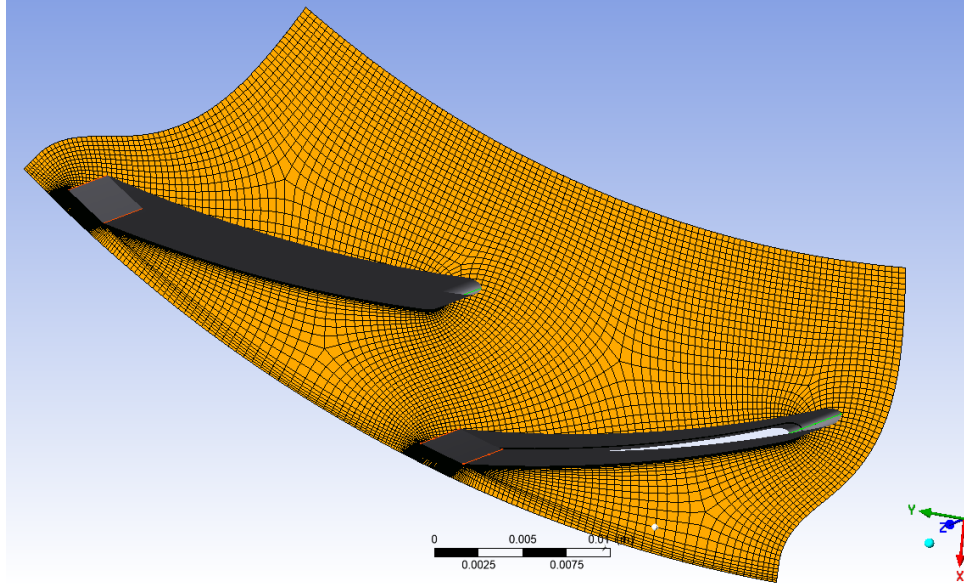


Figure 50 : Mesh at the Diffuser

3.2.3 Mesh in Ansa

The mesh generation of the Volute accomplished using the program of Ansa. The reason for the selection of this program is that the mesh can be produced not only very easily but can also have very good quality. Although the steps of the procedure are quite the same for every geometry, every option is declared with respect to the corresponding geometry.

After the geometry is imported as a *.step* file, starts the geometry cleanup by delaminating the imperfections and the intersections between the surfaces. Then the conditions on every surface are set, as shown in Figure 51 below.

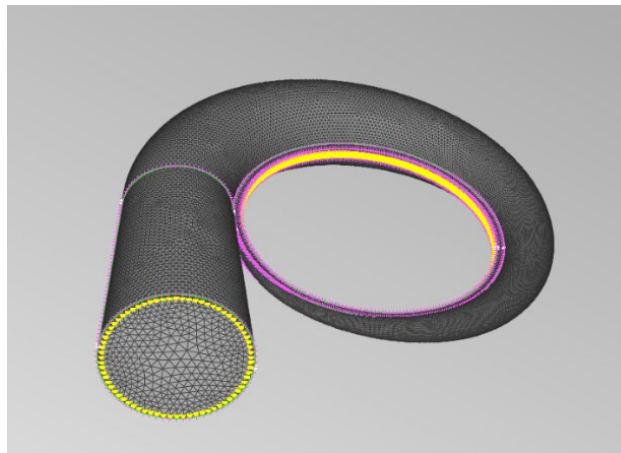


Figure 51 : Volute Mesh Generation

Moving on with the surface mesh on this geometry, the y^+ that is preferred as a target is set at 30, as it can be seen in Figure 52. This value will declare the position of the boundary layer and the total number of them. After the simulations, the other inputs were alternated in order to achieve this target.

Y+ Calculator	
Type of flow	Pipe
Velocity (m/s)	120
Density (kg/m ³)	1.225
Dynamic viscosity (kg/ms)	1.789E-5
Reference length (m)	0.082
Target y ⁺	30.
Reynolds number	6.7e+05
Estimated first cell centre (m)	9.8e-05
Estimated first layer height (m)	2.0e-04
Total boundary layer thickness (m)	2.1e-03
OK	

Figure 52 : y⁺ Calculator

The last part of the mesh generation is the production of the volume mesh. For the volute, it was decided to produce a mesh with tetrahedral cells. The reason is that the resolution in this kind of cells is less time consuming in contrast to hexahedral ones, as the program will use less nodes to solve the corresponding equations. Tetrahedra cells are used in order to improve the quality of the mesh, and the final grid is illustrated in Figure 53.

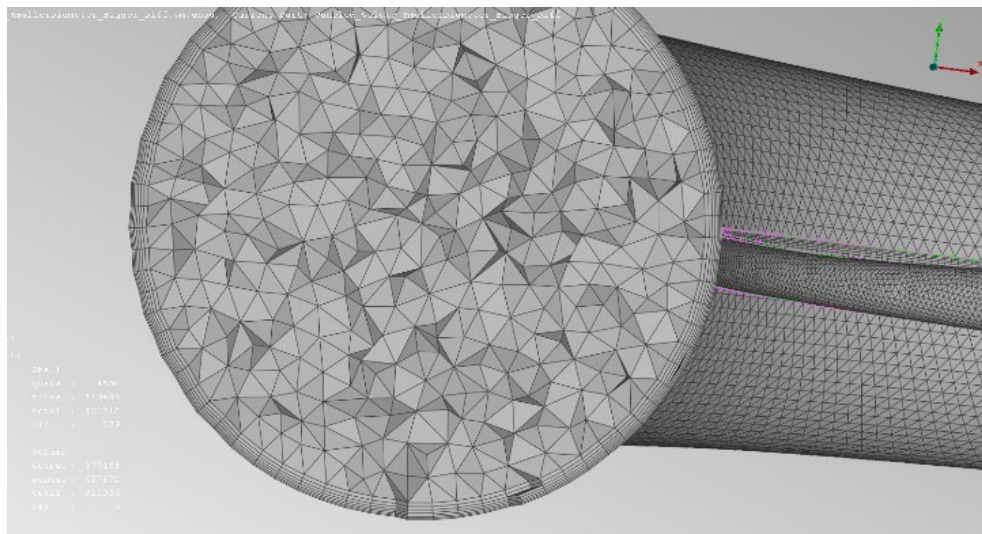


Figure 53 : Volute Volume mesh

As far as the quality of the mesh is concerned, the user must check it at every step, in order to reduce the possibility of an error. Moreover, the user sets standard mesh criteria that warn you if any limit is exceeded after the mesh generation.

Figure 54 presents some criteria that define the CFX for mesh generation. The most important of all of these are the skewness, the aspect ratio, and the warping, which have a huge effect on the quality of the mesh. This method will not be analyzed any further as it is not an object of study for the specific thesis.

Quality Criteria - Presentation Parameters

Name: CFX Standard

Criteria	Calculation	Color	Failed
<input type="checkbox"/> aspect ratio	FLUENT	Yellow	20.
<input type="checkbox"/> skewness	FLUENT	Green	0.92
<input checked="" type="checkbox"/> warping	IDEAS	Cyan	70.
<input type="checkbox"/> squish		Green	0.92
<input checked="" type="checkbox"/> jacobian	ANSA	Blue	0.4
<input checked="" type="checkbox"/> min length		Red	1.E-6
<input type="checkbox"/> max length		Red	0.
<input checked="" type="checkbox"/> min angle tetras	ABAQUS	Orange	15.
<input checked="" type="checkbox"/> max angle tetras	ABAQUS	Orange	165.
<input checked="" type="checkbox"/> min angle pentas	ABAQUS	Orange	15.
<input checked="" type="checkbox"/> max angle pentas	ABAQUS	Orange	165.
<input checked="" type="checkbox"/> min angle hexas	ABAQUS	Orange	15.
<input checked="" type="checkbox"/> max angle hexas	ABAQUS	Orange	165.
<input type="checkbox"/> non orthogonality	FLUENT	Brown	0.08
<input type="checkbox"/> growth ratio	ANSA	Purple	1000.
<input checked="" type="checkbox"/> negative volume	OPENFOAM	Cyan	
<input checked="" type="checkbox"/> left handed		Magenta	
<input type="checkbox"/> min height		Teal	0.
<input type="checkbox"/> h-ratio		Blue	0.15
<input type="checkbox"/> determinant	OPENFOAM	Dark Blue	0.001

Figure 54 : CFX quality criteria Standard

3.3 Mesh Independency Study

In this case, the mesh size is optimized for the vaneless diffuser and the impeller to provide accurate results within the simulation duration. The first tests and simulations concerned the impeller with the vaneless diffuser. The changes in the mesh size and the corresponding results are presented in the below figures. Concerning the results, the magnitude of total pressure and total temperature are compared with those extracted from the preliminary design.

3.3.1 Calculation of Mesh Size of the Vaneless Diffuser

The following graphs (Figure 55 and 56) show how the mesh size of the diffuser and impeller causes fluctuation in temperature, total pressure and the efficiency factor. The time needed for the simulation is also listed. There is interest in finding the golden section between solving time and the degradation of convergence.

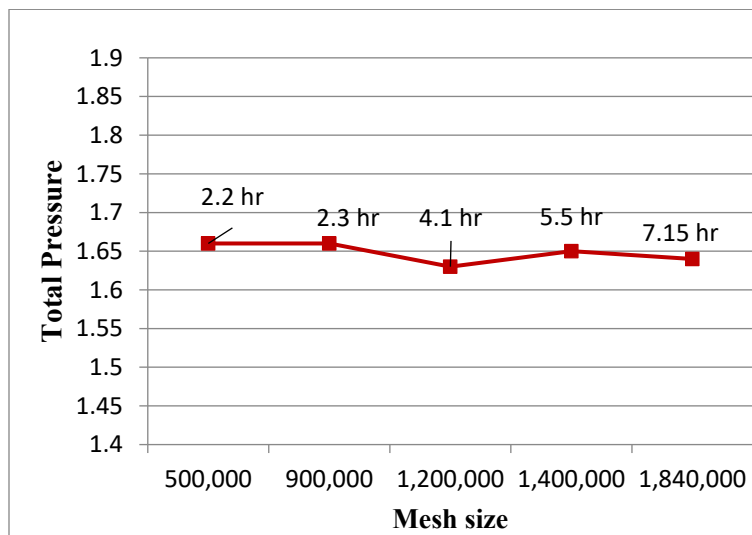


Figure 55 : Total Pressure variation according to Mesh size

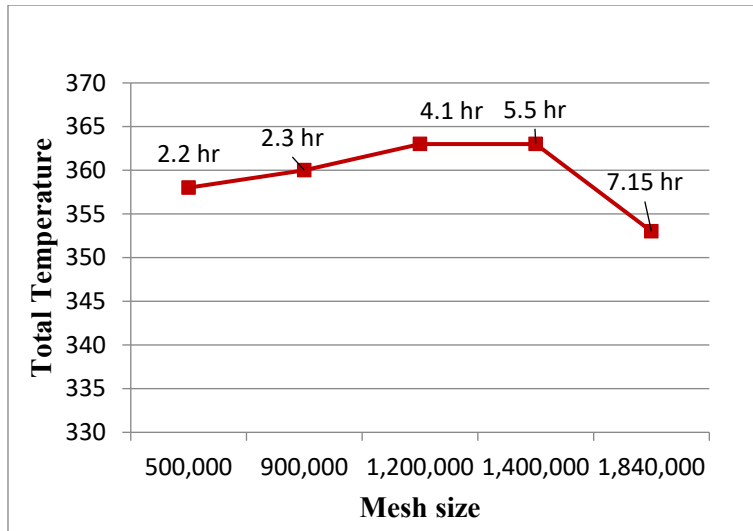


Figure 56 : Total Temperature variation according to Mesh size

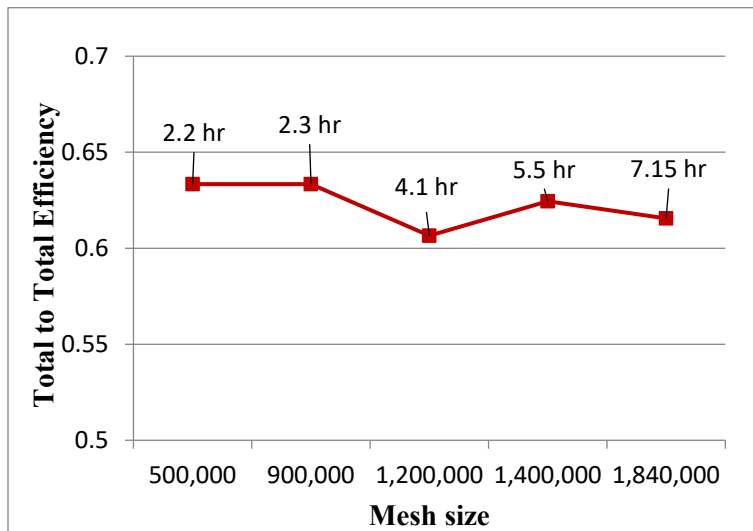


Figure 57 : Efficiency factor variation according to Mesh size

In order to alternate the mesh size, the main change concerned the Global Size Factor, starting from the value of 1.05, and increasing it each time by 0.05, finally reaching the maximum value of 1.3. For critical areas, and especially close to the blades, the factors didn't change since the aim is to keep the analogy of the mesh condensation constant. The number of layers was also kept constant, as was the distance from the hub. The philosophy behind creating the mesh was the same for each case, as described further in sub-section 3.4.

The final mesh size for the impeller with the vaneless diffuser should be 1.000.000 elements. The results are closer to the calculated ones from preliminary design. As far as the efficiency, its fluctuation is small. The y^+ values are below 5 in critical areas and in areas that undergo boundary

layer detachment across the impeller and diffuser parts. The goal was to avoid values from 10 to 30, since within this range the solution is not reliable. The choice to utilize a somewhat bigger mesh size for the impeller with the vaneless diffuser is made because the presence of the vanes necessitates a higher level of detail in the region around them.

3.4 Mesh Generation Criteria

To summarize, the steps for a high-quality mesh in any geometry are:

- Import the geometry of the component
- Decide and maintain a general good grid
- Increase mesh fineness at critical areas
- Focus on boundary layer refinement
- Mesh Dependency study

With the mesh dependency study and after analyzing the results, the process should be repeated.

3.4.1 Final Mesh Generation

In Table 14 below, the final mesh size is calculated and presented for every part of the compressor.

Table 14 : Final Mesh Size

Comparison between the Vaneless and Vaned Diffuser				
	Impeller	Vaneless Diffuser	Vaned Diffuser	Volute
Number of Elements	500.000	500.000	600.000	1.800.000

4. Computational Fluid Dynamics Analysis

The simulation model consists of all the parts of the compressor and aims to represent the physical problem, governed by physics laws and equations. The whole process is performed using the program “CFX-Solver”.

The first step is to import the mesh of each part in a suitable form and define the geometrical relation between them. Then, the solver equations and boundary conditions used in the simulation must be correctly set.

4.1 Modeling

The setup of the simulation is performed in “CFX-Pre”, and it is shown in Figure 58. The graphic interface of the program is presented in the following figure. In order to get more accurate results, the simulation must be set as close to the real conditions as possible. Every setting will be presented in detail further in this chapter.

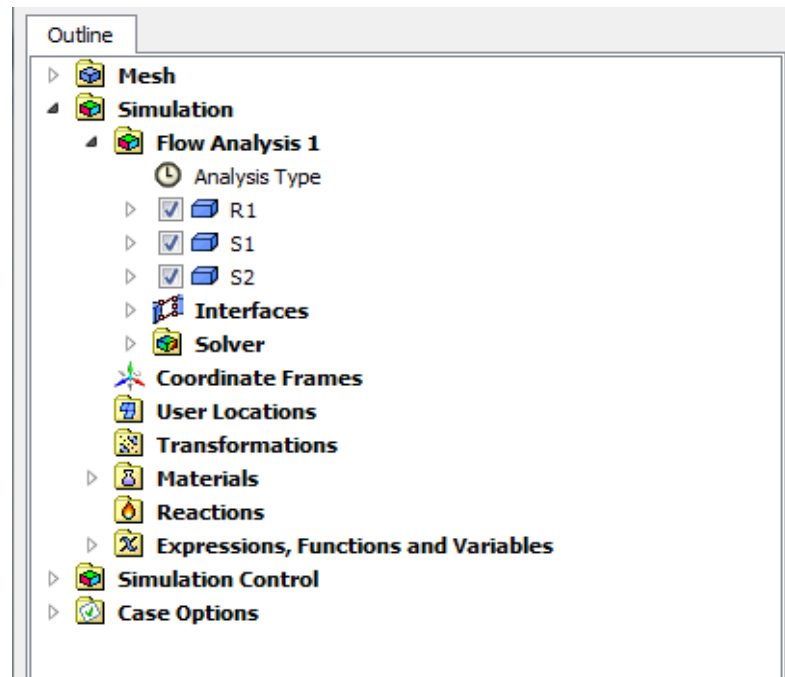


Figure 58 : Interface of CFX

One of the most valuable in “CFX-Pre” tools is “Turbo Mode” and it is portrayed in Figure 59, which makes the simulation setup easier for its users. When using Turbo Mode, the basic parameters are regulated, including the type of turbomachinery and simulation analysis.

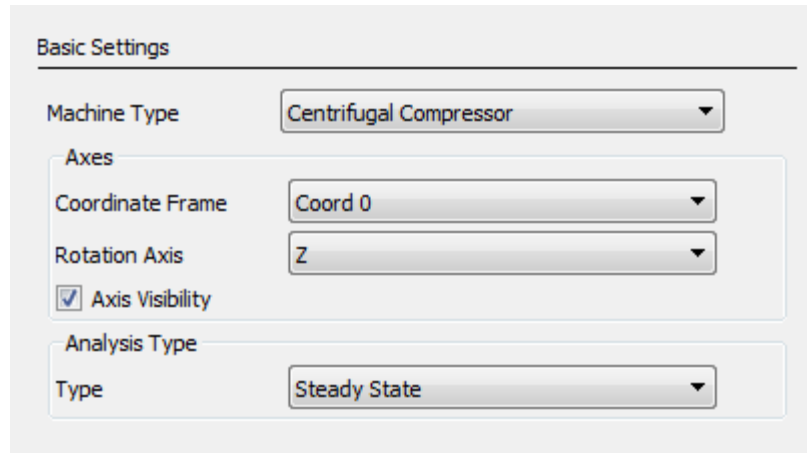


Figure 59 : First slide of Turbo Mode

The next task is to define the components with the desirable volumes and declare whether they are rotating or stationary. If they are rotating, the number of rotations per minute must be set, as must their rotation times. It is important that the last is set correctly to avoid any flow problems. On the other hand, if it isn't a moving part, it must be set as stationary. The rotating component is denoted by R #, while the stationary component is denoted by S #. The order of the components in component definitions has to be the same as the fluid flow inside the compressor (Inlet (S1)→ Impeller (R1)→ Diffuser (S2)→ Outlet (S3)). Lastly, in this slide, the shroud and tip clearance are imported automatically from previous settings from Turbogrid. The component definition is shown in Figure 60 below:

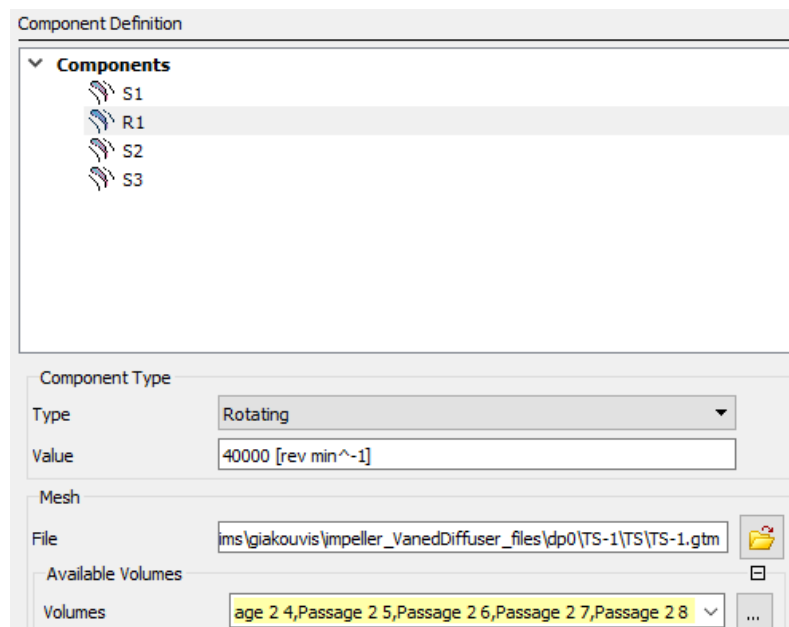


Figure 60 : Component Definition

The following is the physics definition, as shown in Figure 61. Here, the air is set as an ideal gas, with a reference pressure of 0 atm. The most crucial part is to select the suitable turbulence model.

The options are:

- k- ϵ
- k- ω
- SST

Through bibliography [21] and after simulation tests, it is found that the use of the Shear Stress Transport model is more efficient in contrast to the other Eddy Viscosity Models. The SST model is a combination of the other two, and it actually uses the advantages of both, providing accurate computations in a short period of time.

The screenshot shows the 'Physics Definition' dialog box. The 'Fluid' is set to 'Air Ideal Gas'. Under 'Model Data', 'Reference Pressure' is 0 [atm], 'Heat Transfer' is 'Total Energy', and 'Turbulence' is 'Shear Stress Transport'. In the 'Inflow/Outflow Boundary Templates' section, 'P-Total Inlet Mass Flow Outlet' is selected. The 'Inflow' section has 'P-Total' at 105 [kPa], 'T-Total' at 293 [K], and 'Flow Direction' as 'Normal to Boundary'. The 'Outflow' section has 'Mass Flow' as 'Per Component' and 'Mass Flow Rate' as 0.2 [kg s⁻¹]. The 'Interface' section has 'Default Type' as 'Frozen Rotor'. A 'Solver Parameters' checkbox is at the bottom.

Figure 61 : Physics Definition

The best method for defining the boundary conditions of the model should be determined before moving on. The preliminary design calculations were implemented in order to use the total pressure and total temperature for the inlet conditions and mass flow of air for the exit conditions

(inlet conditions are close to environment conditions). This selection is considered the most stable approach for the convergence of the solution [17].

The interfaces created also need to be correctly set (Figure 62 and 63). The mixing model must be selected for all the interfaces. The interfaces primarily declare periodicity or interaction between two distinct components. The periodicity is used in order to run the simulation with just a part of the whole impeller, in order to reduce the time required to be completed. The simulated device has both stationary and rotating parts, making modeling significantly important since it directly affects the accuracy of the solution of the simulation.

The options to define the mixing model are the following:

- None
- Stage Mixing
- Frozen Rotor

Both the “Stage Mixing” and the “Frozen Rotor” models are steady-flow methods [22]. In “Frozen Rotor”, the governing equations are solved for the rotor in a rotating reference frame. The governing equations for the stationary components are solved in an absolute reference frame. Due to the interaction between the rotating and stationary components, the continuity of velocity components and pressure are imposed. Due to the fact that the impeller is at a fixed position during the simulation, the flow field is dependent on the relative position of the impeller and the volute [23]. So, in order to achieve more accurate results, the flow for different relative positions has to be computed.

The “Stage Mixing” model uses absolute and relative reference frames, as in the previous model, but the interaction between the components is characterized by the circumferentially averaged flow quantities. Therefore, the results are independent of the relative position of the impeller and the stationary components. Moreover, it assumes that the losses caused by circumferential mixing are equal to those that arise during a gradual mixing process in the diffuser. Consequently, the flow disturbances that develop inside the impeller blades do not transfer to the downstream of the impeller. Although this assumption is incorrect, the mixing model is mostly used in turbomachinery development.

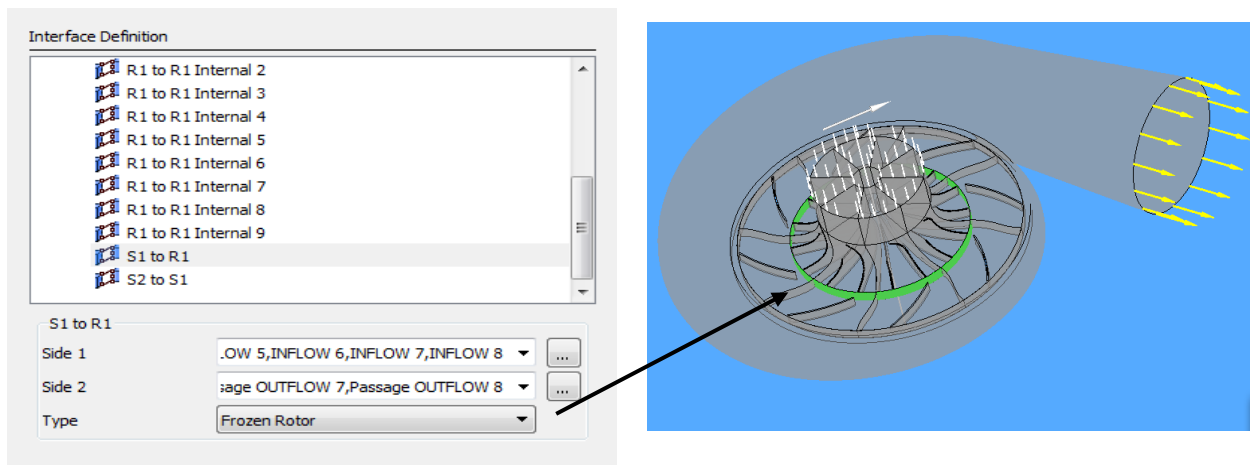


Figure 62 : Frozen Rotor Interface Definition

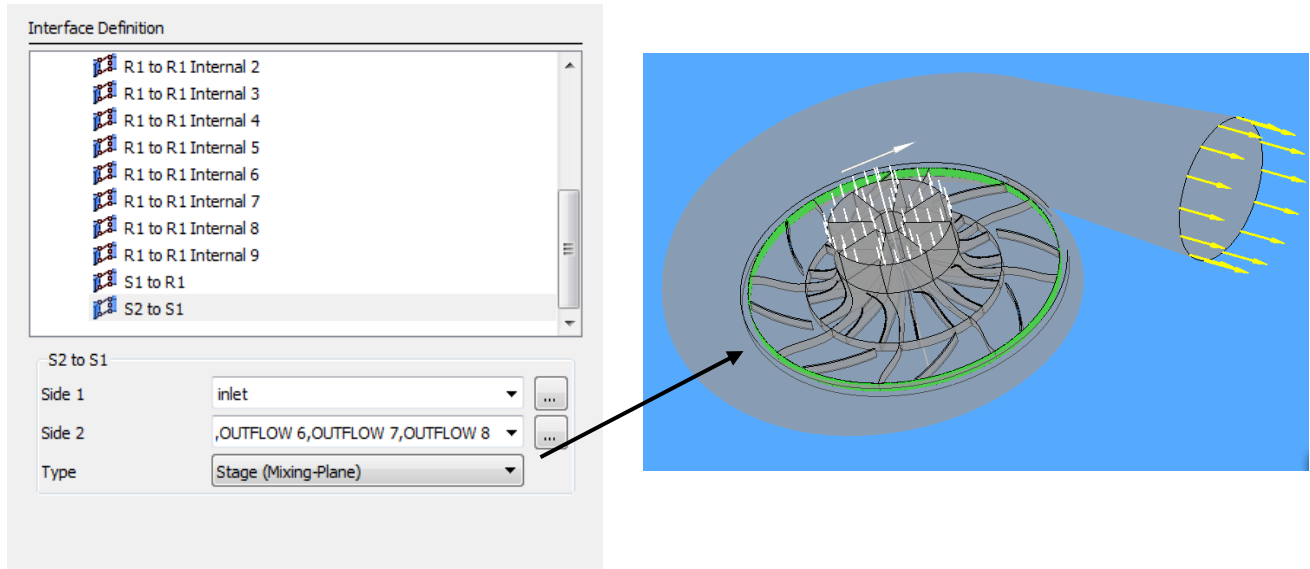


Figure 63 : Mixing Plane Interface Definition

Lastly, another parameter considering the interfaces is defining the gap between the blades of the impeller and the shroud. If it is not set as such, there is a possibility for the simulation to consider it as a solid part, so the user must be careful.

4.2 Boundary Conditions

Figure 64 presents the boundary conditions of the simulation. The boundary conditions accompany the solver equations, using the inlet and outlet conditions, in order to produce the solution for the simulation model.

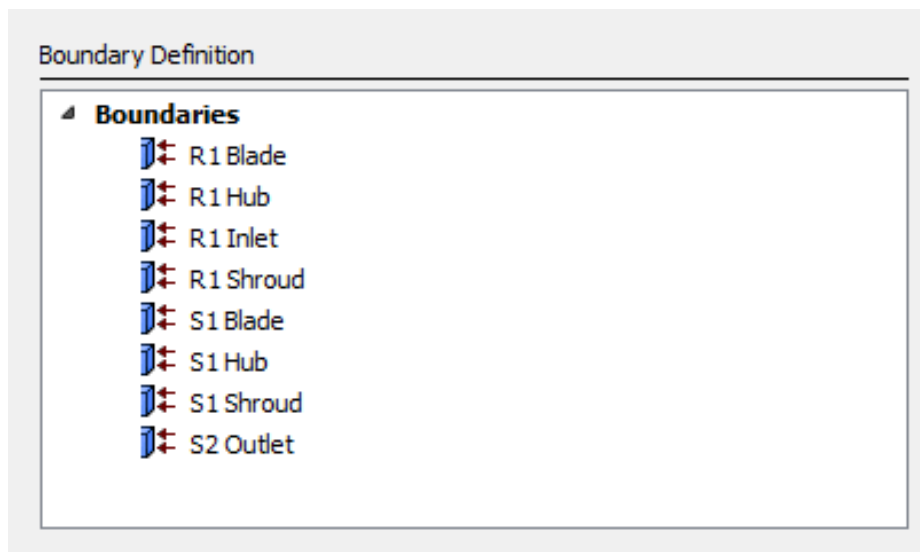


Figure 64 : Boundary Conditions Definition

Figure 65 is an example of how the boundary conditions are set:

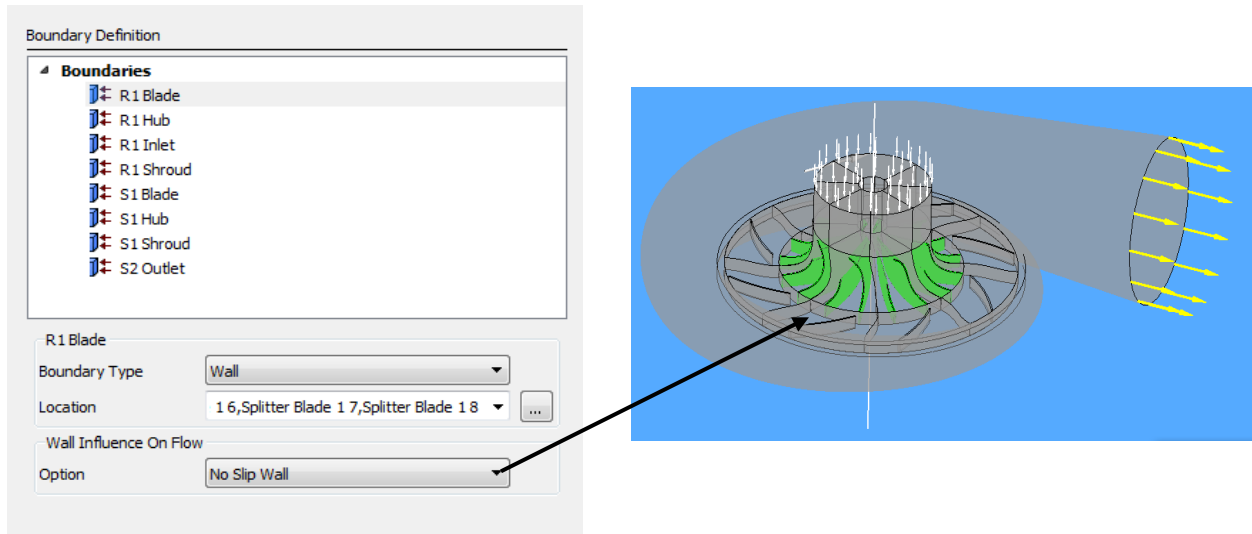


Figure 65 : Blades are set as 'Wall'

Table 15 contains all the boundary conditions set in the model, is presented below:

Table 15 : Detailed Definition for every Boundary Condition

Inlet Boundary Conditions	
S1 Inlet	Inlet Area
S1 Hub	Wall
S1 Shroud	Wall
Impeller Boundary Conditions	
R1 Hub	Wall
R1 Shroud	Counter Rotating Wall
R1 Blade	Wall
Diffuser Boundary Conditions	
S1 Hub	Wall
S1 Shroud	Wall
S1 Blade	Wall
Volute Boundary Conditions	
S2 Outlet	Outlet

Although the shroud at the impeller is imported as part of the rotating impeller, it is stationary. That's why it is set as a "Counter Rotating Wall". All the other boundaries, with type set as Wall, are governed by the no-slip condition. This means that the velocity in this area is set to zero.

4.3 Solver Setup

Then, the solver setup comes after the definition of the boundary conditions is finished. The first step is to declare the units of the simulations and never forget to set the length in millimeters. Figure 66 shows the solver interface:

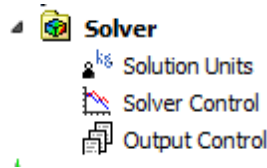


Figure 66 : Solver Setup Interface

The next and most crucial step is the solver control (Figure 67). In this tab there are 3 categories:

- The basic settings,
- The equation class settings
- The advance options

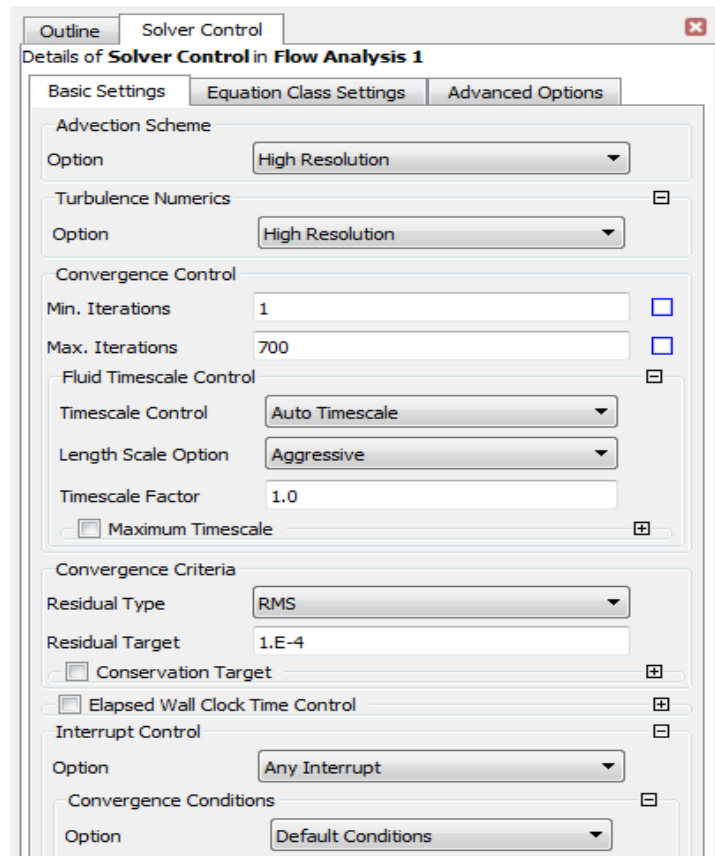


Figure 67 : Solver Control Definition

In the basic setting, the user must set the maximum iterations of the simulation and the residual target for the convergence of the simulation. By the time one of these values reaches its target, the simulation ends. For this simulation, the maximum iterations are set at a value of 800. The reason

behind this choice is that convergence has been reached. At that point, the algorithm stops, and the results created from the last iteration are saved.

For the setting of the "Advection Scheme", there were two possible solutions: "Upwind" and "High Resolution". Using the "Upwind" option, the transfer terms in the Navier Stokes equation show first-order accuracy. Although the stability of the calculations is ensured with this scheme, the first-order accuracy makes them prone to numerical diffusion errors in the flow. While using the "High-Resolution" scheme, the algorithm determines whether to use high-precision or low-precision models for each case, making the whole process easier for the user.

The Turbulence Numerics are then displayed. All the CFX models use first-order Turbulence Numerical errors. In this case, the selection is the "High-Resolution" option, because first-order numerical errors are undesirable in order to have better accuracy in the results, which it usually offers.

The CFX employs the so-called False Transient algorithm, where a timescale (time step) is used to move the solution towards the final answer. A steady-state simulation, like in this dissertation, is a "transient" evolution of the flow from the initial guess to the steady state conditions. The option chosen is "Auto Timescale", with which the solver calculates a timescale based on the boundary or current condition and domain length scale (L/U). The domain length scale is further predicted using the option of "Aggressive", which takes into account the whole control volume. The user also has the opportunity to decide the convergence criteria. When convergence criteria are reached, the solver will stop. At this point, the maximum interactions will probably not be reached. Since iterating towards a solution, there can never be an exact solution to the equations, but one quite close to the analytical. The RMS Residuals are set to a value of 10^{-5} , in order to increase the reliability of the results. However, the results are reliable even with higher values of 10^{-4} or 10^{-3} in some cases.

4.4 Solver Functions

At this point, it is very important to understand the equations solved through Ansys CFX. In this way, the user will have the ability to overcome and solve simulation problems. These four equations are the continuity equations, complied with the three equations of momentum in the three directions.

It is very difficult and time-consuming for someone to solve the Direct Numerical Solution (DNS) because of flow fluctuations [24]. These fluctuations complicate the simulation and that is why the equations solved in Ansys CFX are the Reynolds Averaged Navier-Stokes (RANS). The RANS equations will be explained later in this chapter.

Engineers, in most cases, do not actually need to know the exact velocity at a particular instant, which very often may be difficult to understand and unrepresentative. The time-averaged velocity is all one needs to know. This provides a useful way to approach modeling turbulence.

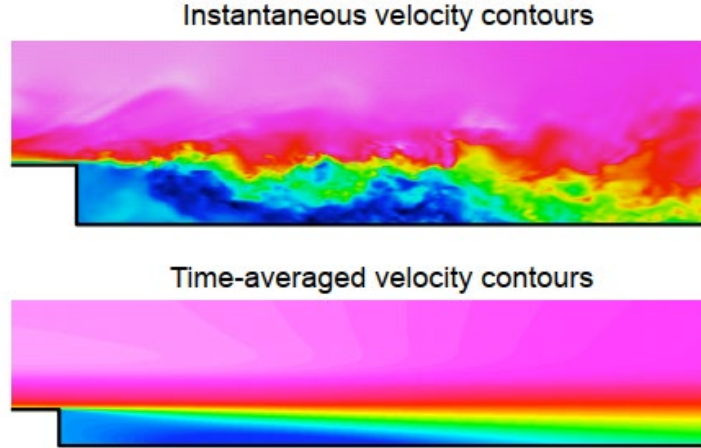


Figure 68 : Time-averaged Vs Instantaneous velocity [25]

4.4.1 Transfer equations

Below, the conservation equations for mass, momentum, and energy are presented. For turbulence flow, which also exists in centrifugal compressors, the equations are solved on average, with the addition of some terms. The turbulence model describes these terms, and it must be pointed out that they are crucial in order to describe the turbulence flow and its consequences.

The equations are written below in general form:

➤ **Continuity Equation**

$$\frac{\partial \rho}{\partial t} + \nabla \cdot (\rho U) = 0 \quad (65)$$

➤ **Momentum equation**

$$\frac{\partial(\rho U)}{\partial t} + \nabla \cdot (\rho U \times U) = -\nabla p + \nabla \cdot \tau + S_M \quad (66)$$

Where the tensor τ , is described from the equation:

$$\tau = \mu(\nabla U + (\nabla U)^T) - \frac{2}{3} \delta \nabla \cdot U \quad (67)$$

➤ **Energy Equation**

$$\frac{\partial(\rho h_{tot})}{\partial t} - \frac{\partial p}{\partial t} + \nabla \cdot (\rho U h_{tot}) = \nabla \cdot (\lambda \nabla T) + \nabla \cdot (U \cdot \tau) + U \cdot S_M + S_E \quad (68)$$

Where h_{tot} is total enthalpy, which connects to static enthalpy $h(T, p)$ through the equation:

$$h_{tot} = h + \frac{1}{2}U^2 \quad (69)$$

The term $\nabla \cdot (U \cdot \tau)$ is the one that defines the heat production of the fluid due to shear stresses, and in most cases, can be neglected. Additionally, the term $U \cdot S_M$ describes the work that derives from momentum from external factors.

4.5 Averaging the Navier-Stokes

By averaging the Navier-Stokes equations [24], one can obtain that every instantaneous field is defined as the sum of the mean and the fluctuating component as:

$$p = \underline{p} + p' \quad \text{and} \quad u_i = \underline{u}_i + u_i'$$

So, all the equations are transported as:

$$\frac{\partial \rho}{\partial t} + \frac{\partial (\rho \underline{u}_i)}{\partial t} = 0 \quad (70)$$

$$\frac{\partial (\rho \underline{u}_i)}{\partial t} + \frac{\partial (\rho \underline{u}_i \underline{u}_j)}{\partial t} = -\frac{\partial \underline{p}}{\partial x_i} + \frac{\partial}{\partial x_j} \left[\mu \left(\frac{\partial \underline{u}_i}{\partial x_j} + \frac{\partial \underline{u}_j}{\partial x_i} - \frac{2}{3} \delta_{ij} \frac{\partial \underline{u}_m}{\partial x_m} \right) \right] + \frac{\partial}{\partial x_j} (-\rho \underline{u}_i' u_j') \quad (71)$$

Using the Eddy Viscosity Model, with the only new unknown to be an effective turbulent viscosity μ_t , there can be an estimation of the term $-\rho \underline{u}_i' u_j'$, as:

$$-\rho \underline{u}_i' u_j' = \mu_t \left(\frac{\partial \underline{u}_i}{\partial x_j} + \frac{\partial \underline{u}_j}{\partial x_i} \right) - \frac{2}{3} \delta_{ij} \left(\rho k + \mu_t \frac{\partial \underline{u}_m}{\partial x_m} \right) \quad (72)$$

Reynolds stress tensor

Eddy viscosity

4.5.1 Constitutive Equation

The transfer equations are accompanied by the constitutive equations in order to consider the system as a closed one. In general form, these are:

$$\rho = \rho(p, T) \quad (73)$$

$$dh = \left. \frac{\partial h}{\partial T} \right|_p dT + \left. \frac{\partial h}{\partial p} \right|_T dp = c_p dT + \left. \frac{\partial h}{\partial p} \right|_T dp \quad (74)$$

$$c_p = c_p(p, T) \quad (75)$$

The form of all equations changes according to the type of every problem. In this case, where the air is considered ideal, the density is calculated through the fluid ideal law, which depends only on the temperature:

$$\rho = \frac{MW \cdot p_{abs}}{R_0 T} \quad (76)$$

$$dh = c_p dT \quad (77)$$

$$Cp = Cp(T) \quad (78)$$

Where w : air molar mass, p_{abs} : absolute pressure and R_0 : fluid constant

4.6 Turbulence Models

Turbulent flow is an unsteady and very complicated phenomenon to research as it is three-dimensional. Therefore, the eddy viscosity turbulence model must be carefully selected. These models are based on the fact that the turbulence consists of small eddies that are continually being created but also destroyed.

The Eddy Viscosity models are divided into the following three categories depending on the number of additional equations used in order to achieve sufficiency (closure):

- The Zero equation model
- The One equation model
- The Two equation model

The CFX uses 3 different models with belong in the category “two equation model”, which are:

- k-epsilon turbulence model (k-ε)
- k-omega turbulence model (k-ω)
- Shear stress transport turbulence model (SST)

The k-epsilon and k-omega models correspond to the Reynolds stresses with the mean velocity of the turbulence and the turbulence viscosity. The viscosity of the flow is simulated as the product of the turbulence velocity and its length scale. The term K symbolizes the kinetic energy of the turbulence, while the other term, “epsilon”, represents the eddy dissipation rate and the term “omega” the kinetic energy.

4.6.1 k-epsilon model

The most commonly used model is the k-epsilon model because it provides accurate estimations for different types of flows. However, there are some cases in which someone should avoid the use of this model. These cases are:

- Flows with boundary layer detachment
- Flows in rotating fluids
- Flows in curved surfaces

4.6.2 k-omega model

K-omega, in contrast with k-epsilon, is more accurate because it doesn't contain the nonlinear function used in the latter. Another advantage of this model is that it gives better results near wall treatment (Figure 69) for calculations near low Reynolds numbers. K-omega is reliable for:

- Flows with boundary layer detachment
- Transient flows
- Low Reynolds number

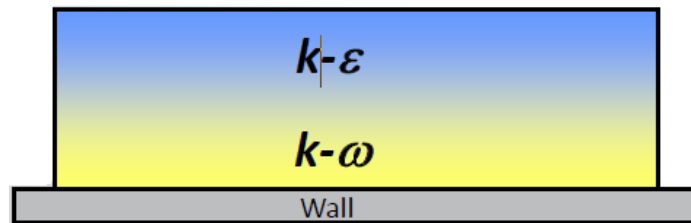


Figure 69 : k-ε and k-ω [26]

4.6.3 SST model

The Shear Stress Transport turbulence model is a mix of the previous models, having the advantages of each. The SST model is based on k-omega and considers the transfer of the shear stresses of turbulence and gives accurate results even with boundary layer detachment. Also, the SST prevents the overestimation of the viscosity of the flows. Moreover, this model can also handle the full range of values, with values from less than 1 up to 300. It is clear that for the study of the flow in the centrifugal compressor, the SST model gives better results.

4.6.4 Modeling of y^+

As mentioned previously, the choice of the eddy viscosity model, as well as the way the flow is modeled near the wall, constitutes a very important parameter. For this reason, the appropriate y^+ plays a major role (Figure 70).

The y^+ is calculated by means of the following equation using the dimensional velocity, the height of the boundary layer, and the dynamic viscosity:

$$y^+ = \frac{y \cdot U_\tau}{\nu} \quad (79)$$

Where:

$$U_\tau = \sqrt{\frac{\tau_{wall}}{\rho}} \quad (80)$$

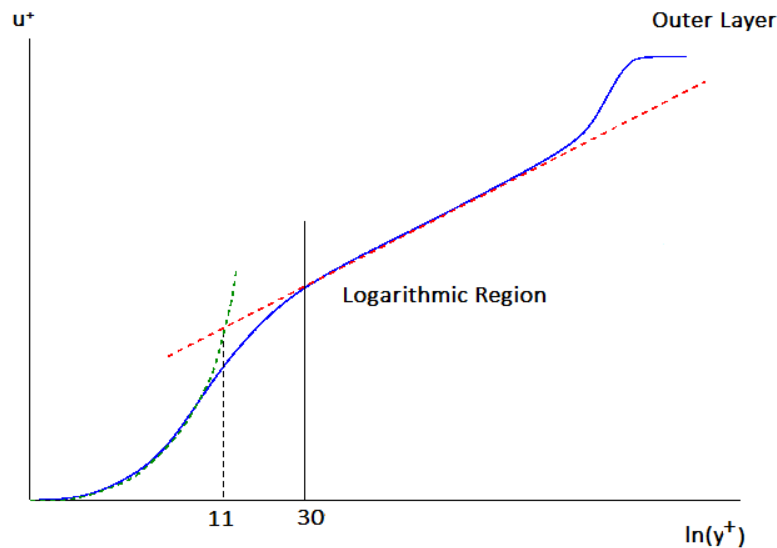


Figure 70 : y^+ [27]

It should also be underlined that the SST model in Fluent and CFX applies so-called "automatic wall functions". The wall treatment is automatically adjusted to the near-wall y^+ . If y^+ is small (like $y^+ < 5$), then no wall functions are used anymore. Wall functions are equations empirically derived and used to satisfy the physics in the near wall region.

4.7 Finite Volumes

The finite volume method is the way that Ansys uses to discretize any problem in order to solve it. The analytical solutions of the RANS can only be found when the flow is very simple and solving them is very time-consuming. In a complicated system, like that of a centrifugal compressor, where the flow is turbulent, the problem must be approached numerically. Using this finite volume method, the partial equations are transformed into the form of algebraic equations.

Ansys-CFX uses the method of finite volumes (Figure 71), which discretizes the control volume using a mesh grid [28]. This mesh grid produces finite volumes, which the program uses in order to store information (quantities like momentum, mass, and energy). In the figure below, a two-dimensional mesh is displayed. The control volume is produced around any node of the mesh and is defined by edges, which join the centers of element edges with the centers of neighboring elements.

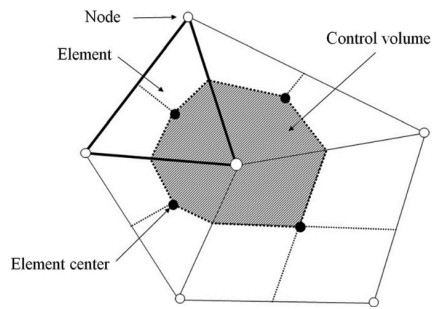


Figure 71 : 2-D Finite element volume [29]

The next step of this method is the discretization of the spatial and surface integrals in every section of the element. It is important to point out the difference between the finite volume method and the finite difference method. Using the finite difference method, the information is stored at the element nodes, while in the finite volume, the information is stored in the center of the finite volume. This method will not be analyzed any further as it is not an object of study for the specific thesis.

5. Computational Fluid Dynamics Analysis Results

When the computational fluid dynamic analysis of the flow is over, the results of the simulations are going to be presented at every stage of the compressor. The CFX-Post is used for the visualization and analysis of the results. This procedure is called "Post Process". As is referred to many times, the centrifugal compressor studied consists of the impeller, the vaneless and vaned diffuser, and the volute. So, all the thermodynamic properties will be presented, as well as the velocity streamlines, at every stage. All the results derived from the CFD analysis will be compared with those from the preliminary design further in this chapter.

5.1 Impeller-Vaneless Diffuser

Total Pressure

The graph below (Figure 72) shows the total Pressure in a Standard Frame. By the time air reaches the exit of the impeller, its pressure value has increased to 199513 Pa. After it exits the impeller and goes into the diffuser, there seems to be a pressure drop, at 152331 Pa. A total pressure drop is expected when entering the stationary part due to the flow losses. The fluid loses its kinetic energy, leading further to a static pressure rise. At the exit of the diffuser, some of the total pressure loss is regained, at 181290 Pa. However, the total pressure is reduced in the diffuser.

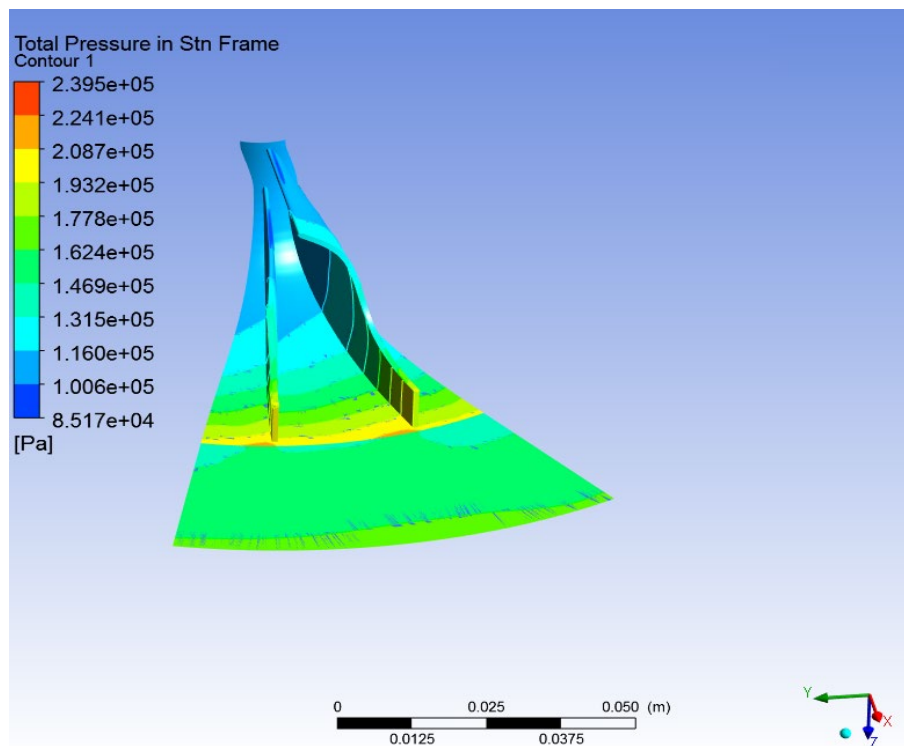


Figure 72 : Contour of Total Pressure at Vaneless Diffuser

Static Pressure

Figure 73 below provides the static pressure values within the impeller and diffuser, which increases throughout both parts. Through the impeller, the fluid is compressed and, consequently, there is a pressure rise. Apart from that, there is also an increase in pressure in the diffuser as the kinetic energy transforms into static pressure, rising from the value of 145277 Pa to the value of 163249 Pa. The order of magnitude of 200 mbar is very important and has a great effect on the performance of the compressor.

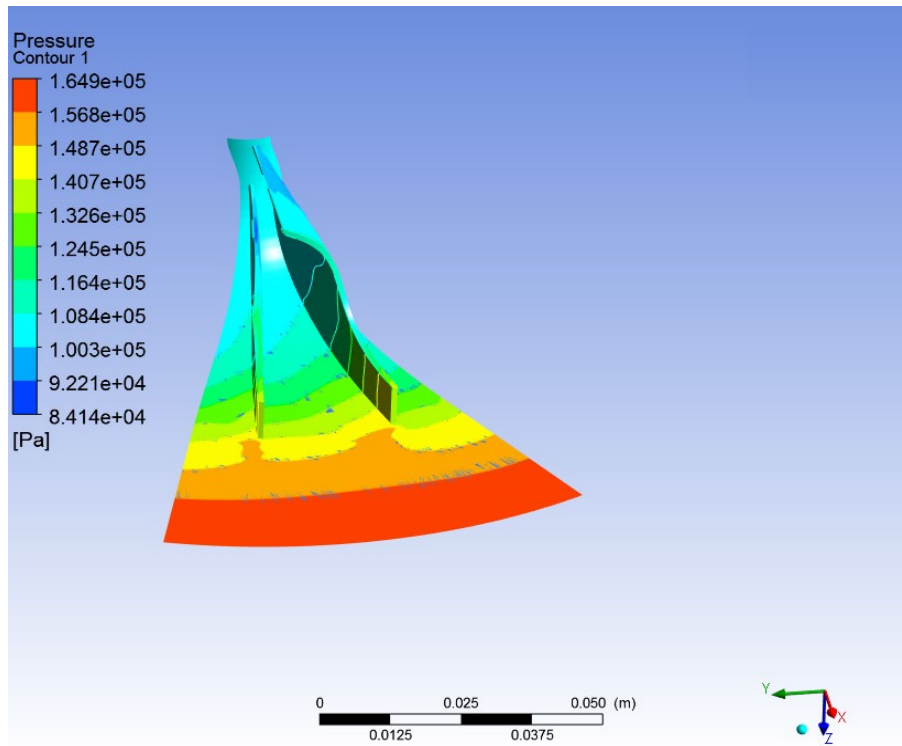


Figure 73 : Contour of Pressure at Vaneless Diffuser

Streamlines

The velocities are shown in Figure 74. It's easy to see that the flow reaches the impeller eye axially and that the angle of attack between the flow and the blades is constantly changing. It reaches very high values at the exit of the impeller, whilst it gradually decreases in the diffuser, transforming into static pressure. The velocity at the exit of the impeller is 245 m/sec, while at the exit of the diffuser it is around 155.4 m/s.

Total Temperature

Figure 75 illustrates the contour of Total Temperature in a Standard Frame. It's clear to see that total temperature behaves the same way total pressure does. The fluid enters the impeller at 293 K and gradually increases its temperature in layers, reaching a value of 362.2 K. After leaving the impeller, it seems to maintain a fixed value of 362 K, since no work is produced in the diffuser and the total enthalpy remains constant.

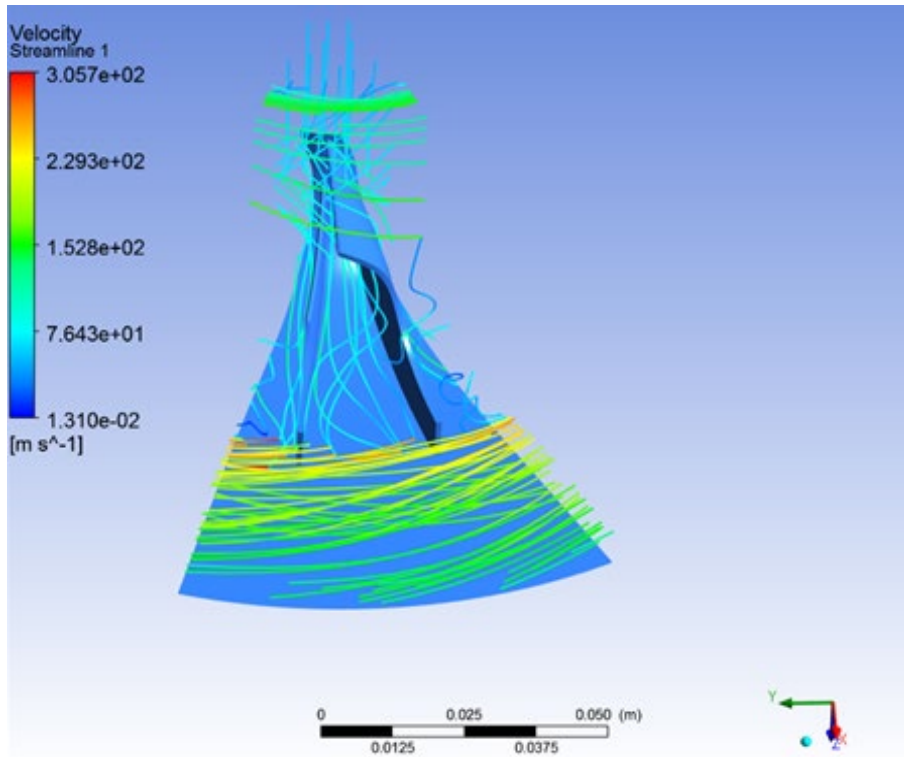


Figure 74 : Velocity Streamlines at Vaneless Diffuser

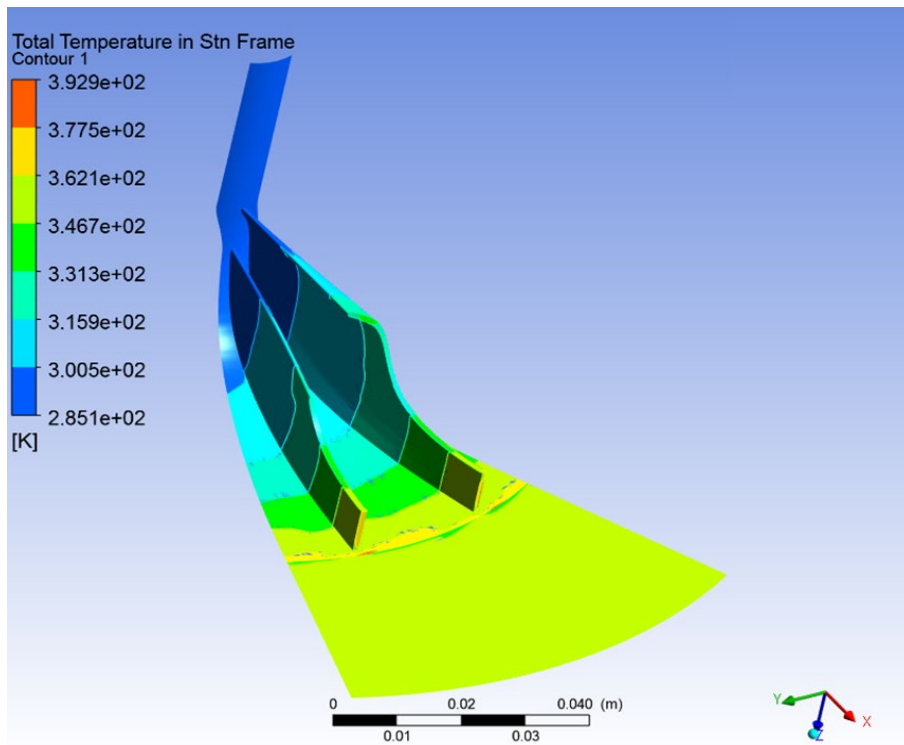


Figure 75 : Contour of Total Temperature at Vaneless Diffuser

Static Temperature

Figure 76 depicts the contour of the static temperature. The temperature of the fluid is increasing through the impeller due to the compression that takes place. At the inlet, the temperature is 289 K and reaches a value of 327 at the outlet of the impeller. One can also observe that the biggest increase in the static temperature takes place at $2/3$ of the blade. In the diffuser, in contrast to the total temperature that remains constant across it, the static temperature increases even further until the value of 356 K. Another observation for Figure 76, but also for previous figures, is about the blue spots on the color borders. These marks are unexpected at these points, and they may be caused by insufficient meshing. These spots became visible once the number of contours increased.

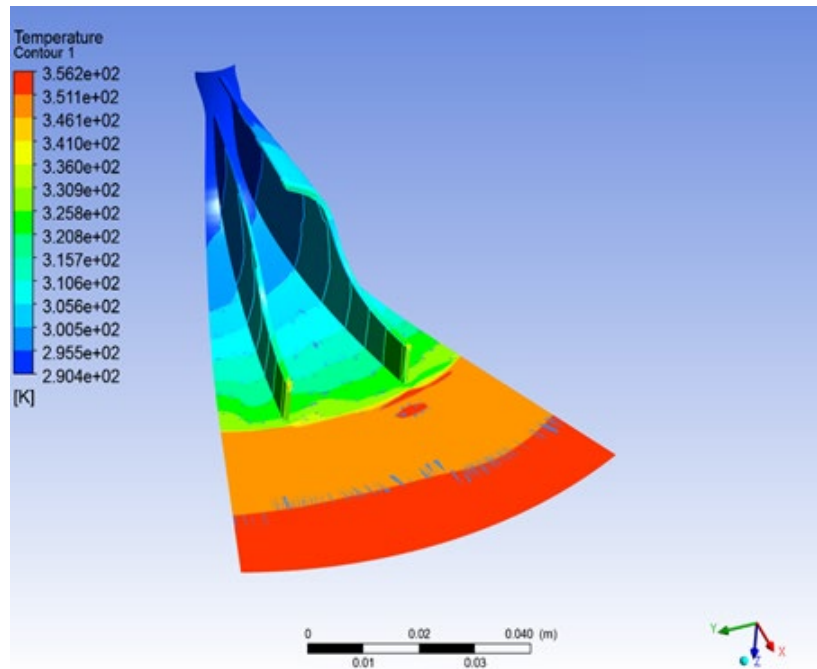


Figure 76 : Contour of Static Temperature at Vaneless Diffuser

Density

Figure 77 shows the contour of Density across the impeller. Even though both the pressure and the temperature are increasing, the density, which is more sensitive to the changes in pressure, increases. The fluid is leaving the impeller at 1.48 kg/m^3 . At the exit of the diffuser, it reaches a value of 1.65 kg/m^3 . The rise in density due to the diffuser and its contribution consequently to the increase in engine power is very important.

Mach Number

Mach number stays at acceptable levels throughout the whole compressor. It gradually increases from hub to tip at the impeller eye, as shown in Figure 78. Figure 79 displays the Mach

number in the middle width. At the exit of the impeller, it reaches a value of 0.69, while at the exit of the diffuser it is at 0.41. It is very crucial to keep this number at low levels.

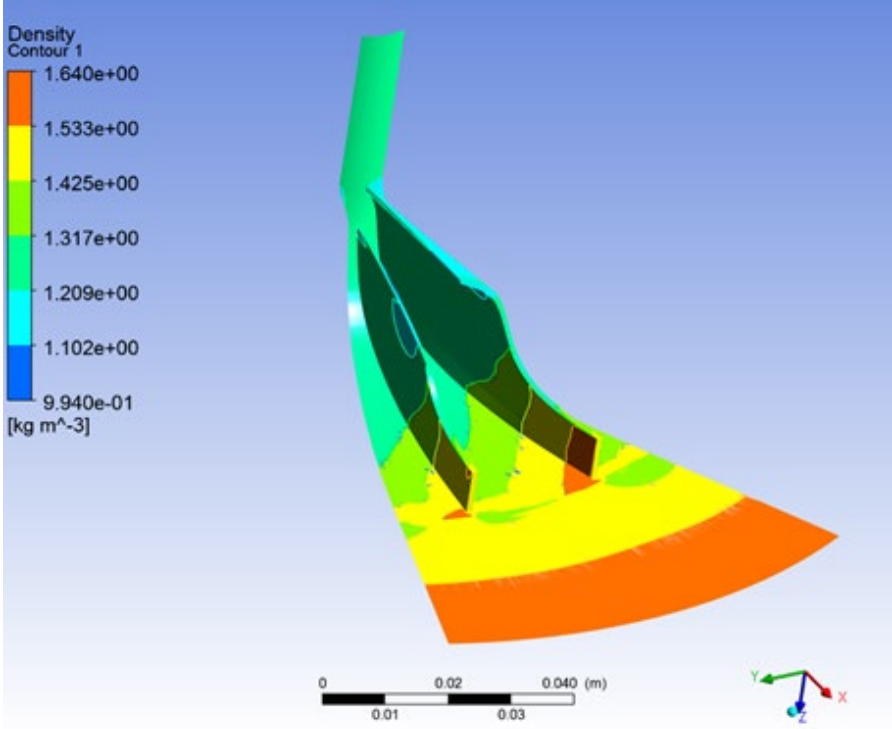


Figure 77 : Contour of Density in Vaneless Diffuser

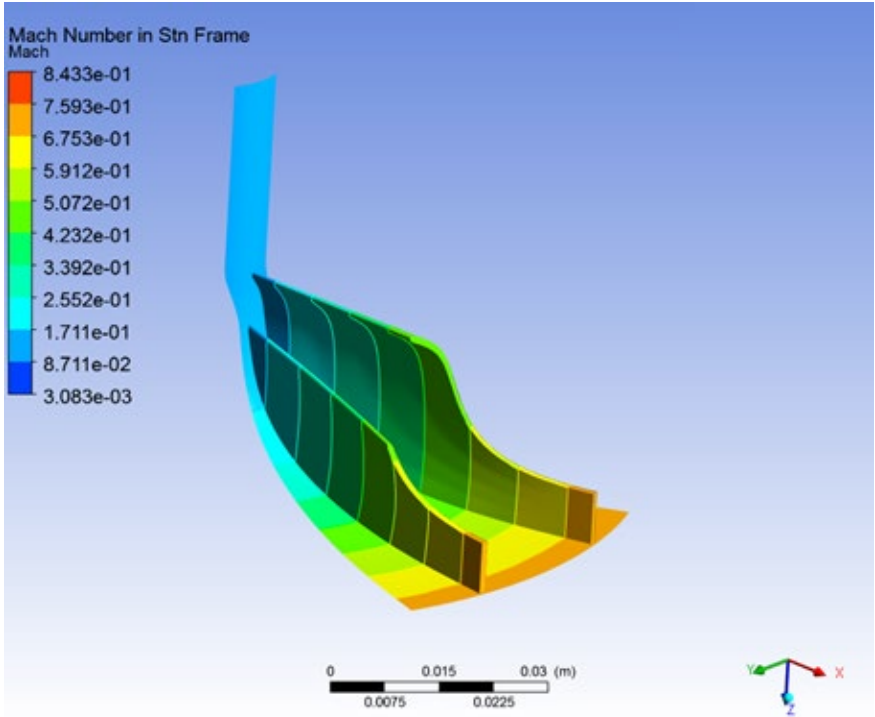


Figure 78 : Mach number at the Impeller

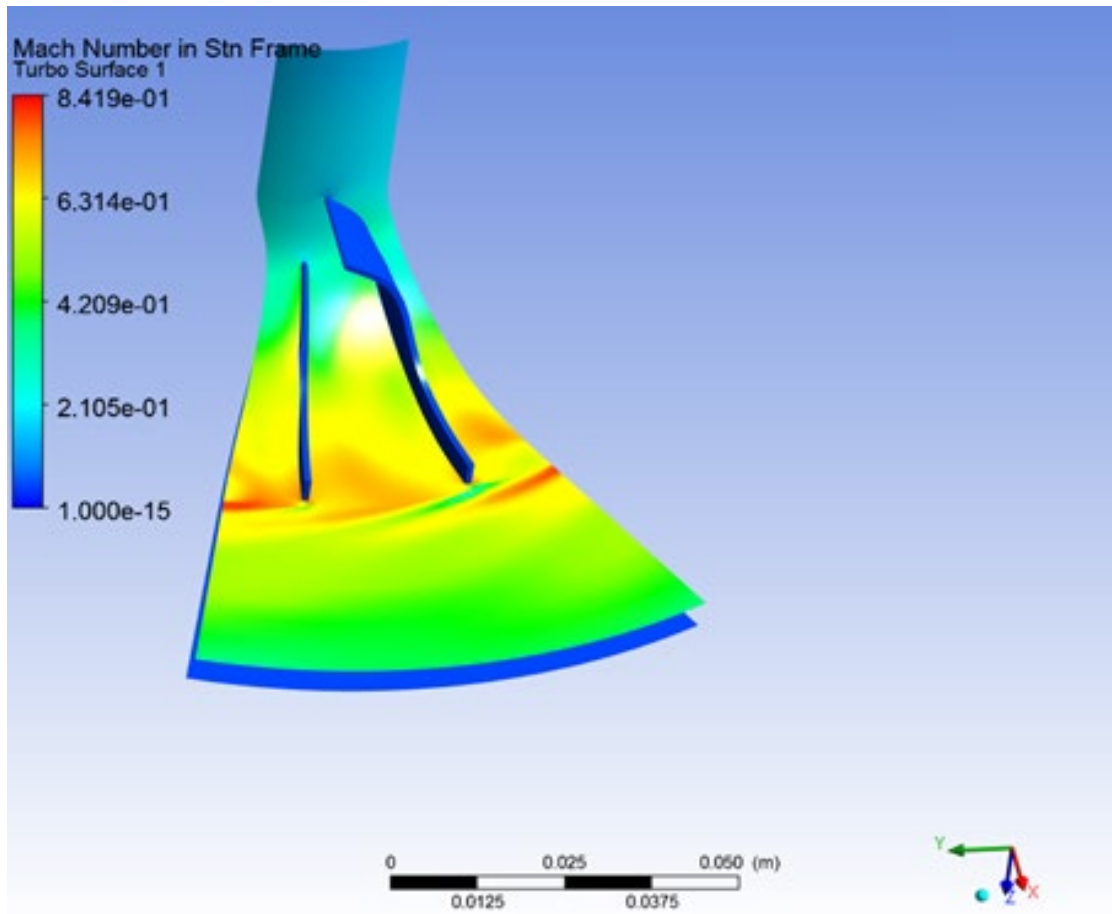


Figure 79 : Mach Number at the Vaneless Diffuser

Flow Field

In Figure 80, the flow field can be seen at the exit of the vaneless diffuser. It is clear that the passage wake remains close to the shroud. The result is the low velocity near it. Also, the radial component of the velocity is high on the suction side of the main blade, in contrast to other regions. This means that the mixing of the flow is not good enough and will result in poor efficiency.

Static Entropy

Figure 81 depicts the contour of static Entropy at the exit of the Vaneless Diffuser. Entropy is a measure of disorder and randomness. Here, there is high entropy across the whole area. It is an estimation that the flow is not stabilized enough.

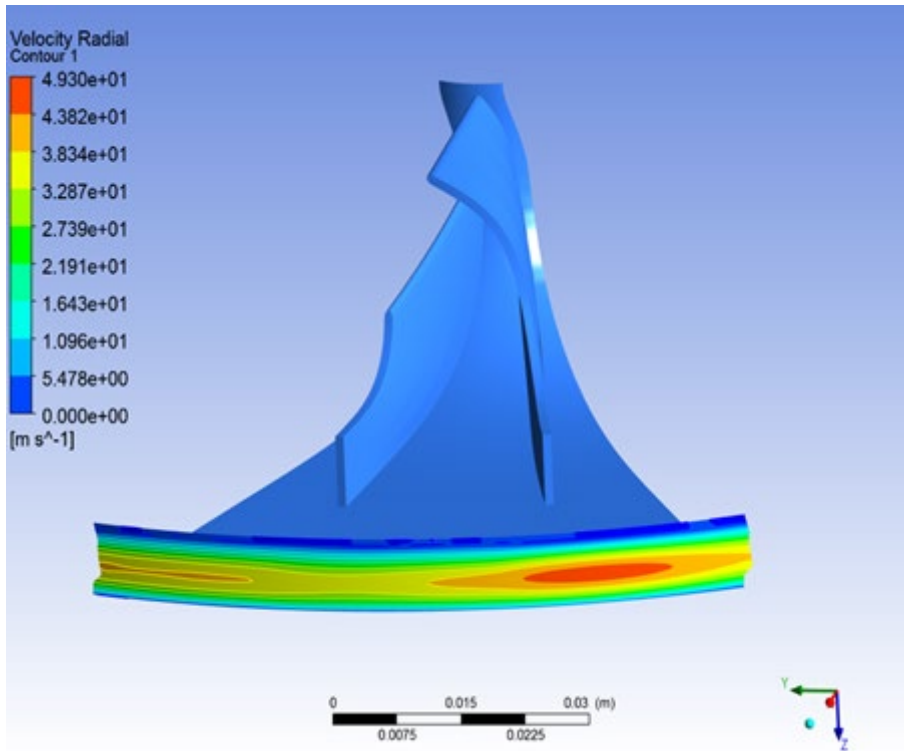


Figure 80 : Flow Field of Vaneless Diffuser

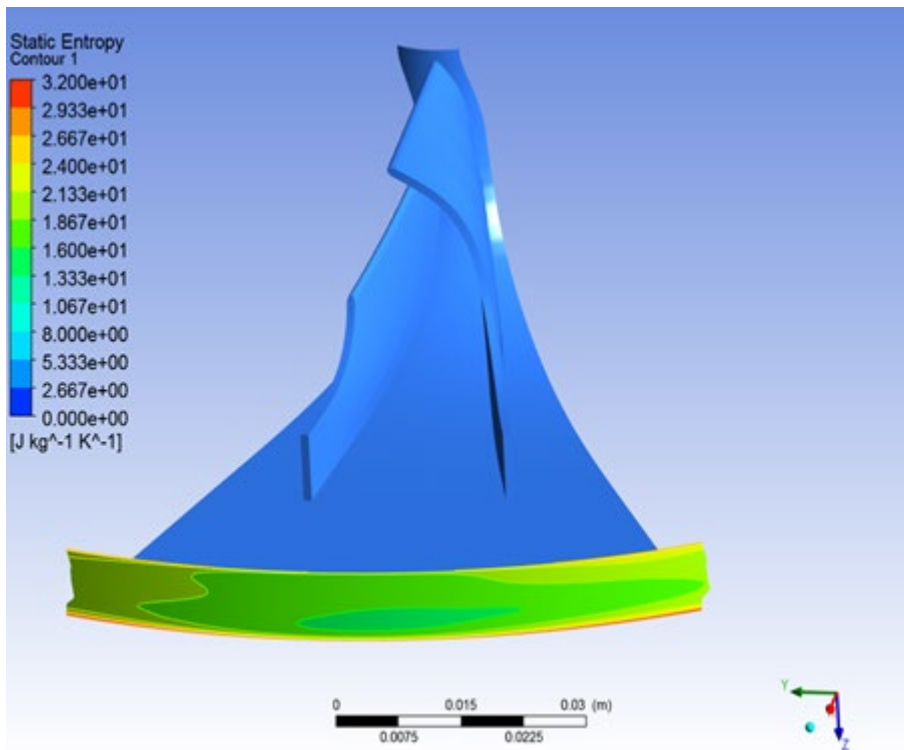


Figure 81 : Static Entropy at the Vaneless Diffuser

In Table 16, the results accrued from the Computational Fluid Dynamic analysis of the impeller with the vaneless diffuser are presented in contrast with those taken from the preliminary design. The deviation between the values reaches the maximum value of 9.8% in only one unit. The deviation that exists is expected as the flow inside the compressor is very complicated and it cannot be simulated at its maximum level. However, all the results have qualitatively expected values. This fact shows that the simulation model is quite well set up and can be efficiently used to simulate the real problem.

Table 16 : Results of CFD vs pre-design for the Vaneless Diffuser

Results Presentation of CFD Vs pre-design				
Unit		Anslys CFX	Excel	Deviation (%)
Total Pressure	P_{01}	108467	105000	3.3
	P_{02}	216381	197985	9.3
	P_{02d}	177285	196540	9.8
Static Pressure	P_1	104281	103148	1.1
	P_2	148752	145957	1.9
	P_{2d}	165249	177511	6.9
Total Temperature	T_{01}	293	293	0
	T_{02}	362	357.7	1.2
	T_{02d}	362	357.7	1.2
Static Temperature	T_1	288.9	291.6	0.9
	T_2	327	327.8	0.3
	T_{2d}	356	346.7	2.7
Density	ρ_1	1.24	1.21	3
	ρ_2	1.49	1.5	1
	ρ_{2d}	1.65	1.72	4.7
Mach Number	$M_{1m,rel}$	0.33	0.31	4.8
	$M_{2,abs}$	0.69	0.67	3
	$M_{2d,abs}$	0.41	0.39	5.1

5.2 Impeller-Vaneless Diffuser-Volute

Static Pressure

As seen in previous figures, the static pressure increases through the compressor. In Figure 82, the most remarkable point is that the pressure of the fluid gradually increases until it reaches a value of 1.66 bar. Very important, not only in the pressure increase but also to reduce the flow, is the contribution of the diffuser part of the volute. Its role is to slow down the flow and aim to achieve successful static pressure recovery. This type of diffuser must have the appropriate length in order to normalize and stabilize the flow and achieve the optimum outer diameter. These parameters have a huge effect on flow losses and must be carefully selected.

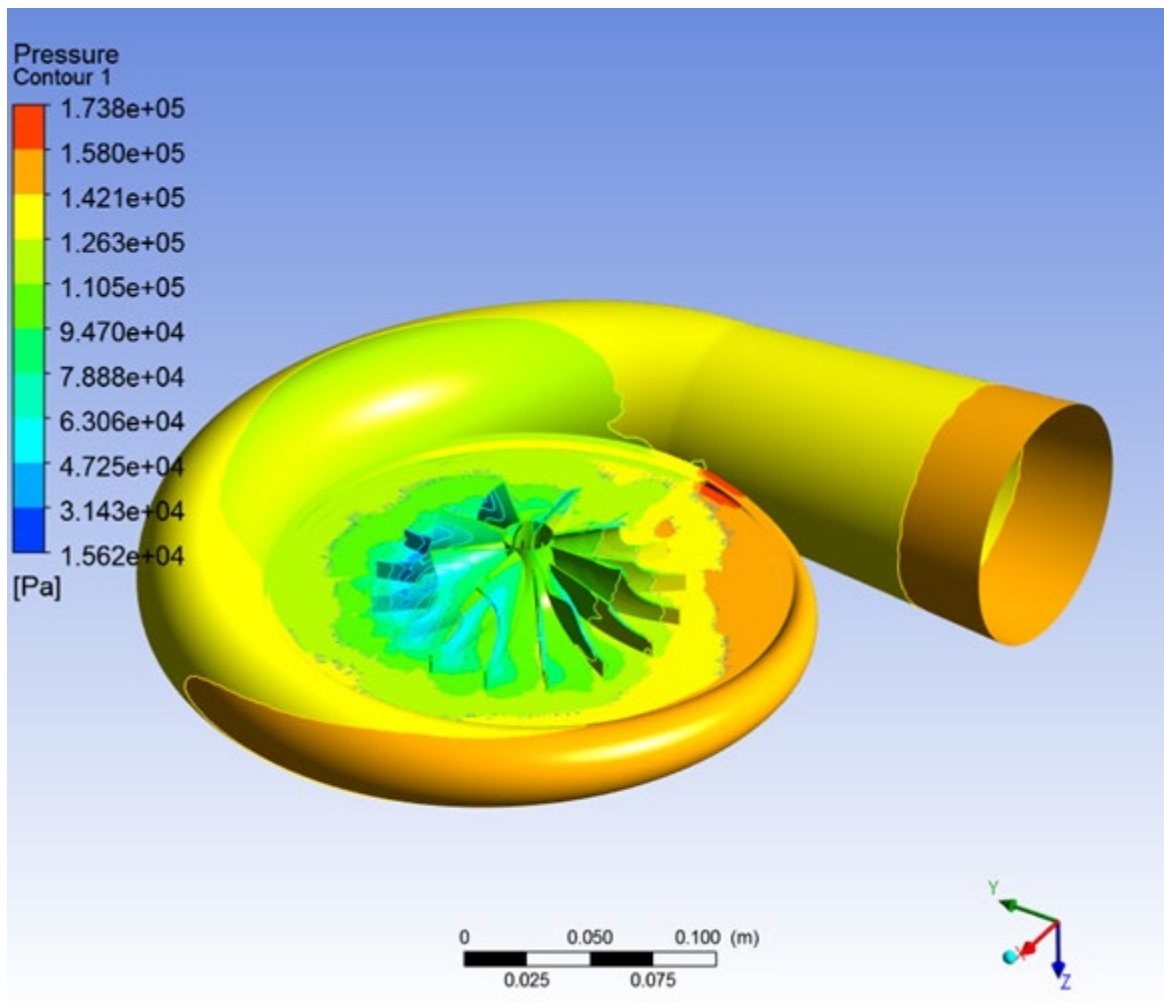


Figure 82 : Contour of Static Pressure

Figure 83 shows the contour of the static pressure at the XY plane. The results of the CFD are not close to those one would expect, due to numerical errors of the algorithm. The deviation at some points is around 20%.

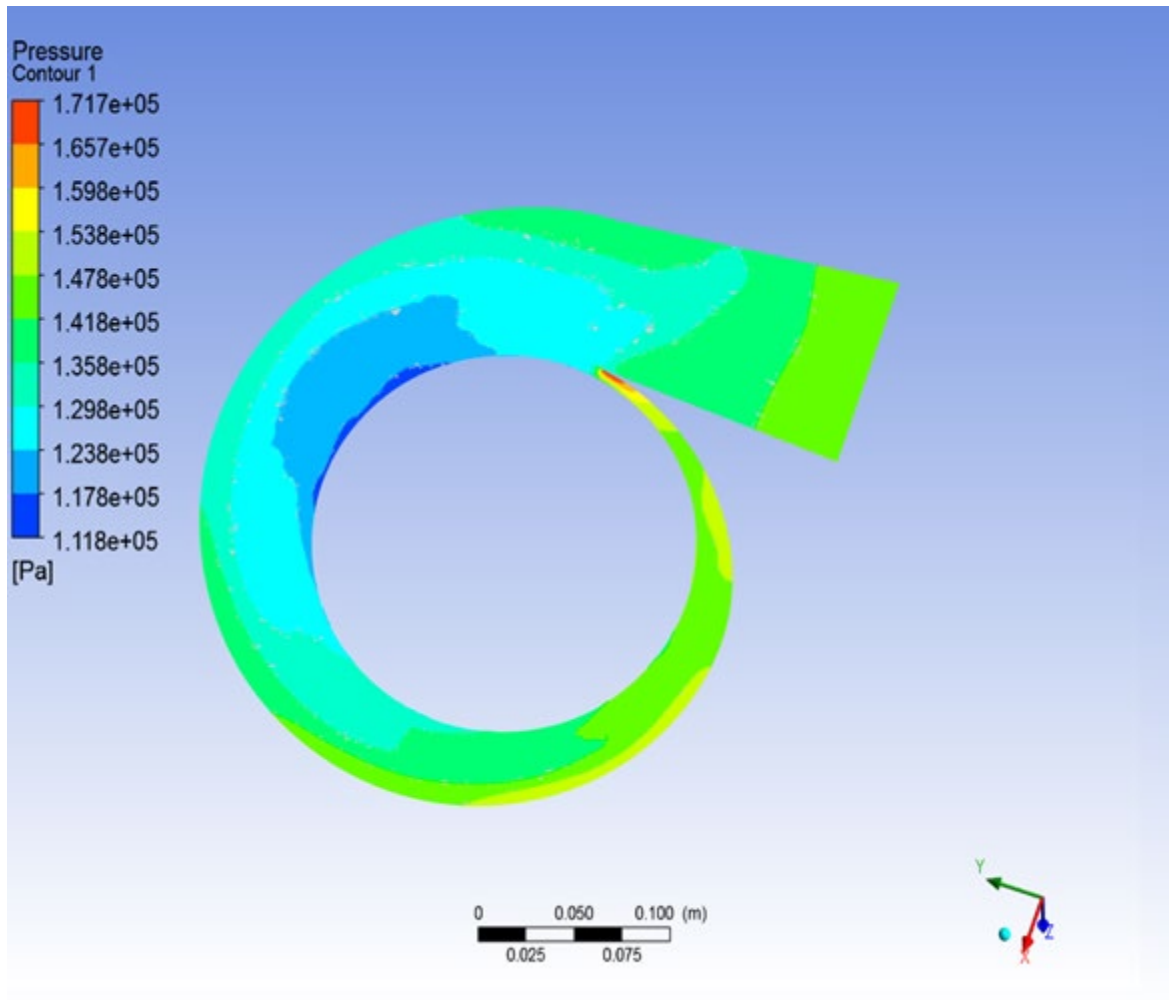


Figure 83 : Contour of Static Pressure at XY plane

Total Pressure

Figure 84 illustrates the contour of Total Pressure across the compressor. While the total pressure is gradually increasing in the impeller, there is a reduction through the diffuser and the volute. In the diffuser, the total pressure is gradually reduced in every ring section, whereas in the volute, the total pressure decreases in some specific areas, where streamlines become more or less dense. In Figure 85, a cross-section of the compressor is represented, where the Total Pressure decreases as the diameter of the volute increases. In this figure it is clearer that in smaller diameters the total Pressure is high and it decreases as the diameter of the volute increases.

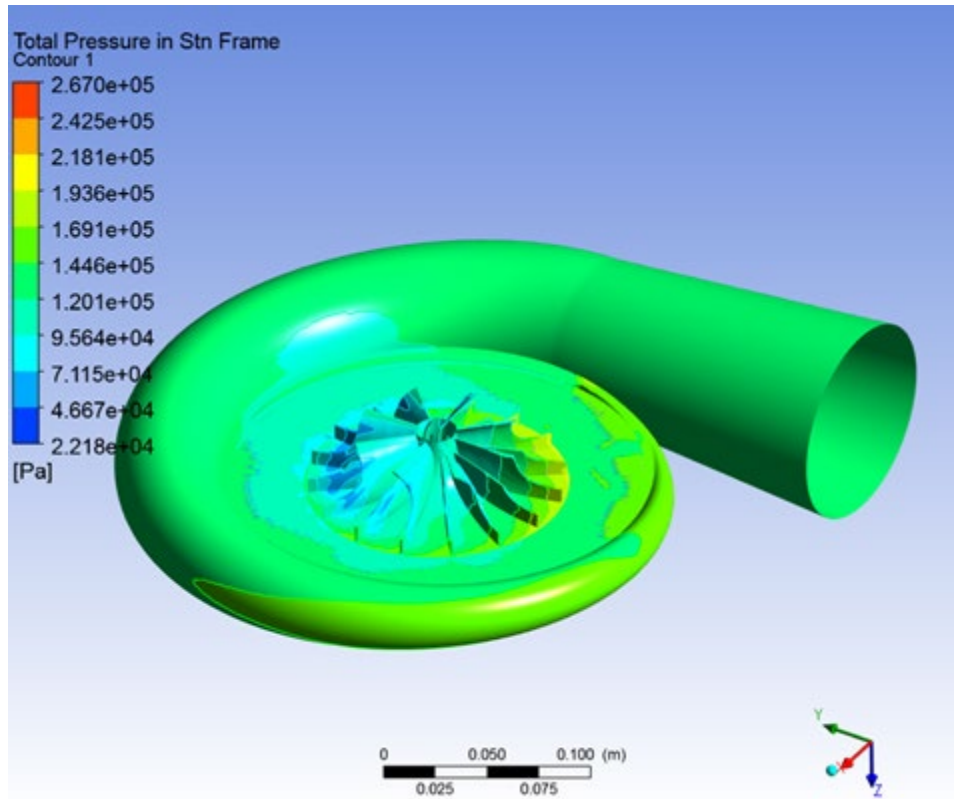


Figure 84 : Contour of Total Pressure

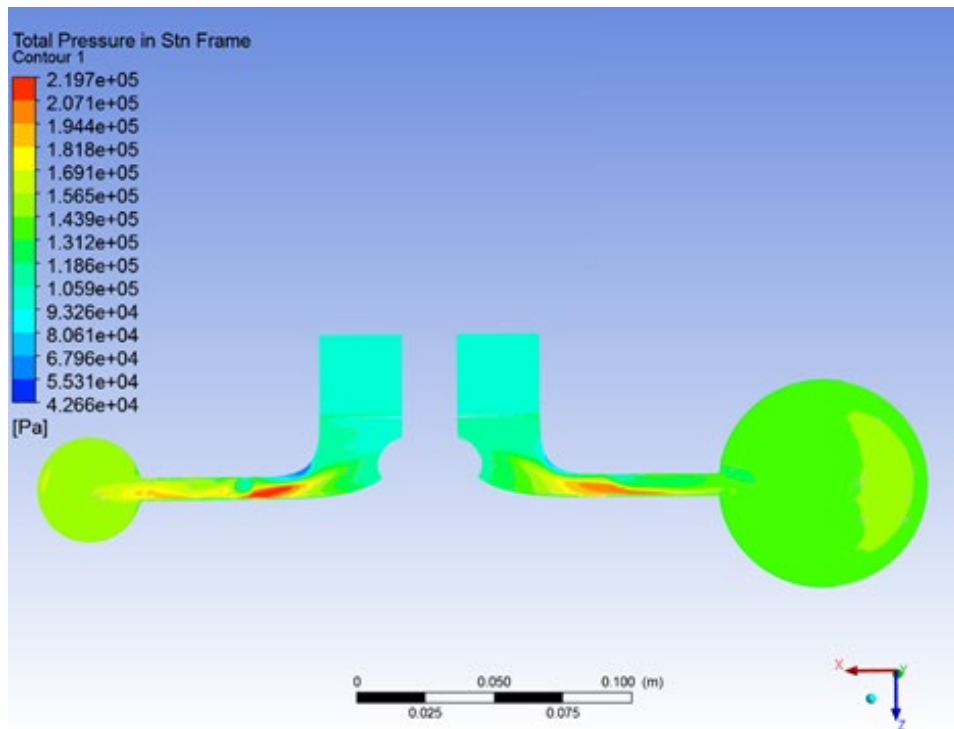


Figure 85 : Total Pressure distribution at XZ plane

Streamlines

In Figure 86, it can be observed that the fluid enters the impeller eye with an axial velocity. Then, the impeller increases the kinetic energy of the fluid as it passes through it. At the exit of the impeller, the velocity of the fluid reaches a value of 286 m/sec. Next, in the diffuser, the fluid slows down at 220 m/sec in order to achieve static pressure recovery. The volute then guides the flow to the exit while the fluid retains its velocity.

The fluid in areas before the impeller tongue has lower velocity due to the huge blockage that it has to deal with. Moreover, it is important to note that the flow of the fluid in the final diffuser part of the volute is normalized and tends to become laminar. This means that the length of this part was selected correctly. The fact that the flow tends to become laminar at this point is very crucial, as the flow becomes more controllable, and the flow losses are lower. However, the results are not exactly logical, since some streamlines take a quite unexpected course and exit the diffuser in a tangential direction. That is why it may need further investigation.

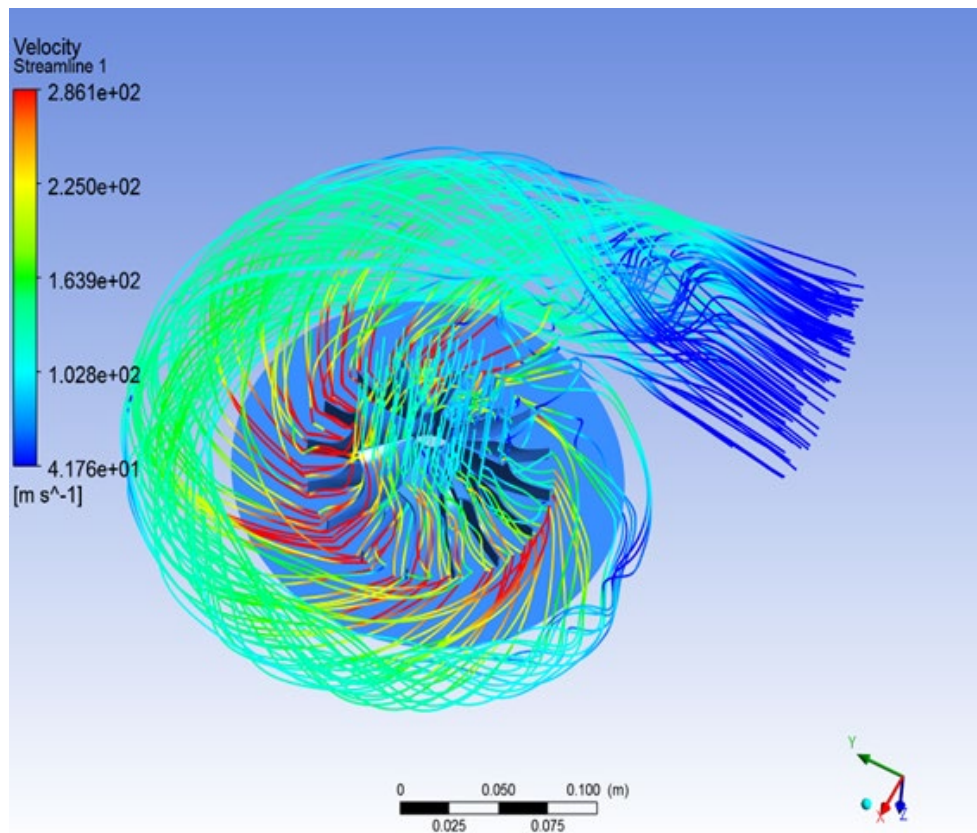


Figure 86 : Velocity Streamlines

Total Temperature

Figures 87 and 88 display the Total Temperature of the fluid. Across the impeller, the enthalpy gradually increases due to the offered work through rotation, resulting in a total temperature

increase. At the diffuser, the total temperature remains constant. However, this doesn't happen at the volute. Due to the fact that no work is produced or consumed at the volute, the Total Pressure must remain constant. The numerical errors of the software produce the deviation from the expected results (around 13%).

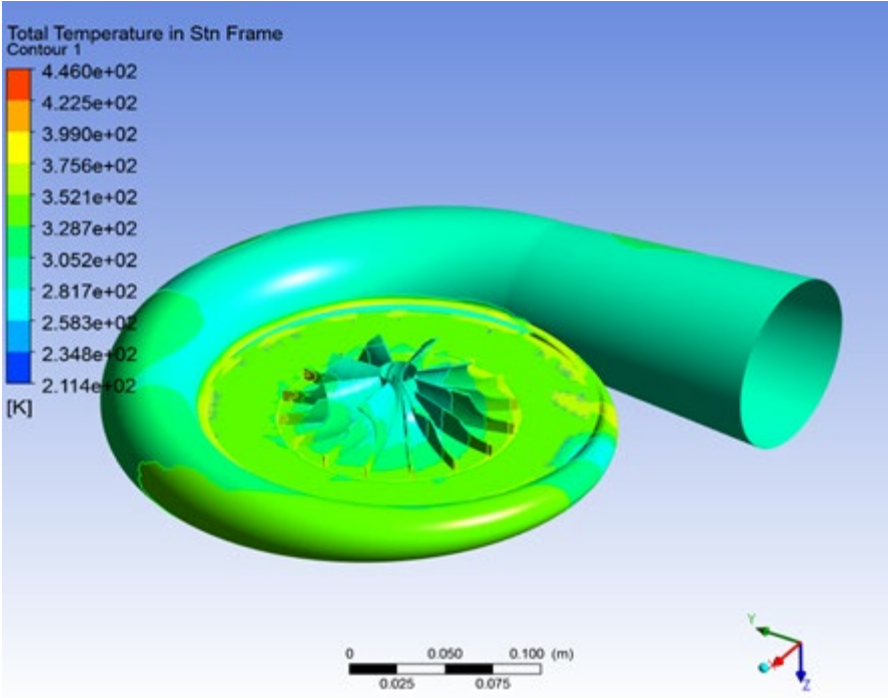


Figure 87 : Contour of Total Temperature

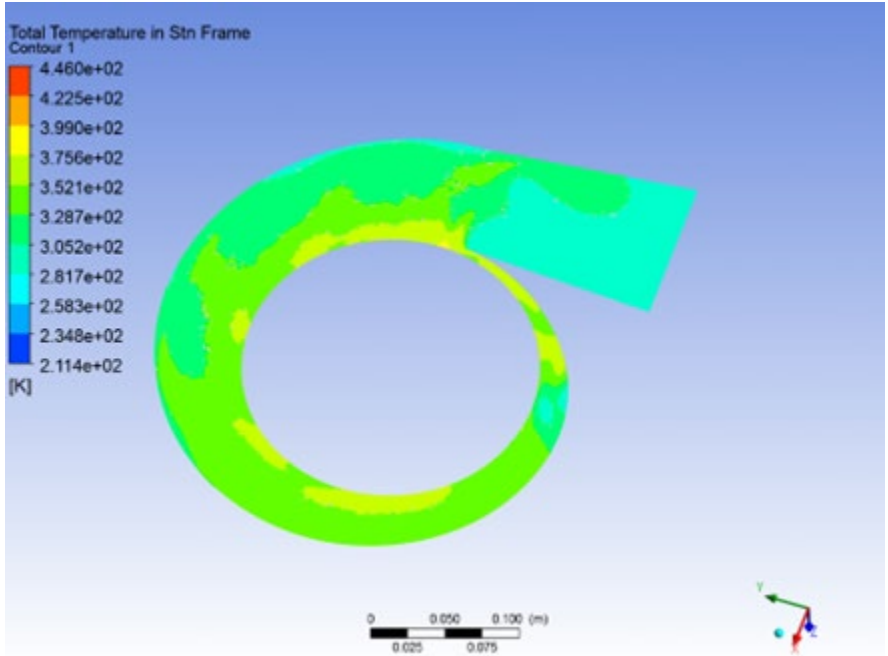


Figure 88 : Contour of Total Temperature at XY plane

Static Temperature

The Static Temperature, as shown in Figures 89 and 90, behaves similarly to the Total Temperature. As shown in previous Figures, the Temperature across the impeller and the diffuser is constantly rising. With the same way, the Static Temperature should behave at the Volute. The numerical errors that exist, cause this weird decrease in Temperature.

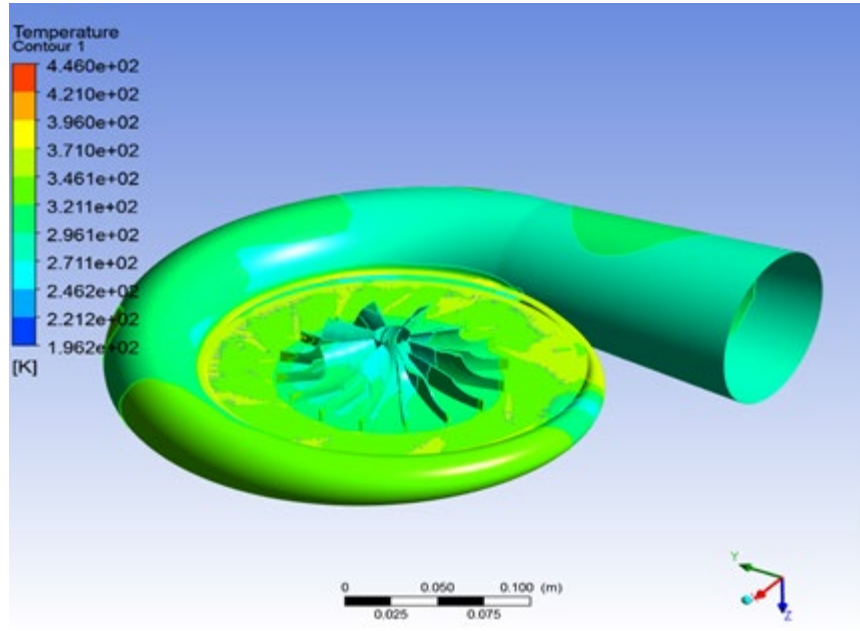


Figure 89 : Contour of Static Temperature

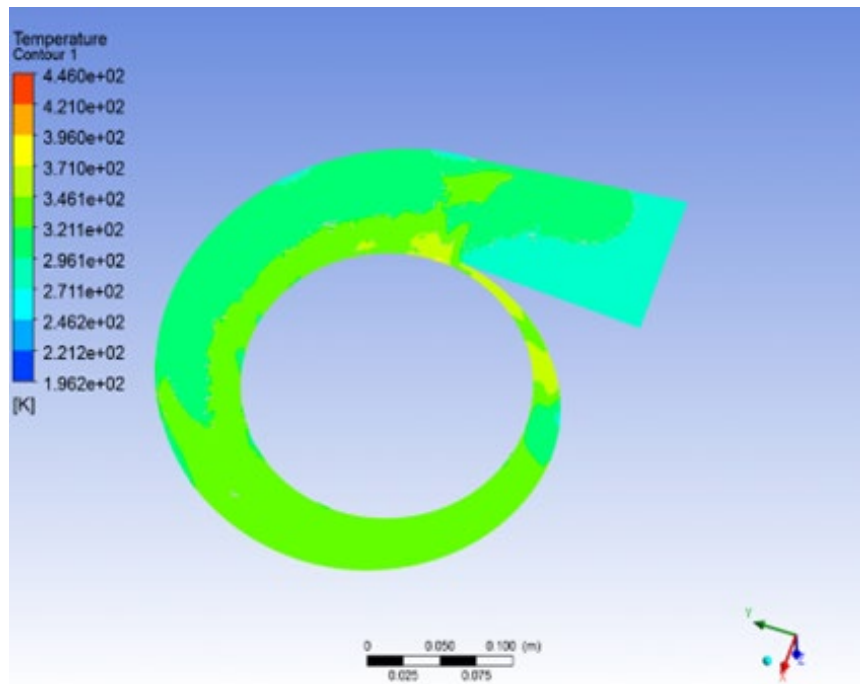


Figure 90 : Contour of Static Temperature at XY plane

Density

The fluid gets denser, as can be seen from the data in Figures 91 and 92, which depict how density behaves throughout the compressor. Leaving the impeller at a value of 1.4 kg/m^3 , it finally reaches a value of 1.751 kg/m^3 at the exit of the volute. The great pressure increase produced by the diffuser part at the exit contributed mainly to the density increase.

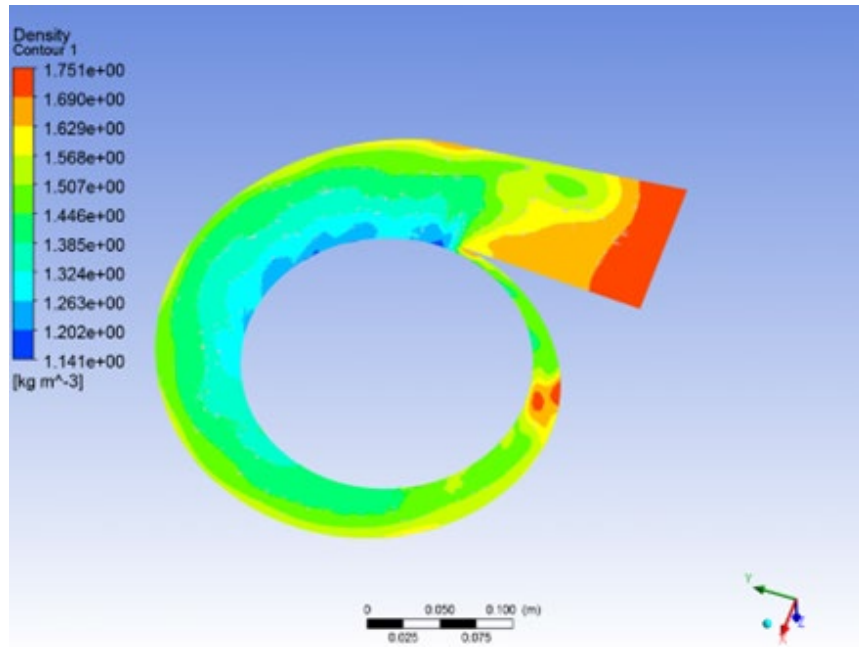


Figure 91 : Contour of Density at XY plane

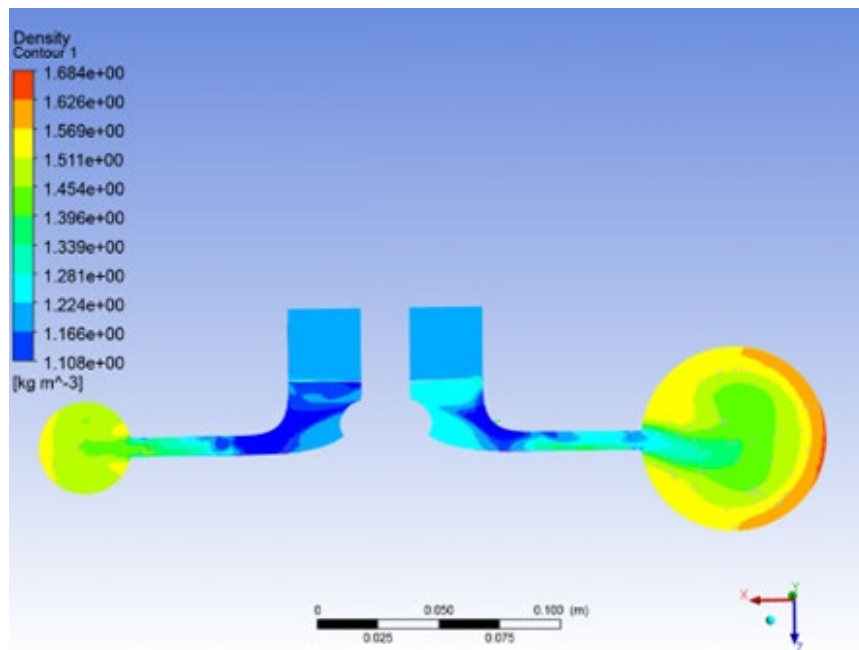


Figure 92 : Density Distribution at ZY plane

5.3 Impeller- Vaned Diffuser

The use of a diffuser with vanes is expected to increase the overall pressure ratio of the compressor. Although the width of a vaned diffuser is shorter than that of a vaneless, the diffusion caused by the vanes is big enough to slow the flow and achieve static pressure recovery. It is important to note that the phenomenon of the boundary layer detachment in the vanes, in combination with the maximum possible mesh size due to the high computer needs, made the CFD analysis even more complicated. This fact didn't allow us to aim to achieve the highest accuracy in the results, but rather to aim to get satisfactory results at every geometrical change made. That's why a series of tests were conducted, that included changes with respect to:

- the number of the vanes
- the angle of the vanes
- the width of the diffuser

The initial geometry started with the values used in the preliminary design. As far as the angle of the vanes, it was determined that they must be set in order to aim at a +2 angle of attack of the flow. A sensitivity analysis of the two other parameters has been carried out. From the diagram below, one can get a lot of information about the effect of each one on performance and the relation between the two on the specific compressor that is concerned in the study.

Several simulations were carried out in order to determine not only the exact number of the diffuser vanes but also the final outer diameter of the diffuser. Three different diffusers were tested with outer diameters of 82 mm, 88 mm, and 94 mm. In each of them, the effect of the diffuser vanes can be seen both on static and total pressure (Figure 93 and 94).

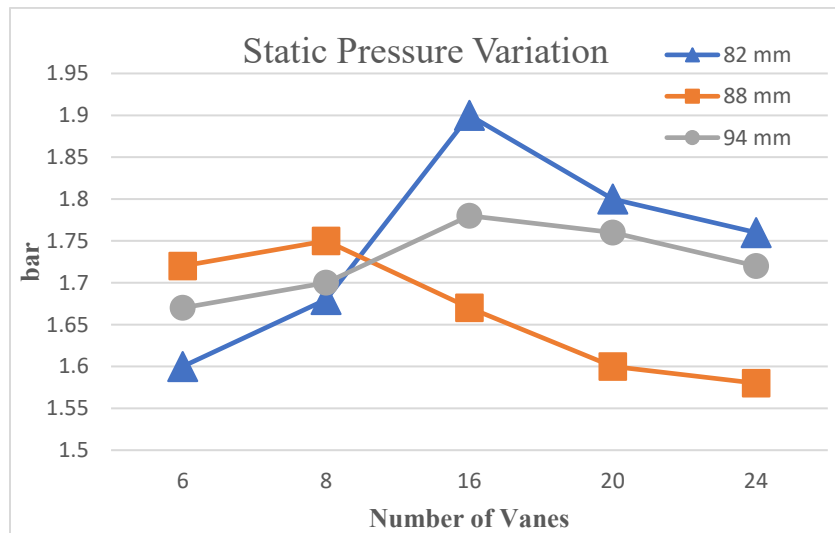


Figure 93 : Static Pressure Variation

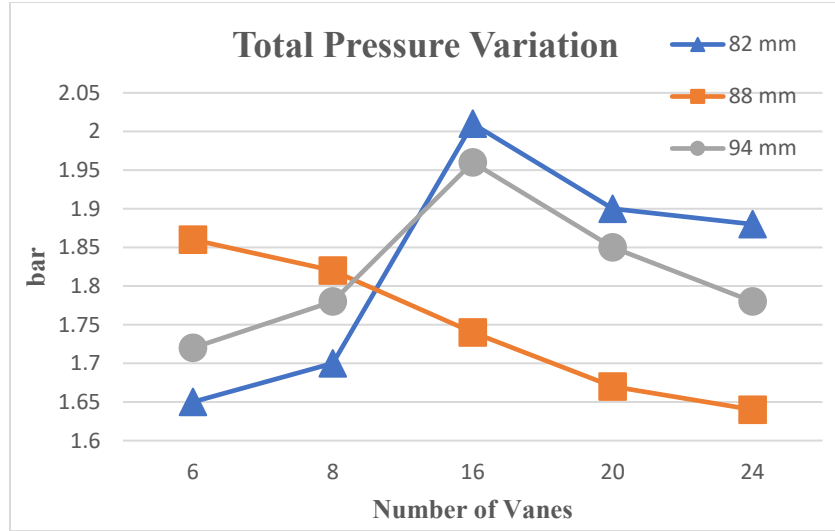


Figure 94 : Total Pressure Variation

Based on the previous figures, the optimum diffuser for this case is the one with an 82 mm outer diameter and with 16 diffuser vanes in terms of pressure. However, there are also some critical parameters that characterize the performance of every diffuser and must be examined. The performance of the diffuser is defined in terms of pressure recovery and loss coefficient, as mentioned by Heinrich [30] and Methel [31]. These parameters are calculated using the following equations, and the results are presented further.

$$K_{pr} = \frac{P_{o2} - P_{o2d}}{P_{o2} - P_2} \quad (81)$$

$$C_p = \frac{P_{2d} - P_2}{P_{o2} - P_2} \quad (82)$$

Using these terms, the diffuser effectiveness can also be estimated by this approximation:

$$\zeta = \frac{C_p}{C_{p,ideal}} = \frac{C_p}{C_p + K_{pr}} \quad (83)$$

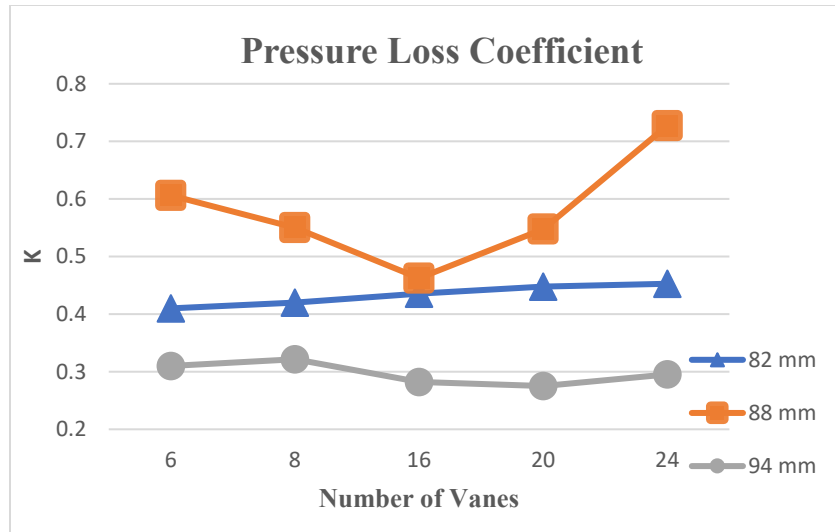


Figure 95 : Pressure Loss Coefficient Variation

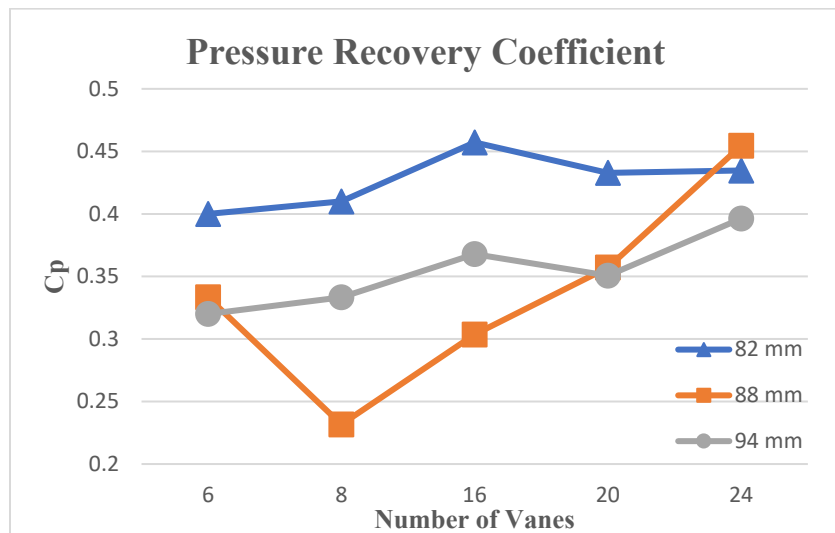


Figure 96 : Pressure Recovery Coefficient

From Figures 95, 96 and 97, it was found that the diffuser with an 82 mm outer diameter appears to have the larger pressure recovery for any number of vanes. The curve of the pressure loss coefficient for the diffuser with an 82 mm outer diameter lies between the other two. Figure 92 shows the effectiveness of all combinations. Although the diffuser with a 94 mm outer diameter has higher effectiveness, the design of the diffuser with an 82 mm outer diameter is more challenging, as it is quite smaller but can achieve a higher pressure rise.

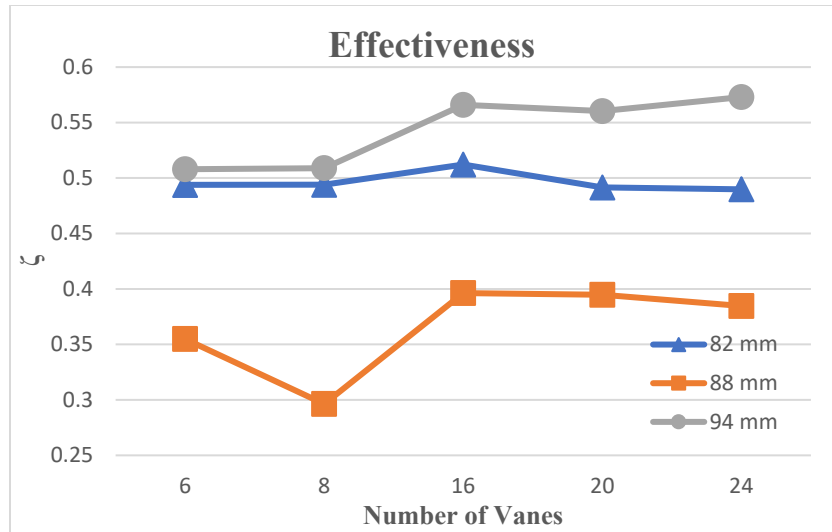


Figure 97 : Diffuser Effectiveness Variation

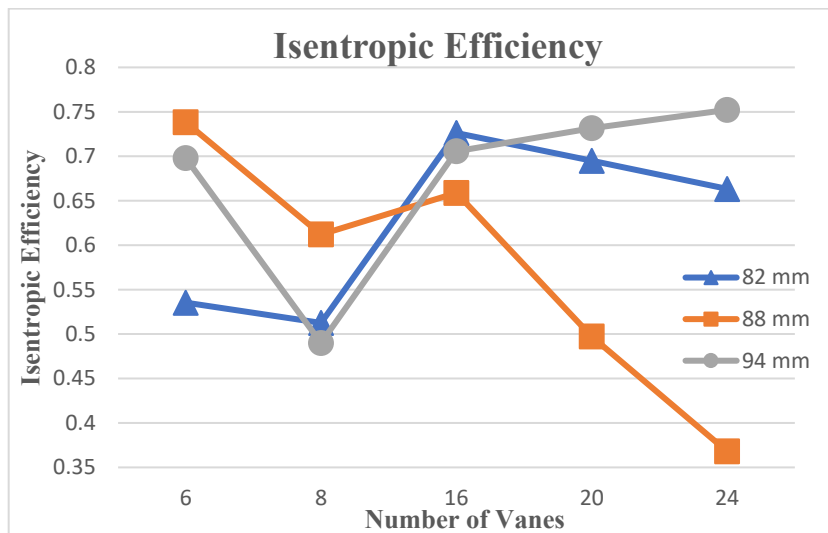


Figure 98 : Isentropic Efficiency factor

Figure 98 illustrates the isentropic efficiency of the diffuser. This unit is a performance parameter that can be used as a pressure recovery coefficient $\frac{P_{o2}}{P_{o1}}$. The diffuser with 82 mm outer diameter and 16 vanes appears to have about the same isentropic efficiency with the one with 88 mm outer diameter and 6 vanes and the one with 94 mm outer diameter and 24 vanes.

$$n_D = \frac{\frac{T_{2s}}{T_1} - 1}{\frac{T_2}{T_1} - 1} \quad (84)$$

This unit is more convenient to be expressed as a function of total pressure ratio as:

$$n_D = \frac{\frac{P_2}{P_1} \left(\frac{\gamma}{\gamma-1}\right) - 1}{\left(\frac{P_{o1}}{P_{o2}} * \frac{P_2}{P_1}\right) \left(\frac{\gamma}{\gamma-1}\right) - 1} \quad (85)$$

So, the choice is to select the diffuser that has an outer diameter of 82 mm and consists of 16 diffuser vanes.

Lastly, another critical parameter that identifies the performance of a diffuser is the blockage coefficient [31]. Although it is not investigated in this thesis, it is important to be referred to for any further research. The Blockage Coefficient is calculated as:

$$B = 1 - \frac{A_{effective}}{A_{geometric}} \quad (86)$$

Where $A_{effective}$ is the reduced flow area due to the presence of viscous boundary layers at the walls, and $A_{geometric}$ is the geometric area at the throat that corresponds to the maximum possible flow area assuming no losses in the passage

Pressure

Figure 99 displays the contour of the Static Pressure. Across the impeller, the static pressure increases due to the work offered by the rotating impeller. It is also confirmed that the vanes increase the static pressure of the fluid through the diffuser. The great increase in the static pressure starts at the leading of the vanes and reaches a value of 171483 Pa at the exit of the diffuser. One can also distinguish the surface of overpressure and underpressure in the vanes. At the upper surface, there appears to be a thickening of the streamlines of a fluid, as it can be observed through the following figure, and due to Bernoulli's equation, there is a corresponding effect on the pressure.

Total Pressure

Figure 100 depicts the change in the total pressure across the components. The contour of the total pressure of the vanes reduces the total pressure of the fluid, as they slow down the flow in order to achieve static pressure recovery.

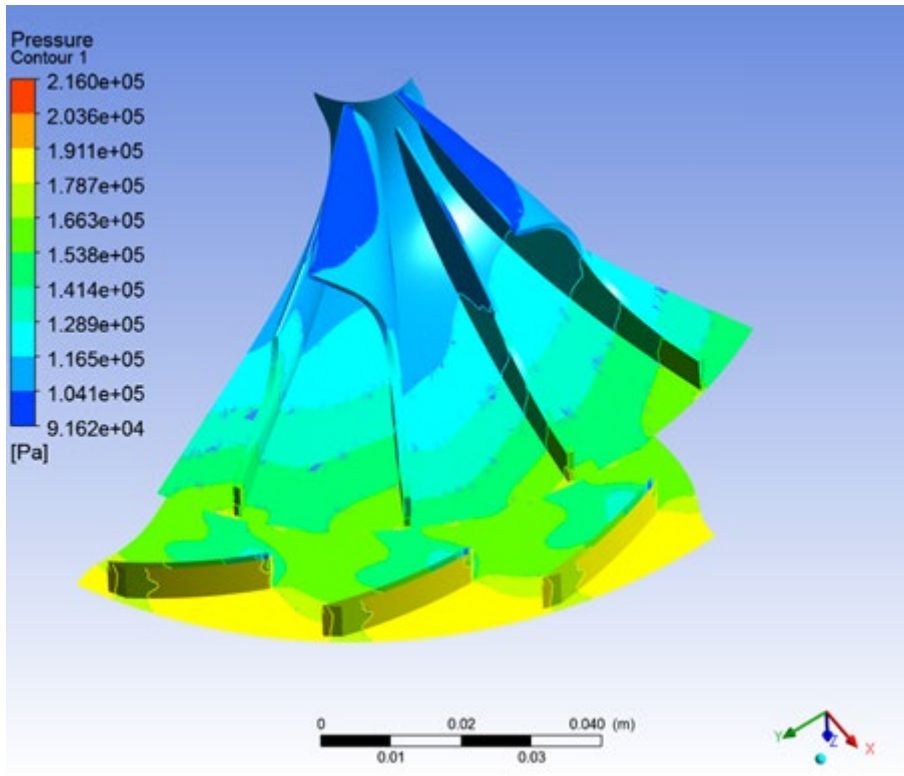


Figure 99 : Contour of Static Pressure at Vaned Diffuser

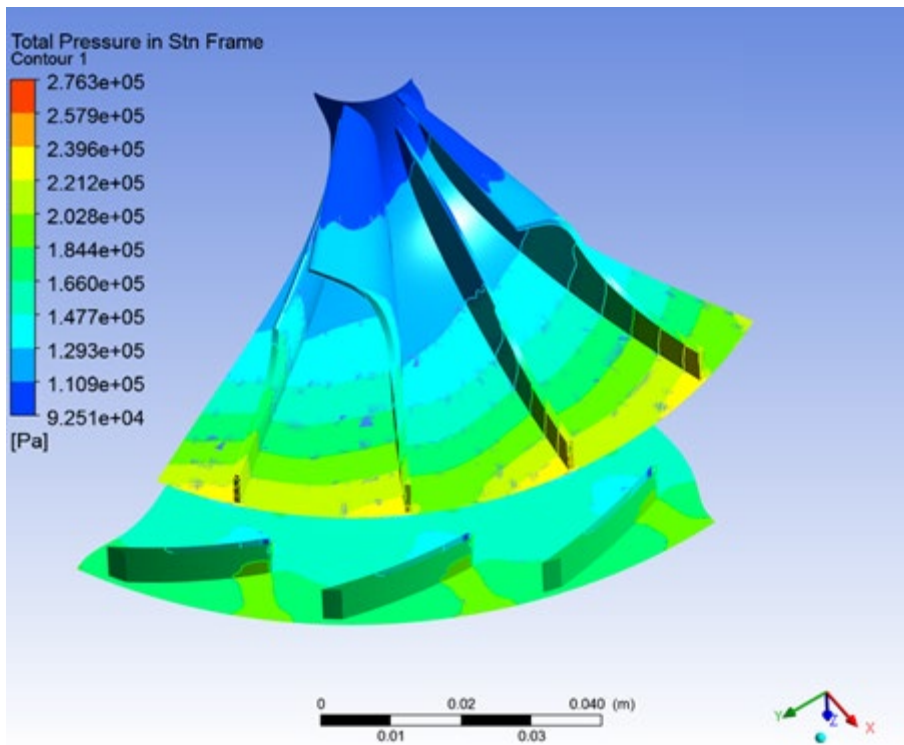


Figure 100 : Contour of Total Pressure at Vaned Diffuser

Streamlines

Streamlines are a family of curves that are instantaneously tangent to the velocity vector of the flow. These show the mean direction in which a massless fluid element will travel at any point in time. The streamlines accompanied by the magnitude of their velocity are shown in the figure below.

In Figure 101, the velocity enters the vaneless part of the diffuser at 260 m/sec and exits at 110 m/sec on average. The position of the vanes is set with respect to the angle of attack of the flow to the leading edge of the vanes. It is found that the optimum angle of attack is 0 degrees. In this way, the possibility of boundary layer detachment through the vane is eliminated.

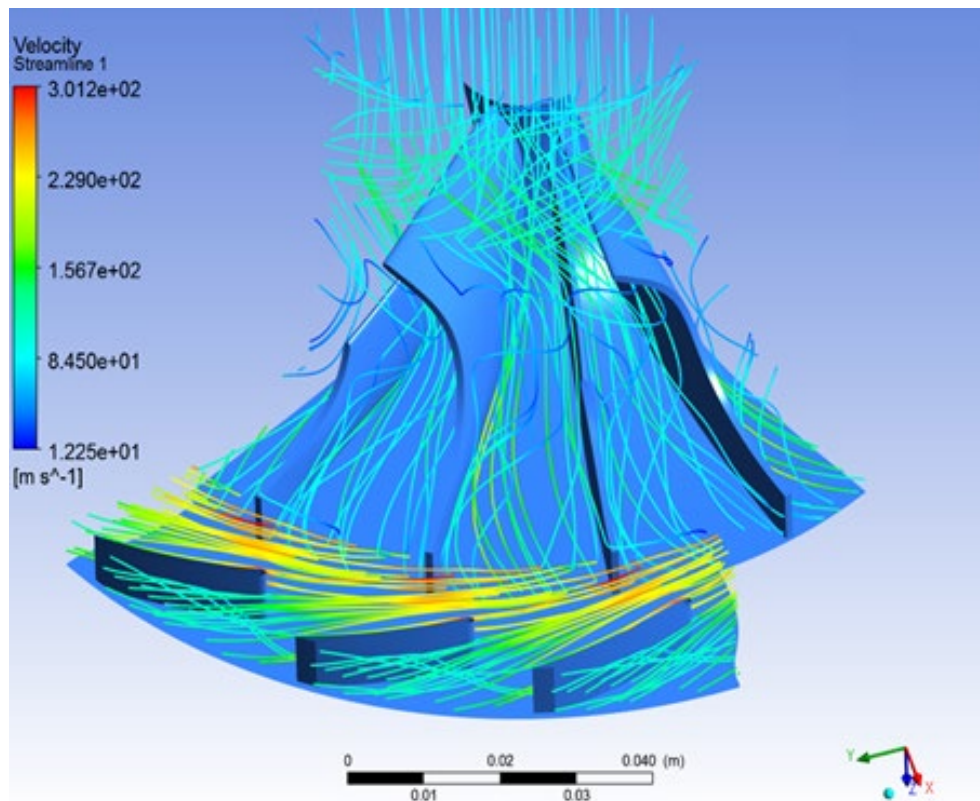


Figure 101 : Streamlines in Vaned Diffuser

Figure 99 shows the overpressure and the underpressure areas over the diffuser vanes. By the side, where the streamlines become denser, the pressure decreases, as can also be observed in Figure 102.

Total Temperature

Figure 103 displays the contour of total temperature across the impeller and the vaned diffuser. As expected, the total temperature remains constant through the diffuser. Across it, the total temperature is at 370 K due to the total enthalpy, which remains constant.

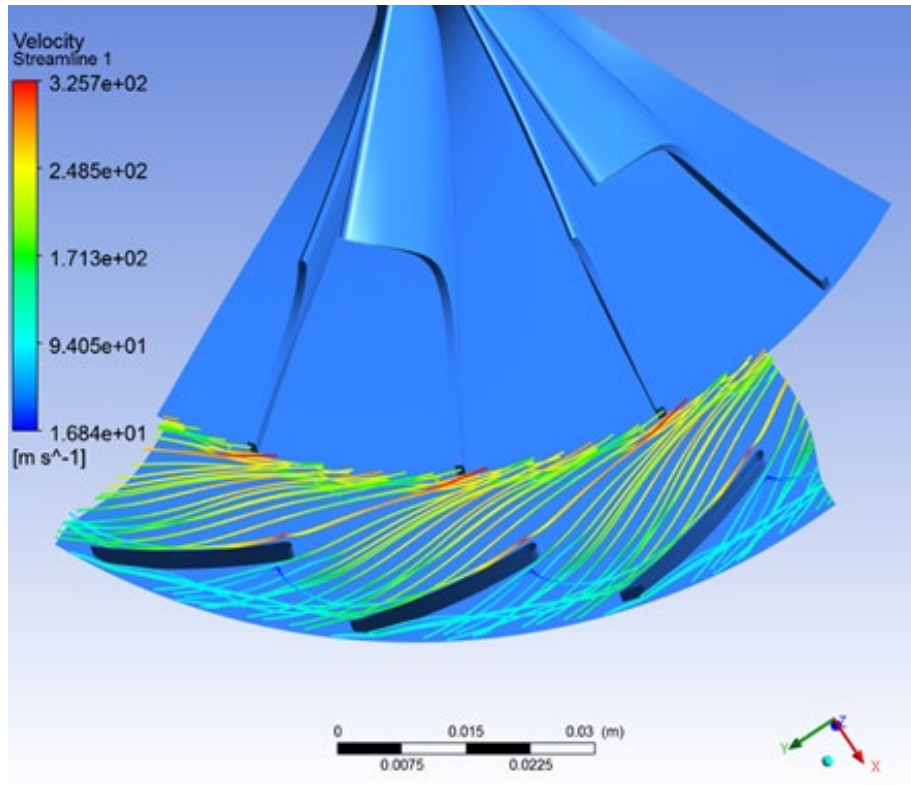


Figure 102 : Streamlines over and under the vanes

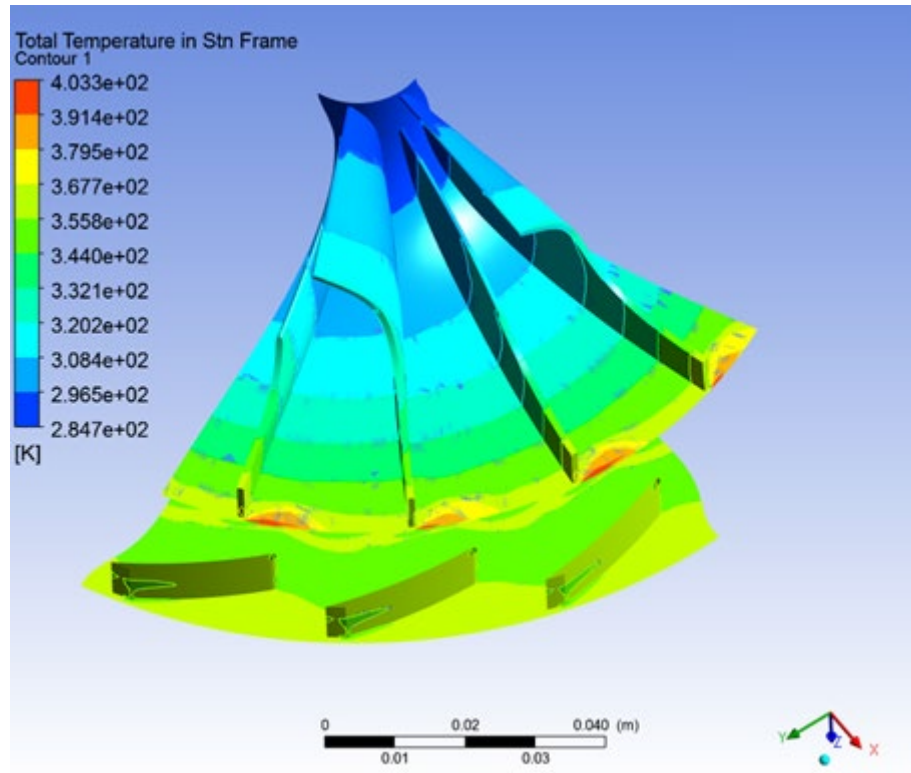


Figure 103 : Contour of Total Temperature at the Vaned Diffuser

Static Temperature

Figure 104 displays the contour of Static Temperature. Across the impeller, the static temperature gradually increases due to the compression caused. At the exit of the impeller, the temperature reaches a value of 340 K. As can be seen in the diffuser, there appear to be fluctuations in temperature. However, the vaned diffuser causes an increase in the temperature of the fluid. The static temperature at the exit of the diffuser is 365 K.

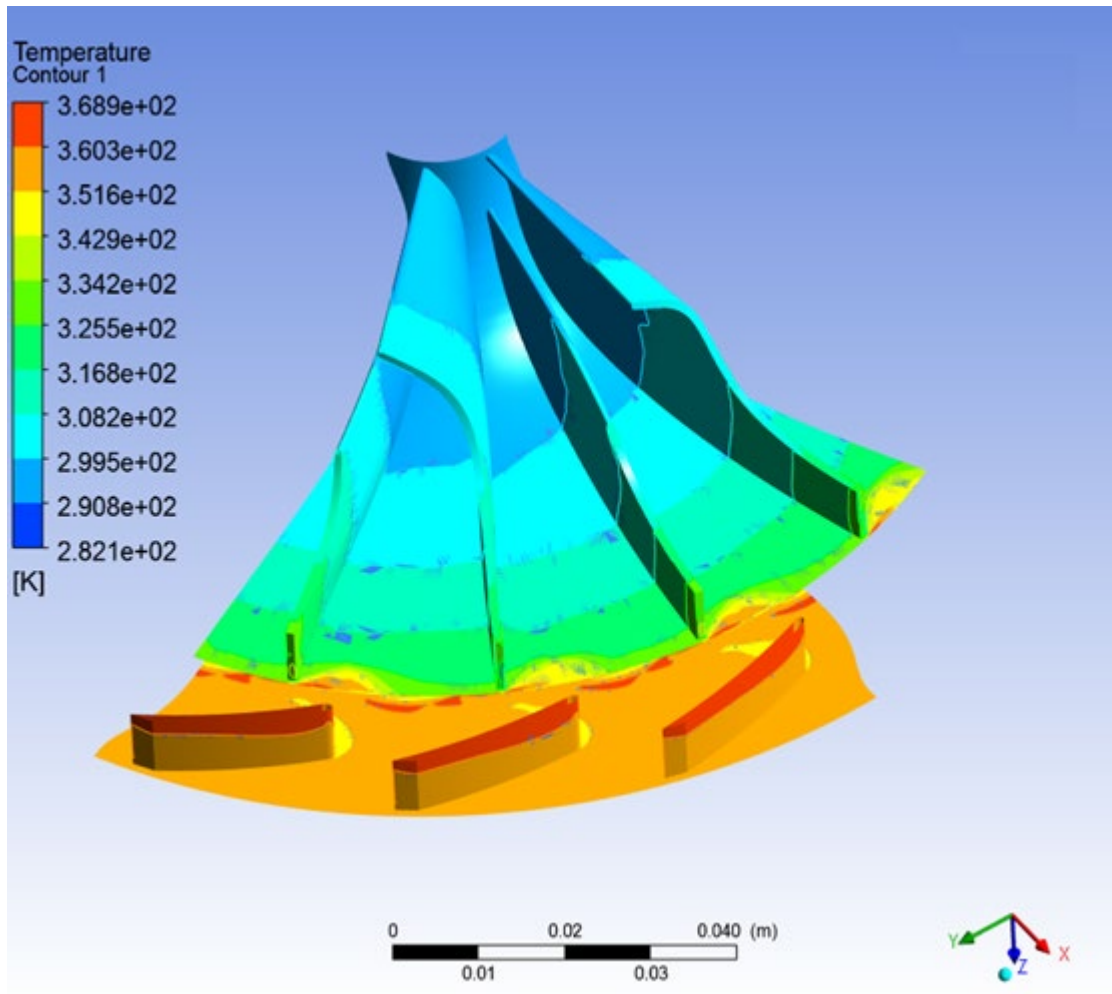


Figure 104: Contour of Static Temperature in Vaned Diffuser

Density

Concerning the Density, it increases throughout all the parts. Finally, the fluid exits the vaned diffuser with a density of up to 1.86 kg/m^3 .

Flow Field

Figure 106 displays the flow field at the outlet of the Vaned Diffuser. As expected from previous studies (Jaatinen-Värri et al. 2014 [9]), the backflow close to the shroud is smaller in contrast to the one seen in the vaneless diffuser. In the vaned diffuser, the jet and the wake mix out

faster. The faster mixing leads to lower losses and is the reason for the better efficiency in the Vaned Diffuser.

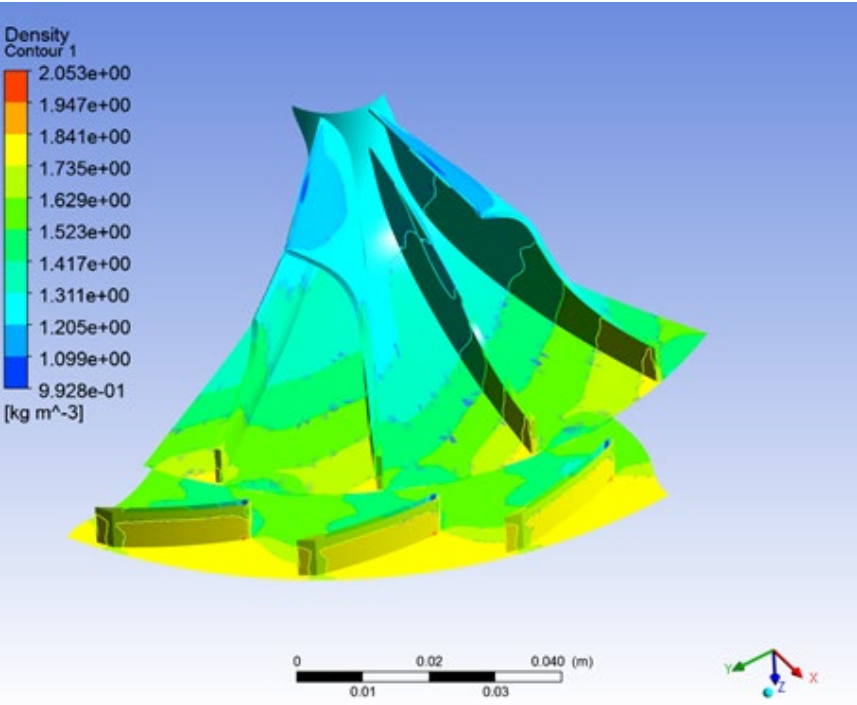


Figure 105 : Contour of Density of Vaned Diffuser

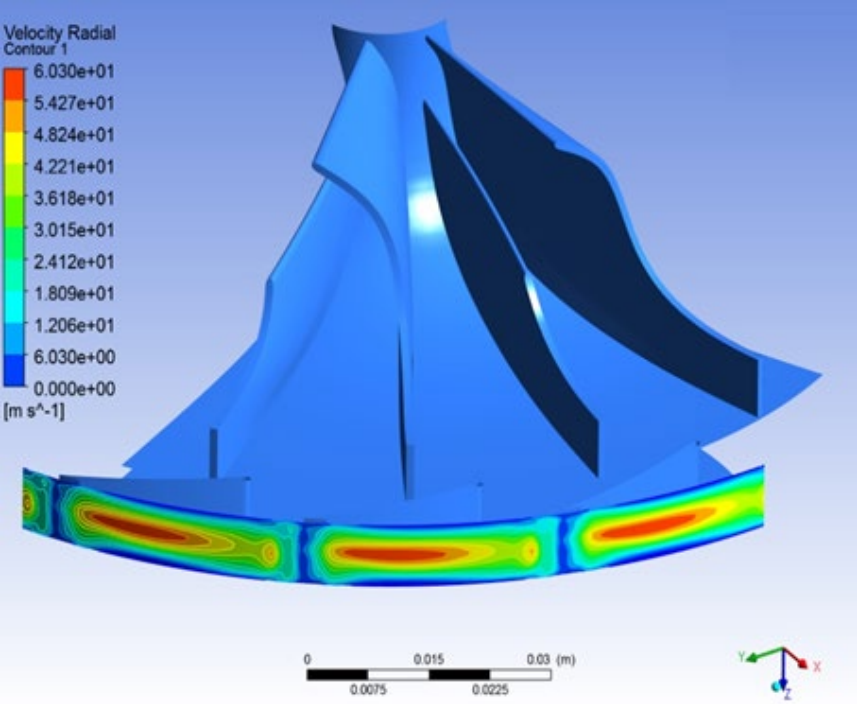


Figure 106 : Flow Field at Vaned Diffuser

Static Entropy

The static entropy at the vaned diffuser's outlet is displayed in Figure 107. It is clear that this unit is low enough across the area. Because the diffuser width is reduced and diffuser vanes exist, entropy generation in the passage wakes is reduced in comparison to the vaneless diffuser. The diffuser vanes make the flow more uniform at the impeller exit and the diffuser inlet. It is also confirmed that there is a significant reduction in the wake region at the impeller exit when comparing the vaned with the vaneless diffuser.

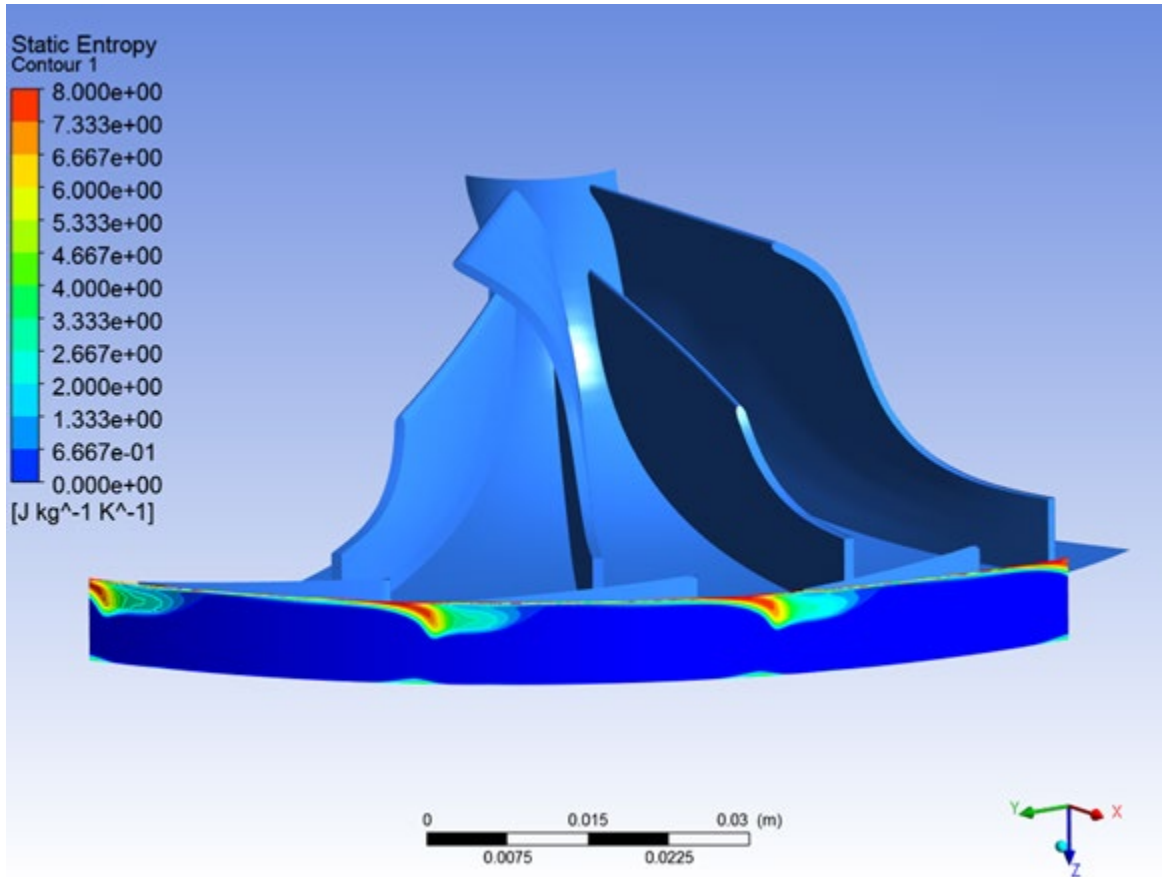


Figure 107 : Static Entropy at Vaned Diffuser

In Table 17, the results accrued from the Computational Fluid Dynamic analysis of the impeller with the vaned diffuser are presented, in contrast with those calculated from the preliminary design. The deviation between the values reaches the maximum value of 9.8% in only one unit. The deviation that exists is expected as the flow inside the compressor is very complicated and it cannot be simulated at its maximum level. However, all the results have qualitatively expected values. This fact shows that the simulation model is quite well set up and can be efficiently used to simulate the real problem.

Table 17 : Results CFD vs Pre-design for the Vaned Diffuser

Results Presentation of CFD Vs pre-design				
Unit		Ansys CFX	Excel	Deviation (%)
Total Pressure	P_{01}	105000	105000	0
	P_{02}	220453	197985	11.34
	P_{02d}	219942	182583	19.5
Static Pressure	P_1	103068	103148	0.07
	P_2	150186	145956	2.89
	P_{2d}	197242	226824	13.04
Total Temperature	T_{01}	293	293	0
	T_{02}	372	357.7	4
	T_{02d}	370	357.7	3.4
Static Temperature	T_1	290.7	291.6	0.28
	T_2	340.2	327.8	3.78
	T_{2d}	365	353.5	3.25
Density	ρ_1	1.20	1.23	2.11
	ρ_2	1.64	1.49	10.06
	ρ_{2d}	1.87	2.16	13.42
Mach Number	$M_{1m,rel}$	0.32	0.31	1.58
	$M_{2,abs}$	0.68	0.66	3.03
	$M_{2d,abs}$	0.22	0.20	10

5.4 Impeller-Vaned Diffuser-Volute

Due to the very complicated geometry in accordance with the high computational power needed, the simulation of the whole compressor became unattainable. Consequently, two distinct approaches to modelling the whole compressor were used. The first way included only a part of the impeller, a part of the vaned diffuser, and the entirety of the volute. Although the flow direction suggested that the components were working together well, the remainder of the data proclaimed that this method of modeling was ineffective, as can be seen in the figures below.

The second way, as presented in this subsection, was to divide the compressor into two separate parts, one with the impeller and diffuser, and one with the volute. In the first simulation, the results at the outlet of the diffuser are extracted and set as inlet conditions for the volute. Using this tactic, Ansys provided us with better results, as presented below.

Static Pressure

Figure 108 illustrates the distribution of Pressure across the volute. The pressure decreases as the cross-section area of the volute increases. As is confirmed in the next figure, the velocity of the fluid is lower in the area before the tongue of the volute and the pressure is high. In the final part, the diffuser, a small rise in static pressure stands out.

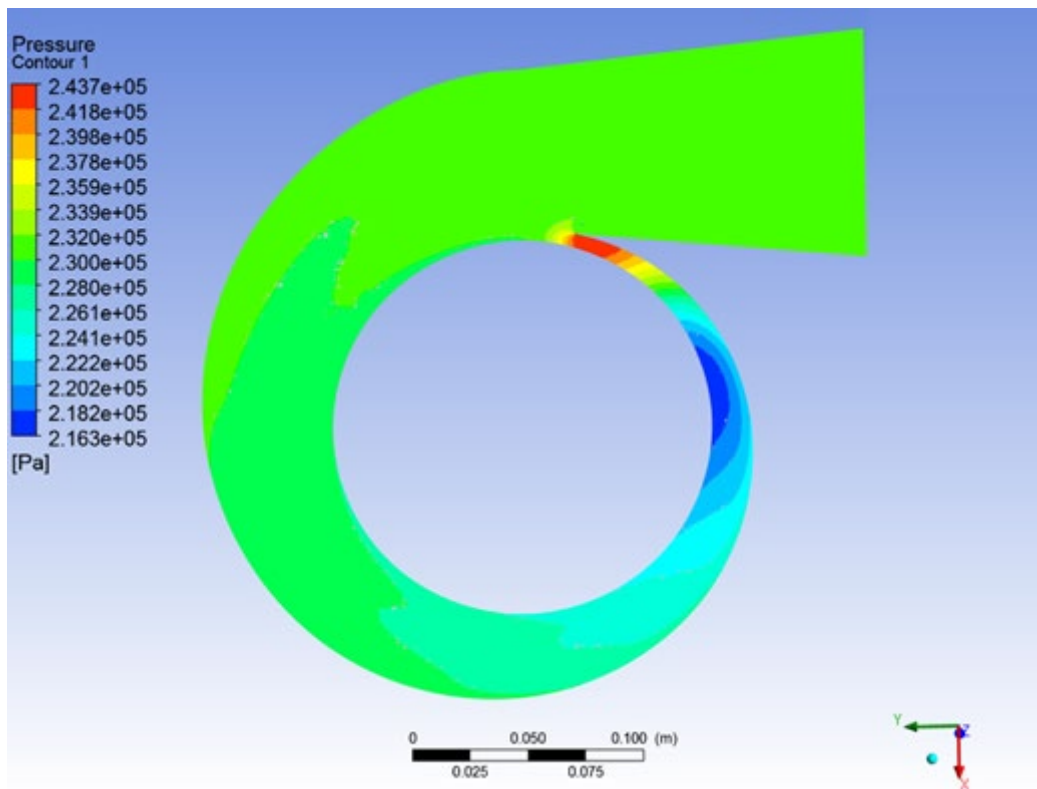


Figure 108 : Contour of Static Pressure at XY plane

Total Pressure

Figure 109 displays the contour of Total Pressure at the Volute. One can see that the Total Pressure is constantly decreasing. This is caused by the flow losses throughout the volute. According to Watson, the total losses in the volute are considered about half of the dynamic pressure of the diffuser. Finally, the Total Pressure at the exit reaches a value of 2.31 bar.

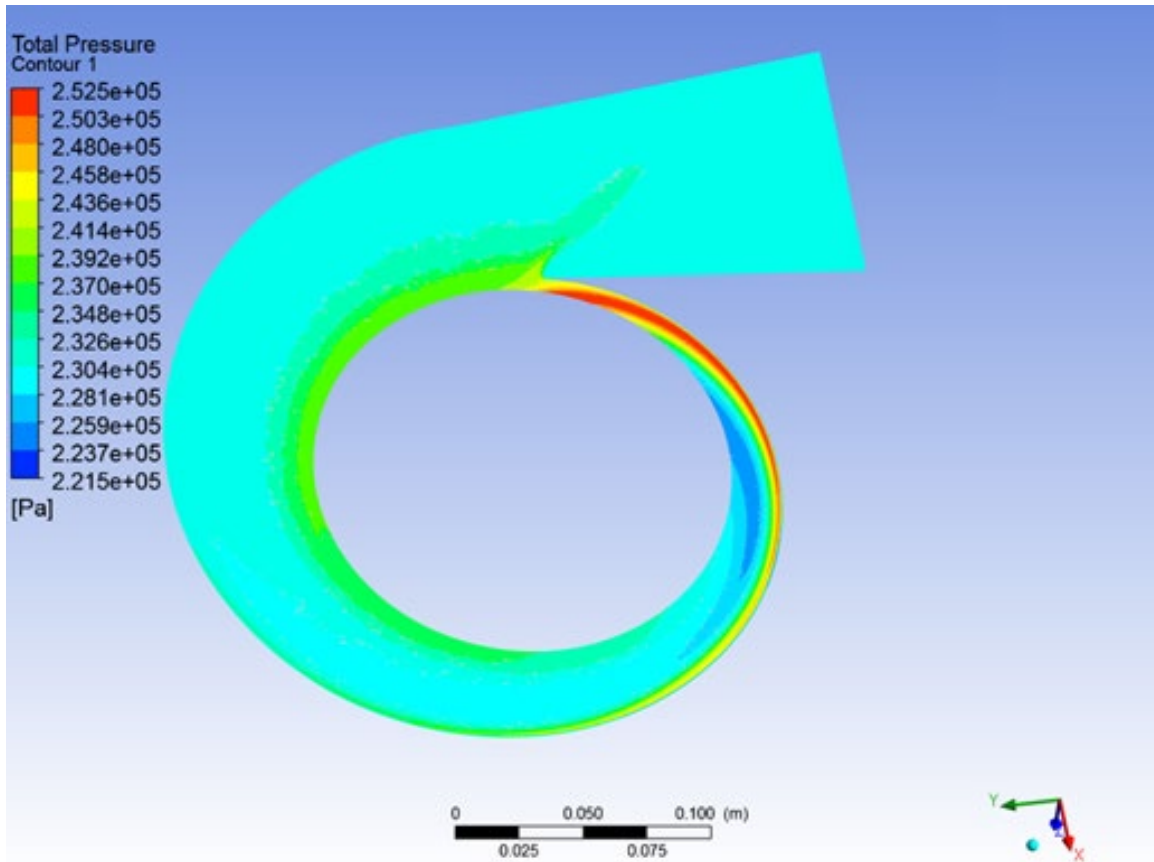


Figure 109 : Contour of Total Pressure at XY plane

Streamlines

In Figure 110, the streamlines are depicted. It is clear that the velocity near the wall is very low due to the no-slip condition. The velocity profile of the exit of the vaned diffuser is set as the boundary condition for the inlet. This leads to a 10 m/sec velocity on average.

Static Temperature

In Figure 111, the contour of the Static Temperature is depicted. The Volute neither produces nor consumes work, so the Total Temperature remains constant across it, while the static temperature increases. Static Temperature gradually increases up the value of 384 Kelvin.

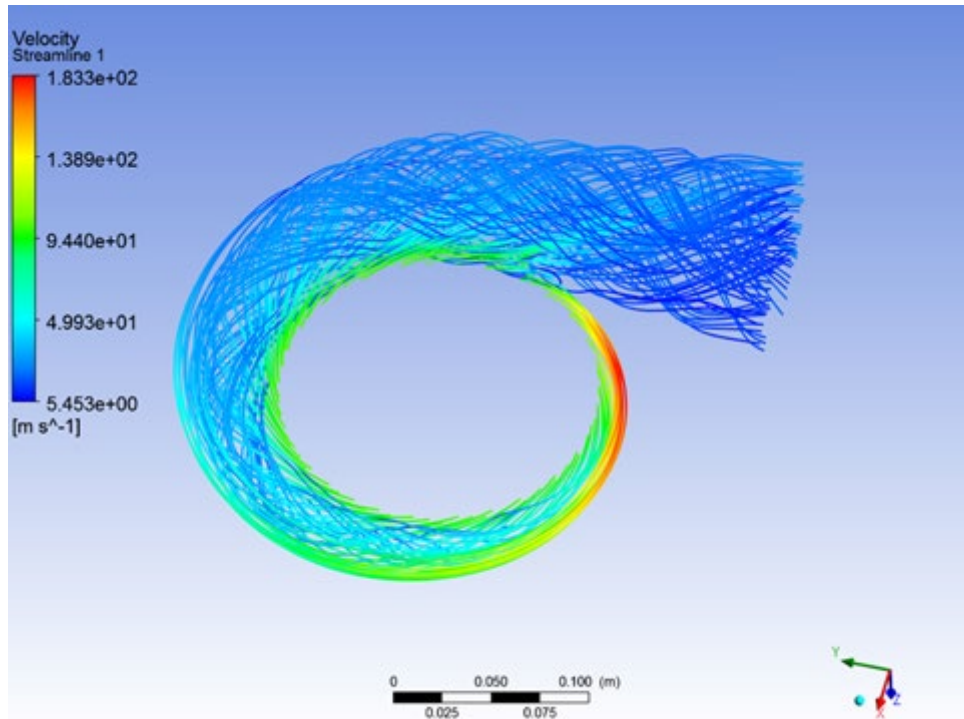


Figure 110 : Velocity Streamlines

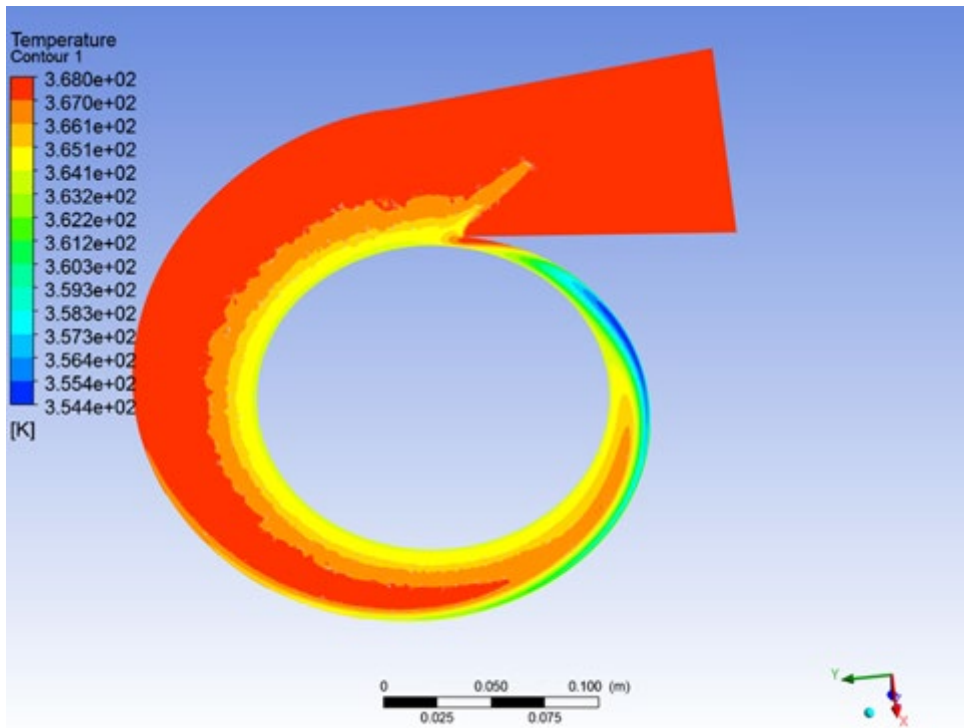


Figure 111 : Contour of Static Temperature

Density

Lastly, Figure 112 depicts the contour of Density. Density depends on the values of Temperature and Pressure, as described from the conservation law, and so it is already known what to expect based on the previous results. At the exit of the volute, it reaches the value of 2.168 kg/m^3 .

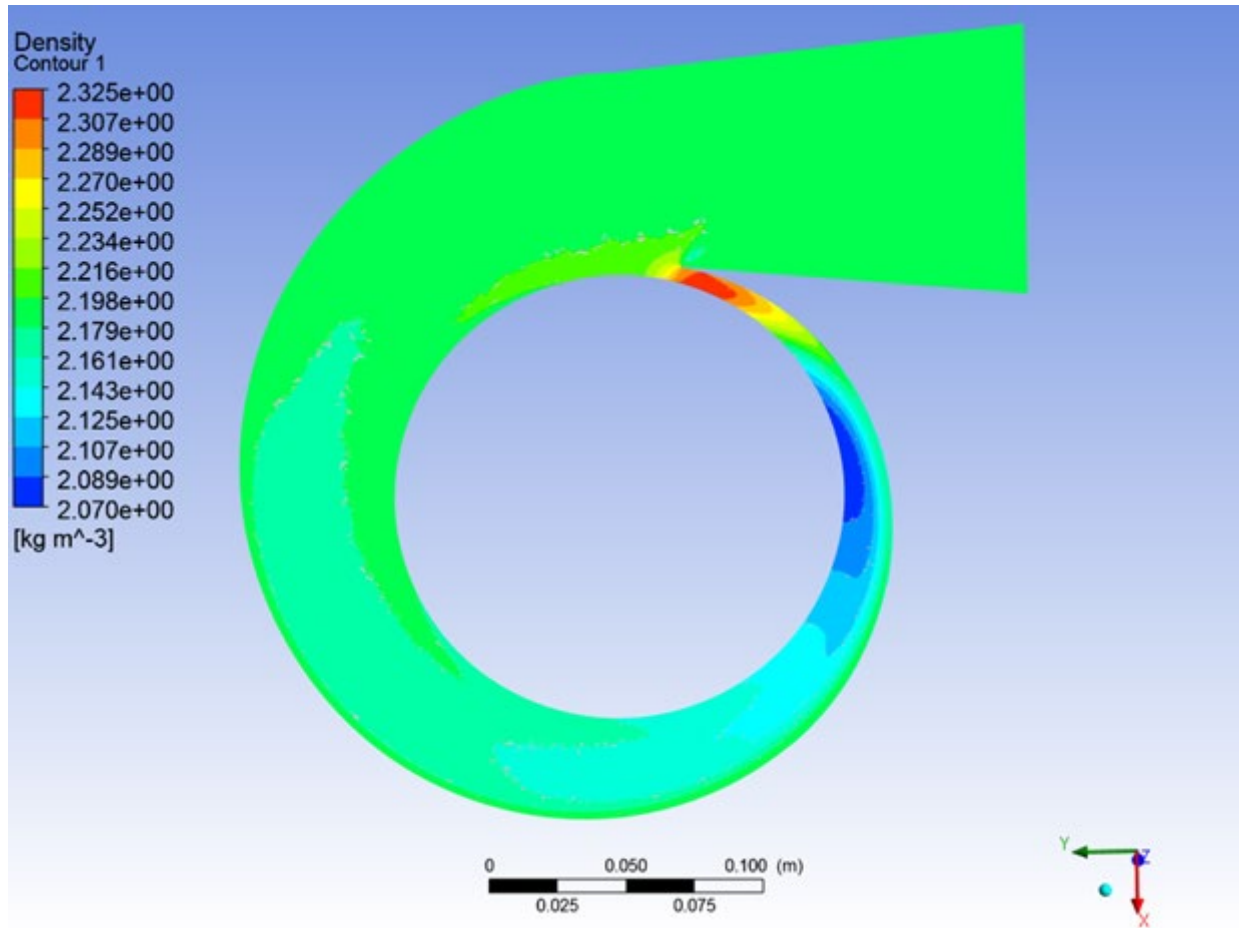


Figure 112 : Contour of Density

Turbulence Kinetic Energy

Figure 113 illustrates the Turbulence kinetic energy throughout the Volute. At inlet of the volute there is high turbulence kinetic energy due to the sudden change in area. Throughout the volute, this unit remains at low levels. At the area of the tongue there are eddies that causes losses to the flow and that is why it must be carefully designed.

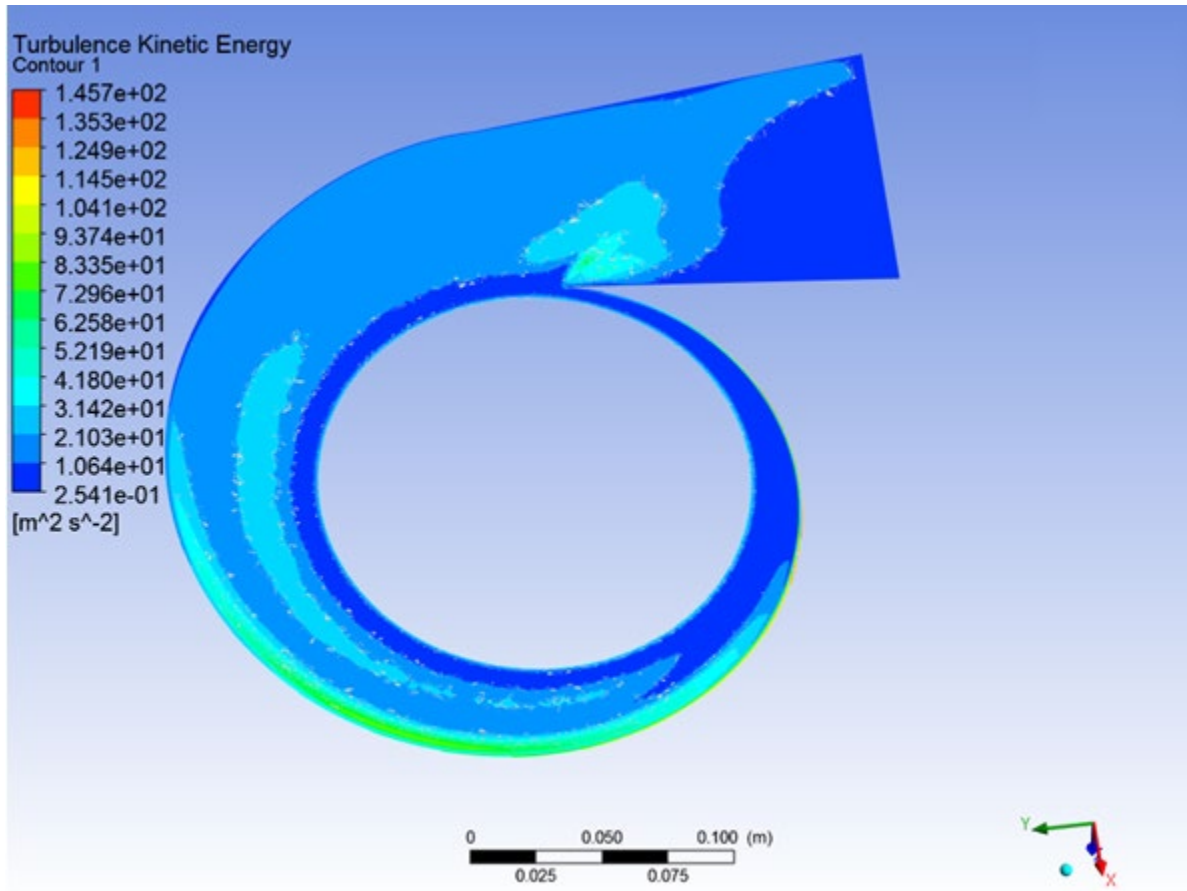


Figure 113 : Contour of Turbulence Kinetic Energy

5.5 Comparison of CFD Results with the two types of diffusers

The findings of the CFD study previously discussed in this chapter are gathered and compared in this paragraph. Furthermore, most differences and deviations concerning values that describe the fluid state in the compressor were expected from the preliminary report but confirmed further through the CFD process.

From the table below, a lot of information about the two different concepts can be extracted. Firstly, the compressor with the Vaned Diffuser can achieve higher static and total pressure, increasing by 32.06% and 29.26% respectively in comparison with the compressor with the Vaneless Diffuser. Consequently, the density further increases by 18.28%. This order of magnitude is crucial to the performance not only of the compressor but also of the engine.

Table 18 : Comparison between the CFD results

Presentation of CFD Results for the two different versions				
Unit		Compressor with Vaned Diffuser	Compressor with Vaneless Diffuser	Deviation (%)
Total Pressure	P_{01}	105000	105000	0
	P_{02}	220453	216381	1.88
	P_{02d}	219942	177285	24.06
	P_{03}	231263	169812	36.18
Static Pressure	P_1	103068	104281	1.16
	P_2	150186	148752	0.96
	P_{2d}	197242	165249	19.36
	P_3	238153	166153	43.33
Total Temperature	T_{01}	292.6	293	0.13
	T_{02}	372	362	2.76
	T_{02d}	370	362	2.2
	T_{03}	365	330	11.12
Static Temperature	T_1	290.8	289	0.62
	T_2	340.2	328.5	4.04
	T_{2d}	365	353.6	2.53
	T_3	370	321	15.26
Density	ρ_1	1.2	1.24	3.22
	ρ_2	1.64	1.48	10.81
	ρ_{2d}	1.87	1.64	14.02
	ρ_3	2.17	1.75	23.88

Based on the data extracted by the simulations for both versions, the Pressure Ratio and efficiency factor are calculated, which are the main indicators of the performance of the compressor.

Table 19 : Final Calculations

Results			
	Compressor with Vaneless Diffuser	Compressor with Vaned Diffuser	Deviation %
Total Pressure	187026	231264	23.65
Efficiency Factor	0.66	0.71	5.48

6. Concluding remarks

In this chapter, the most important conclusions about this thesis are presented. In the first subsection, as we can see in the table below, a brief overview of the work in terms of time spent on each stage is presented. In subsection two, the crucial design parameters that directly affect the performance of the compressor are shown. The effects of most of them were known from the bibliography but were confirmed through the simulations. In subsection three, we recommend a couple of future research topics in order to improve the design of the compressor even further. In the final subsection, we analyze the ways in which we cooperated and acted in order to achieve this great result. Mistakes in the way we worked and in the time spent are also mentioned so that other colleagues can avoid them.

6.1 Software

The study began with the Ansys workbench, which contains a number of softwares for geometry, meshing, flow analysis, etc. Ansys is a software that contains multiple apps that have simulation and 3D design, and is widely used by companies for product testing, design, and operation. The programs we used were Bladegen for the geometry construction for the impeller and diffuser, Turbogrid for their meshing and CFX for the fluid analysis. For the geometry of the Volute, we used Solidworks, which is one of the most commonly used 3D design programs by students and companies, because its interface is found to be more friendly to their needs. The mesh of the volute was completed in ANSA, since its geometry was quite complicated, and the quality of the mesh could be better than using an ANSYS meshing software. ANSA is ANSA is the leading multidisciplinary CAE pre-processor and is constructed by BETA CAE Systems, providing maybe the best mesh quality compared to other softwares.

The software of Ansys was available to us through the University of Thessaly. The computer of the Laboratory of Thermodynamics and Thermal Engines gave us access to ANSA and lastly, the Department of Mechanical Engineering owns a license of Solidworks.

6.2 Time Management

As shown in the table, the most important and most time-consuming part of this thesis was the preliminary design. It was the first part of the thesis, and it was crucial to make sure that all the calculations were correct, as the results of the preliminary were also going to be a reference point for those of the Computation Fluid Dynamics Analysis.

Concerning the design of the parts, it was the shortest part of the work. The geometry of the impeller was already available to us from a previous thesis at the University of Thessaly. The design of the diffuser was produced using Turbogrid, setting the appropriate options, while for the volute, we needed more time in order to finish the design, due to its geometrical complexion.

As far as mesh generation and preprocessing go, we studied very well all the available options and their functions before starting to use the program. However, we ran many tests and simulations with a variety of inputs in order to conclude the final settings that give the best results.

The solver modeling and the postprocessing were the biggest parts of this thesis. For the modeling, we tried deeply to understand the way that CFX solves the problem and the discretization methods that it uses. By doing so, the user can not only avoid errors but also correct them easily.

Table 20 :Review of the tasks of the thesis

Review of tasks	
Tasks	Time Spent %
Preliminary Design	20
Geometries	10
Mesh	10
Pre-Process	15
Solver	25
Post Process	20

6.3 Conclusions

Based on our experience gained during our Thesis work, we realized the preliminary design remains the most basic, fast, and useful tool in our search to pre-assess the effect of any geometrical and design modifications on the parts of the compressor, on its performance, expressed in terms of the evolution of the thermodynamic properties of air across. By making changes in the inputs of the preliminary design, the user may observe trends those that must be studied further. It also provides a view very close to reality, offering us a way to expect the outcome of every process.

As far as the geometries of the parts go, our CFD computations confirm that the number of the diffuser vanes is a very important design parameter. On the other hand, this number is directly connected to the outer diameter of the diffuser. The suggested vane numbers and dimensions are based on rough estimation based on from theoretical findings and experience of previous studies. In order to find the optimal balance between the diameter of the vaned diffuser and the number of vanes, CFD assists us in better understanding the flow, pressure, and temperature field variation, giving more insight in the process of comparing many different combinations. Further, we found the design and modeling of the volute a most crucial and demanding task. As it known from specialized literature, there are many flow losses in this part due to its complicated shape. Unfortunately, we did not have available any detailed measurement results to validate CFD modeling, thus, we have been very conservative in the interpretation of the CFD results. There are many ways in order to improve the volute's design that could be studied further.

Our experience confirmed the well-known role of mesh generation in the analysis of various parts of the compressor. The mesh size affects the accuracy and the convergence of the results and had to be selected with care, with respect to our computer capabilities and time required for multiple runs. The mesh independency study was very helpful in concluding the final mesh size among the three main components. As regards the meshing tools, we used Turbogrid for the Impeller and Diffuser and Ansa for the Volute, since they offered a better, easier, and less time-consuming way in each case.

The boundary conditions and the interfaces in the CFX must always be correctly set. False values caused errors in the simulation process, making it impossible to derive any reasonable solution. So, for each option, the user must understand its function. During this work, we lost a significant amount of time in try and error attempts, in order to better understand and optimally select certain critical options.

Since there were no detailed test data for validation of the results from the CFD simulations, we employed field checks and control volume boundaries' balances of thermodynamic and fluid dynamic variables (total temperature, total pressure etc.). In this way, we spotted some minor numerical errors which limit the accuracy of CFD predictions. Overall, we understood that one should be careful in interpreting the CFD results and not base his design purely on the CFD study. The CFD study is supposed to provide us with more insight about certain parts of the device under study, which cannot be known from the zero or 1-D approach of the preliminary design. Furthermore, during the preliminary design there are some certain indices that are based on thermodynamics and rule of thumb values from basic theory and experience. With the CFD, one can estimate these values with higher accuracy and improve his preliminary design.

6.4 Recommendations

Based on our experience through this thesis, we have pointed out some topics that must be studied further not only in order to improve the accuracy of this simulation but also to accompany this one and get something more complete. These topics are:

- Transient simulation analysis in order to observe the dynamic behavior of the compressor
- Variable diffuser vane angle in respect to mass flow of the compressor
- Study of the compressor map in respect to the engine map
- Design and simulation of the turbine of the particular compressor and the study of these systems working together
- Tip clearance effect on Impeller efficiency

6.5 Time plan

The first thing that we did when we undertook this thesis was to make a timetable with deadlines. Although we could never follow it, we knew every period on which topic we should focus. It is very logical that you may face difficulties with certain topics, and you can't estimate the exact amount of time spent on each. So, in the time plan, a safety time period should be added in each section. The time plan that we made and followed through with our thesis is presented in Table 21.

The fact that this thesis demanded the cooperation of two students gave us the opportunity to find out its importance. First of all, problem-solving becomes easier as there are two people thinking of different ways to solve the problem simultaneously. Having another pair of eyes also helps with small details that sometimes play a major role when setting up a simulation or meshing a geometry. Through this procedure, we also learned from each other. Moreover, we divided the main responsibilities. Although each of us is capable of running a simulation correctly, one was responsible mainly for the mesh generation and the other was for the CFX setup. This gave us the opportunity to deepen in each field and improve our research.

Table 21 : Time plan for the thesis

February	1-15	General Study of centrifugal compressor	Bibliography collection
	15-30	Study of Dixon Preliminary Design	Study of Previous Thesis
March	1-15	Start of Preliminary Design	
	15-30	Correct mistakes on Preliminary	
April	1-15	Study for CFD procedure	
	15-30	First simulations from previous thesis	
May	1-15	Study for the mesh generation	First use of Turbogrid
	15-30	Mesh Dependency Study	Volute Design
June	1-15	Study of CFX set up	Study of solver modeling
	15-30	Simulations with the Vaneless Diffuser	
July	1-15	Simulations with Vaned Diffuser	
	15-30	Simulations with Vaned Diffuser	
August	1-15	Simulations with Volute	
	15-30	Simulations with Volute	
September	1-15	Start of Thesis's Draft	Last simulations
	15-30	Getting ready for the Presentation	Last simulations
October	1-15	END	

Bibliography

- [1] *Air Compressor Types and Controls*. (2005). Canada Natural Resources. (accessed 5 Jul. 2022, www.nrcan.gc.ca/).
- [2] Neundorf, M. (2013). *How Turbochargers Work*. *Gear Patrol*. (accessed 5 Jul, 2022, www.gearpatrol.com/).
- [3] *Turbochargers vs Superchargers how they work*. (n.d.). Mobil. (accessed 5 Jul, 2022, www.mobil.com/).
- [4] *Learn what a Roots Blower is*. (n.d.) Robuschi. (accessed 2 Sep, 2022, www.gardnerdenver.com/).
- [5] Slashme. [Image]. (2016). Wikipedia (accessed 2 Aug, 2022, en.wikipedia.org/).
- [6] Watson, N., & Janota, M. S. (1982) Turbocharging the Internal Combustion Engine, 1st ed. London: Red Globe Press London, p. XVI–608
- [7] Heywood, J. B. (1988). *Internal combustion engine fundamentals*. New York: McGraw-Hill.
- [8] Im, K. (2012). *Development of a Design Method for Centrifugal Compressors*. University of Michigan.
- [9] Statharas, J. & Vlachakis, N. (2019). Industrial Centrifugal Compressors Design Validation, using Rapid Method Evolutionary Algorithms to Predict Map Characteristics Evaluation. *International Journal of Engineering and Technical Research*. V8.
- [10] Dixon, S.L. & Hall, C.A. (2014). *Fluid Mechanics and Thermodynamics of Turbomachinery*. UK: Butterworth-Heinemann.
- [11] *Unsteady dynamics of corner separation in a linear compressor cascade* -Scientific Figure on ResearchGate. (accessed 5 Sep, 2022, www.researchgate.net/).
- [12] Bitter, J. (2017). *Important Considerations When Designing a Volute*. Concepts NREC. (accessed 2 Aug, 2022, <https://www.conceptsnrec.com/>).
- [13] Παλάσκας, Α. & Χατζηκόρκου, Μ. (2020) Σχεδιασμός και CFD προσομοίωση συμπίεστη για στροβιλοϋπερπληρωτή κινητήρα Honda CBR600RR. Πανεπιστήμιο Θεσσαλίας.
- [14] Cumpsty, N. A. (2004). *Compressor Aerodynamics*. Florida: Krieger Publishing Company, Malabar.
- [15] *Ansys TurboSystem User's Guide*. (2013). Ansys Inc. (www.academia.edu/)
- [16] Zahed, A. & Bayomi, N. (2014). Design Procedure of Centrifugal Compressors. *ISESCO JOURNAL of Science and Technology*. 10. 77-91

- [17] Ζάμπος, Α. & Ζαρμακούπης, Ι. (2017) Λεπτομερής σχεδιασμός συμπιεστή ΚΚΚ3HD454 με χρήση του λογισμικού ANSYS/CFX. Πανεπιστήμιο Θεσσαλίας.
- [18] Shyam2791. [Image]. (2012). Wikipedia. (accessed 10 Aug., 2022, en.wikipedia.org/)
- [19] Sliffa & Mysid. [Image]. (2006). Wikipedia. (accessed 10 Aug., 2022, de.wikipedia.org/)
- [20] Zureks, I. [Image]. (2007). Wikipedia. (accessed 10 Aug., 2022, en.wikipedia.org/)
- [21] Λουκάς, Γ. (2019). Ανάλυση της λειτουργίας ελίκων μη επανδρωμένων αεροσκαφών, υπό την επίδραση γεωμετρικών σφαλμάτων. Πανεπιστήμιο Πατρών.
- [22] Voorde, J. & Dick, E. & Vierendeels, J. & Serbmyns, S. (2022). Performance prediction of centrifugal pumps with steady and unsteady CFD-methods. Department of Flow, Heat and Combustion Mechanics. Ghent University.
- [23] Denton, J. D. (2010) Some limitations of turbomachinery CFD. In: Proceedings of ASME Turbo Expo 2010: Power for Land, Sea and Air. Glasgow
- [24] *Introduction to Ansys Fluent Lecture 7 : Turbulence Modeling* (2014) Ansys Inc. [PowerPoint slides] (www.academia.edu/)
- [25] *Introduction to Introduction to ANSYS FLUENT*. (2010). Ansys Inc. [PowerPoint slides] Fluent_13.0_lecture06-turbulence. (imechanica.org/)
- [26] Pachpute, S. (n.d.) Turbulent Heat Transfer and Its CFD Modeling. CFD Modeling of Turbulent Heat Transfer: Forced, Natural and Mixed Convection.
- [27] *Y-plus: Boundary Layer Resolution* [Image] (n.d.) (accessed 10 Sep., 2022, www.cfdyna.com/CFDHT/Y_Plus.html)
- [28] Jasak, H. (1996). Error analysis and estimation for the finite volume method with applications to fluid flows. London: Imperial College.
- [29] Kim, J. & Lee, H. & KIM, J. & Choi, Y. & Yoon, J. & Yoo, I. & Choi, W. [Image] (2015). Improvement of Hydrodynamic Performance of a Multiphase Pump Using Design of Experiment Techniques. *Journal of Fluids Engineering*. 137. Paper 081301 (15pp).
- [30] Heinrich, M. (2016). Genetic Optimization of Turbomachinery Components using the Volute of a Transonic Centrifugal Compressor as a Case Study.
- [31] Methel, C. J. (2016). An experimental comparison of diffuser designs in a centrifugal compressor. Purdue University.